Doctoral theses at NTNU, 2018:124

Lars Gullbrekken

Climate adaptation of pitched wooden roofs

Doctoral thesis

ISBN 978-82-326-3038-7 (printed ver.)
ISBN 978-82-326-3039-4 (electronic ver.)
ISSN 1503-8181

NTNU
Norwegian University of
Science and Technology

NTNU
Norwegian University of Science and Technology
Thesis for the Degree of
Philosophiae Doctor
Faculty of Engineering
Department of Civil and Environmental
Engineering

Doctoral theses at NTNU, 2018:124

NTNU
Norwegian University of
Science and Technology

Lars Gullbrekken

Climate adaptation of pitched wooden roofs

Thesis for the Degree of Philosophiae Doctor

Trondheim, May 2018

Norwegian University of Science and Technology
Faculty of Engineering
Department of Civil and Environmental Engineering

NTNU
Norwegian University of
Science and Technology

NTNU
Norwegian University of Science and Technology

Thesis for the Degree of Philosophiae Doctor

Faculty of Engineering
Department of Civil and Environmental Engineering

ISBN 978-82-326-3038-7 (printed ver.)
ISBN 978-82-326-3039-4 (electronic ver.)
ISSN 1503-8181

Doctoral theses at NTNU, 2018:124

Printed by NTNU Grafisk senter

PREFACE

This PhD is funded by SINTEF Building and Infrastructure and is part of the Klima 2050-project, which falls within the remit of the Centre for Research-based Innovation (SFI). The aim of Klima 2050 is to reduce the societal risks associated with climate changes, enhanced precipitation and flood water exposure within the built environment. More information about the research project can be found at www.klima2050.no. The thesis investigates potential adaptations of wooden roofs to accommodate climate change. The main work has involved laboratory studies as well as field measurements. In addition, some simulation results are presented.

I would like to thank everyone who has helped me to finish my thesis. All my colleagues at SINTEF Building and Infrastructure, NTNU Department of Civil and Environmental Engineering and Klima 2050 need special thanks.

Special thanks go to the following people:

My main supervisor and co-supervisor, Tore Kvande and Berit Time: you have been valuable discussion partners and contributed with necessary input, guidance and motivation along the way.
Stig Geving, who has also been a co-supervisor.
Sivert Uvsløkk, you have been an appreciated discussion partner and have contributed with your advice to several parts of the thesis. You have also been a co-author on several of the articles.
The laboratory personel and in particular Øystein Holmberget, Ole Aunrønning and Egil Rognvik.
CAD operators Bjørnar Nørstebø and Remy Eik also need to be acknowledged.
Positive feedback and encouragement from the industry partners among them Jørgen Young from Isola has also been appreciated along the way.

Finally, I would like to thank family and friends for always supporting me.

December 2017

Lars Gullbrekken

SUMMARY

In this thesis, wooden roofs are defined as roof structures where the load-bearing structure consists of wood. Such structures are normally built with a ventilated air cavity between the underlayer roof and the roofing. The main purpose of this air cavity is to transport excessive moisture away from the roof structure as well as to transport heat and avoid snow melt when there is snow on the roof. Hence, the design of the air cavity is crucial in relation to pitched wooden roofs being adapted to the local climate.

Wooden roof structures might have a favourable carbon footprint compared to other building materials. Hence, increased focus on the carbon footprint of building materials and components makes wooden roofs more relevant, including for large buildings. Changes in climate can provide more intense precipitation in the form of torrential rain in parts of the country. Climate-adapted solutions must both protect against the ingress of water and ensure rapid drying-out of moisture in the structure.

The SINTEF Building Design Guides (Byggforskserien) serves as a collection of standard building designs that fulfil the Norwegian building regulations. The collection declares a maximum roof length from eaves to ridge of a pitched, ventilated wooden roof of 15 m. The minimum roof pitch is set to 10-15°. The guidelines are based on long-term experience in the Norwegian climate. Roofs with larger spans and lower angles must be planned in detail for every building project, which is not very efficient.

The objective of this thesis is to increase the knowledge about moisture safety and air flow through the air cavity of pitched wooden roofs. Experimental research, field measurements and numerical simulations have been used to assess and characterise the driving forces and resistances for roof ventilation.

Analysis of the SINTEF Building Defects Archive shows that moisture from precipitation and indoor air leakages is the dominating source of building defects for pitched wooden roofs. This is critical when we bear in mind the anticipated climate changes with wetter and warmer climate in Nordic countries. An airtight vapour retarder and use of balanced ventilating is proposed as an effective means to increase moisture safety. These means are also important in the climate-adapted roofs of tomorrow.

Air movement inside the thermal insulation layer is found to significantly increase the thermal transmittance of roof and wall structures. The effect may also redistribute moisture inside the insulated layer causing increased moisture in the colder parts of the structure with an increased risk of condensation and moisture damage. Dividing the insulation layer using a vapour-open convection barrier is therefore suggested to increase the moisture safety for roof structures with more than 200 mm of insulation.

Increased interest in renewable energy production increases the relevance of using facades and especially roofs for energy production. The possibility to combine PV (Photo Voltaic) systems as roofing and to harvest solar energy, hereafter called BIPV (Building Integrated Photo Voltaic), is therefore relevant. Such systems can lead to building-

physical challenges. In particular, hazards due to downfall of snow and ice during the winter and ventilating requirements during warm sunny periods to ensure low temperatures and thereby higher efficiency are challenges that need to be dealt with.

The air change rate of the air gap between the roofing and the underlayer roof is given by the driving forces and resistances. The driving forces are given by wind and thermal buoyancy. The resistances are given by the air passing inlet and outlet and the different obstacles inside the air cavity. This thesis and the included papers include studies of both the driving forces of wind and the resistances inside the air cavity. The height of the counter and tile battens as well as the edge design of the tile battens is found to influence the air change rate of a specific air cavity. The driving forces of wind are studied by analysing previous data from field measurements. The wind pressure at the facade was affected by the wind approach angle. A value for the average wind pressure difference coefficient given eaves-to-eaves ventilated air cavities is proposed as Δc_p=0.7.

The field investigation of the ventilated wooden roof at the ZEB Test Cell Laboratory shows a strong correlation between the wind speed and the air speed inside the air cavity. In addition, long periods of lower temperatures compared to the ambient temperature on the lower facing of the roofing material have been found. There is a risk of increased moisture content during these periods. Use of dynamic valves which open the ventilating systems during periods with dry-out conditions and close during periods with moistening conditions is a possible solution to the problem.

This thesis also looks at the possibility to construct long, climate adapted roofs. The study included winter conditions with snow on the roof. Roof insulation thickness and the thermal transmittance affect the snow melt potential of the roof structure to a large extent. A review of the ventilating guidelines of different cold climate countries in Europe as well as Canada and USA (Washington) reveals similar guidelines regarding air cavity design compared to the Norwegian guidelines.

Experimental data established in the thesis is used in a stationary model to calculate the snow melt potential of pitched wooden roofs in order to develop a basis for roof ventilating guidelines adapted for future wooden roofs. Given a 30 m long roof and insulation thickness of 350 mm an air cavity height of approximately 160 mm was proposed for roofs with combined underlayer roofing and wind barrier in order to avoid snow melt problems.

The work shows that pitched wooden roofs adapted to the Nordic climate of tomorrow need:

1) Increased climate adaptation and moisture safety by improved air cavity design.
2) Convection barrier when insulation thickness exceeds 200 mm.
3) More knowledge and relevant documentation if BIPV roofing is used.

Contents

List of papers

Part 1: Motivation, current state and future challenges (Papers 1 and 2)

List of Papers

1) Gullbrekken L, Kvande T, Time B (2016). Norwegian Pitched Roof Defects. *Buildings*, *6*(2), p. 24.
2) Gullbrekken L, Kvande T, Time B (2015). Roof-integrated PV in Nordic climate - Building physical challenges. The 6th International Building Physics Conference - IBPC 2015. *Energy Procedia*, Vol. 78, pp. 1962-1967.

Part 2: Increased insulation, moisture-resilient structures (Paper 3)

List of Paper

3) Gullbrekken L, Uvsløkk S, Kvande T, Time B (2017). Hot-Box measurements of highly insulated wall, roof and floor structures. *Journal of Building Physics*, Vol. 41(1), pp. 58–77.

Part 3: Ventilating guidelines, knowledge base (Papers 4 to 7)

List of Papers

4) Gullbrekken L, Kvande T, Time B (2017). Ventilated wooden roofs: Influence of local weather conditions – measurements, 11th Nordic Symposium on Building Physics, Trondheim, Norway, 11-14. June 2017. *Energy Procedia*, Vol. 132, p. 777-782.
5) Gullbrekken L, Uvsløkk S, Kvande T, Pettersson K, Time B (2018). Wind pressure coefficients for roof venting purposes. *Journal of Wind Engineering and Industrial Aerodynamics*, Vol.175, pp. 144-152.
6) Gullbrekken L, Uvsløkk S, Geving S, Kvande T (2018). Local loss coefficients inside air cavity of pitched wooden roofs. *Journal of Building Physics*. Published online 1. December 2017.
7) Gullbrekken L, Uvsløkk S, Hygen HO, Kvande T, Time B. Air cavity design guidelines for pitched wooden roofs in cold climate. Submitted

1 INTRODUCTION

This section gives an introduction into ventilated pitched wooden roofs. Norwegian traditions of wooden roofs, measures for moisture resistance and climate adaptation, and future possibilities are presented.

1.1 Norwegian traditions of wooden roofs

In the Nordic countries, many buildings have wooden frames. Such structures are especially common for small houses. There is a well-developed tradition of using wood for exterior cladding, load-bearing systems, and interior cladding. The wood-based building tradition has developed due to easy access to high-quality raw materials. According to Edvardsen and Ramstad (2007), in Norway, over 98 % of small houses are built with wooden frames. Most of the single family or detached houses have pitched roofs (Thue, 1993) (Figure 1).

The roof structures of small houses are typically constructed with a wooden load-bearing system, in this thesis referred to as wooden roofs. There are several alternative roof structures. The various design principles for wooden roofs are thoroughly discussed by Edvardsen and Ramstad (2014). They define pitched roofs as roofs with an angle larger than 6°.

Figure 1. Wood frame houses in Okstad Hageby in Trondheim. Photo: Tore Kvande.

1.2 Climate adaptation and moisture resistance

Norway is characterised by an extremely varied climate, the rugged topography and long coastline being one of the main reasons for large local differences over short distances and extreme seasonal variations (O'Brien et al., 2004). The climate puts a great demand on the building envelope of Norwegian buildings. The building envelope and the roof in particular may be exposed to severe winds, snow loads, precipitation, freeze/thaw cycles, and rather large temperature fluctuations. The climate exposure strongly affects the durability of the roof materials and the long-life performance of the roof structures.

The Norwegian report "Climate in Norway 2100" is an updated scientific base for climate adaptation in Norway (Bauer et al., 2015). By assuming a further increase in the greenhouse gas emissions, the climate scenarios show an increase in the yearly precipitation by 10-20 % depending on the climatic model used. Heavy showers will occur more frequently and rainfall flood become more powerful and occur more often.

Increased precipitation is also affecting the strain from wind-driven rain. Wind-driven rain is one of the most important moisture sources affecting the hygrothermal performance and the durability of building facades and roofs (Blocken and Carmeliet, 2012; 2004). Measures to adapt the built environment to the anticipated climate changes were studied by Lisø (2006). Lisø stresses the immediate need for information and research with respect to sensitivities in the built environment and technical solutions. This to prevent or minimize negative climatic impacts on buildings. The proposed increase of precipitation will put additional stress on roof structures.

A recent study of risk of wood decay shows that given a warmer and wetter climate, the rate of wood decay is increasing in most areas of Norway. Given the business-as-usual scenario (RCP 8.5) the rate of wood decay will only remain low in small parts of the mountain regions in the southern parts of Norway and some areas in the northern parts of Norway. Given the business-as-usual scenario, most of the areas end up in the "high risk"-range (Tilley Tajet and Hygen, 2017). The method used to assess the wood decay risk is given by Rydock et al. (2005).

1.3 Ventilated pitched wood frame roofs

The roof structures reviewed in this work are pitched roofs with exterior vertical drainpipes and wood-based load-bearing systems, as given in Figure 2. From the exterior, cold side of the structure, the roof consists of the following:

- Roofing
- Air-ventilated cavity
- Thermal-insulated load-bearing structure
- Vapour retarder
- Interior ceiling

In the Nordic countries, it is typical to use air-permeable mineral wool (rockwool or glass wool) as thermal insulation in pitched wooden roofs. The purpose of the air-ventilated cavity of such roofs is to:

1) Remove heat transferred through the insulated roof structure possible causing snow melt and subsequent icing at the eaves and gutters.
2) To ensure that excessive moisture is removed from the roof structure.

The structure is considered robust if constructed according to the requirements of Roels and Langmans (2016), Edvardsen and Ramstad (2014) and Uvsløkk (1996). The problems with snow melt are related to the relatively low thermal conductivity of fresh snow causing a temperature gradient through the snow (Calonne et al., 2011). Hence, the snow can melt on the roofing even if the exterior temperature is significantly below 0°C. Liquid water can rise several centimetres in snow (Coléou et al., 1999). Hence, the snow will hold some melting water. Water can also be transported downwards along the roofing and freeze on the cold unheated parts of the roof, for example, the eaves and gutters. When ice builds up, this can dam up the water and make it penetrate the roofing. Gutters and drains can also be broken by ice formation.

The design of the air cavity affects the air flow through the air cavity of the roof. The air flow is also affected by the heat transmittance through the roof structure and the local wind and temperature conditions.

Larger insulation thicknesses of the thermal-insulated load-bearing structure increases humidity levels in the exterior parts of the structure and thereby increases the risk of mould growth. There are three main reasons why the risk increases:

1) The outer part of the structure becomes colder, hence the relative humidity in the air increases.
2) Increased time for dry-out due to increased amounts of wood.
3) Increased risk of internal or natural convection.

A field investigation by Geving and Uvsløkk (2000) showed wood moisture redistribution caused by natural convection. The effect has also been studied by Økland (1998). Natural convection will cause the air to circulate in the cavity, rising on the warm side and dropping on the cold side. The amount of natural convection depends on the following driving forces and air flow resistance of the insulated cavities:

1) Temperature difference across the wall.
2) Equivalent air permeability of the insulated cavity.
3) Insulation thickness.

Given a wall insulation thickness exceeding 200 mm, a practical measure to reduce the natural convection is to divide the insulation into two parallel “cavities” using an airtight and vapour-open barrier in the middle of two insulation layers (Uvsløkk et al., 2010).

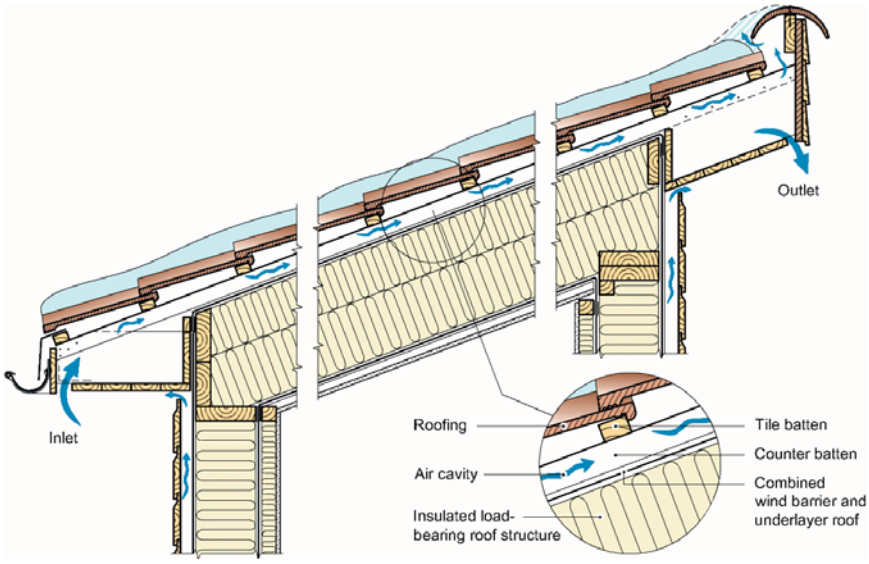

Figure 2. A ventilated lean-to roof structure with snow on the roof. The snow may reduce the air flow through the opening in the upper air cavity opening. The structure has the following build up from the cold face of the structure: roofing, ventilated air cavity, combined wind barrier and underlayer roof and an insulated load-bearing roof structure closed by the vapour retarder and the ceiling at the interior face.

The SINTEF Building Design Guides (Byggforskserien) is a collection of standard building designs in Norway. Use of these guidelines ensures that a building is planned according to the Norwegian building regulations (Edvardsen and Ramstad, 2014). For pitched wooden roofs, Byggforskserien state a maximum roof length from eaves to ridge of 15 m (Bøhlerengen, 2007). However, the air cavity design is only given in detail for roof lengths up to 7 m. The minimum roof pitch is set to 10-15°.

Guidelines for design of wooden roofs in Byggforskserien are largely based on long-term experiences with small houses. Roofs with larger roof spans and lower angles must be planned in detail for every building project, which is not very efficient. The lack of guidelines is one reason for preferring compact roofs.

1.4 Complex and future design

It is the author's belief that nowadays, architects want solutions that use sloping ceilings with minimal eaves even on large buildings and roofs with complex geometry. In several projects, architects are experimenting with the design of pitched ventilated roofs (Figure 3). Several of the Norwegian homebuilders offer houses with low-sloping shed roofs. Some of these houses challenge the existing guidelines for pitched roofs. Thus, it is interesting to explore the possibility to include guidelines for low-sloped roofs in Byggforskserien. The building requirements set from the municipalities are often strict regarding for example building heights. Low-slope shed roofs require a modern building design and a reduction in the height of the buildings.

Figure 3. Complex modern roof geometries. Illustration: Norgeshus

A strong focus on CO_2 emissions from buildings means that in terms of architecture and materials selection, wood-based materials and structures are increasingly relevant for load-bearing structures and insulation materials for large buildings. Roof structures will increasingly have solar cells integrated into the roofing and thus also be used as part of the building's energy solution. In several major research projects in recent years, SINTEF and NTNU have studied some of the issues that need to be solved in order to ensure robust climate-adapted wooden roofs. The national research centre on Zero Emission Buildings (ZEB) (ZEB, 2017), the research centre Klima 2000 (Lisø and Kvande, 2007) and the Klima 2050 Centre for Research-based Innovation (Time, 2014) have been working with climate adaptation of wooden roofs.

Future use of integrated PV systems as the roofing element (BIPV) is introducing new challenges concerning building physics (Gullbrekken et al., 2015b). Hazards of snow falling from roofs, caused by the slippery surface of the PV, the water-tightness of the system and reduced efficiency due to increased temperatures of the PV-panel during sunny summer periods are examples of practical challenges when using BIPV-systems as roofing (Jelle, 2013).

The Powerhouse Brattørkaia in Trondheim represents a large roof structure with a length of 60 m (see Figure 4), which could have been constructed with a wooden load-bearing system if proper air cavity design guidelines existed. The PV roofing of the building is supposed to produce enough energy to make it a plus house[1].
Figure 5 represent another example of a large BIPV-roof which is going to be thoroughly monitored.

[1] A plus house produces more energy from renewable energy sources, over the course of a year, than it imports from external sources.

Figure 4. Powerhouse Brattørkaia is under construction and will have a large BIPV roof facing south. Illustration: Powerhouse/Snøhetta.

Figure 5. ZEB Flexible Lab will be built at NTNU-campus in Trondheim with a large BIPV roof. The building is suitable for monitoring of temperature, humidity and air velocity inside the air cavity beneath the PV roofing. Illustration: LINK Arkitektur/Veidekke.

1.5 Definitions

In this thesis the following definitions are used:

- Air cavity – The cavity between the roofing and the underlayer roof which is ventilated by wind driven forces and thermal buoyancy (Figure 2).
- Air permeable mineral wool insulation – Rockwool or glaswool insulation with low enough density to allow natural convection (Einstabland, 2007).
- Climate adaptation – Normally climate adaptation is defined as measures to increase the robustness towards climate exposure (Time, 2014). In this thesis climate adaptation is defined as: Measures to increase moisture safety of wooden roof structures.
- Compact roofs – Unventilated roofs which are built up with insulation between the vapour barrier and the roofing material. The roof contains no air cavities and has limited dry out capacity. The insulation must be inorganic.
- Convection barrier – Vapour-open wind barrier (s_d-value < 0.5m) used to stop natural convection in a structure (Geving, 2008).
- Flat roof – Roof with a roof angle less than 6°.
- Gable roof – Two roof sections sloping in opposite directions meeting in the ridge of the roof
- Low-pitched roof – Pitched roofs with roof angles less than the air cavity guidelines covered by Byggforskserien 6-10° (Bøhlerengen, 2012).
- Pitched roofs – Roofs with a roof angle larger than 6° (Bøhlerengen and Thommesen, 2017).
- Roof span – The distance between inlet and outlet of the air cavity (Figure 2).
- Shed roof – A roof that slopes in one direction.
- Type A roof – Pitched wooden roofs with separate wind barrier and underlayer roofing including a ventilated air cavity between the wind barrier and underlayer roof as given by Figure 6.
- Type B roof – Pitched wooden roofs with combined underlayer roof and wind barrier (watertight vapour-open membrane) as given by Figure 7.
- Ventilation – Air change rate of the air cavity between the roofing and the underlayer roof.
- Wooden roofs – Roof structures where the load bearing system of the roof structure consist of wood. In this thesis the wood frame is insulated with air permeable mineral wool insulation.

2 THESIS OUTLINE

2.1 Research objective and scope

The objective of this thesis is to increase the knowledge about moisture safety and air flow through the air cavity of pitched wooden roofs. One of the main goals has been to form a basis for development of design guidelines for large low-pitched wooden roofs (> 15 m x 15 m) applicable in the Nordic climate. Today, such roofs must be planned for each individual building project, which is not very efficient.

Experimental research, field measurements and numerical simulations have been collected and applied to assess and characterise the driving forces and resistances for air flow through the air cavity beneath the roofing. This information has been used as input in a stationary model in order to develop a basis for air cavity design guidelines adapted to future wooden roofs.

The thesis does not include compact or flat roofs, nor climate change studies. Roof structures with cold attics or with heated rooms in part of the attic are not treated in detail. A state-of-the art overview is established concerning the building-physical challenges of roof-integrated PV in the Nordic climate; however, no further study of BIPV is covered in this thesis.

2.2 Research questions

Guidelines for design of wooden roofs are largely based on long-term experience on small houses. A potential future option for wooden roofs is long, low-pitched roofs, likely with BIPV as the roofing. The hypothesis of this thesis is that enhanced moisture safety and new air cavity guidelines are needed to facilitate such use. New guidelines are supposed to contribute to risk reduction in the Nordic climate. To address this general challenge, this thesis addresses the following research questions:

1) What are the building physical challenges related to pitched wooden roofs and introduction of BIPV in the Nordic climate?
2) How is the thermal transmittance and the related moisture risk affected by natural convection in highly insulated timber frame structures?
3) How can the complex driving forces and resistances of ventilated pitched roofs be simplified for the design of an air cavity of long, low-pitched roofs?

2.3 Structure of the work

The thesis is divided into three main parts:

Part 1: Motivation, current state and future challenges (Papers 1 and 2)

This part of the thesis is published in ***Papers 1*** and ***2*** and include background and future challenges as well as current challenges related to the air cavity ventilation of pitched wooden roofs. A thorough study of the process-induced building defects is conducted by further studying the SINTEF Building Defects Archive. The study looks in detail at the cases concerning roof defects discussed in Lisø et al. (2005; 2006). In order to obtain an overview of typical roof defects and common sources. A state-of-the-art overview of recent experiences and building physical challenges concerning use of BIPV in Nordic countries was the scope of ***Paper 2***. The paper is mainly based on a literature review focusing on challenges of cold, pitched roofs.

The results of Part 1 formed a basis for the design of the experimental laboratory study and the numerical work.

List of Papers

1) Gullbrekken L, Kvande T, Time B (2016). Norwegian Pitched Roof Defects, *Buildings*, *6*(2), p. 24.
2) Gullbrekken L, Kvande T, Time B (2015). Roof-integrated PV in Nordic climate - Building physical challenges. The 6th International Building Physics Conference - IBPC 2015. *Energy Procedia*, Vol. 78, pp. 1962-1967.

Part 2: Increased insulation, moisture-resilient structures (Paper 3)

The second part of the thesis is published in ***Paper 3***. This paper includes a laboratory study of natural convection inside a highly insulated structure. The effect of the temperature difference across the 500 mm insulated timber frame structure as well as the inclination of the structure was studied.

List of Paper

3) Gullbrekken L, Uvsløkk S, Kvande T, Time B (2017). Hot-Box measurements of highly insulated wall, roof and floor structures, *Journal of Building Physics*, Vol. 41(1), pp. 58–77.

Part 3: Ventilating guidelines, knowledge base (Papers 4 to 7)

The third part of the thesis is published in ***Papers 4*** to ***7***. In order to enhance knowledge about the ventilation behaviour of pitched roofs a field study was conducted with eaves-to-eaves ventilation of such roofs. Three periods within a year is included in ***Paper 4***. ***Paper 5*** includes analysis of a field study conducted by Uvsløkk (1996) in order to find the driving forces of wind driven ventilation of pitched roofs. The laboratory study of ***Paper 6*** is focusing on pressure losses caused by air passing the air cavity inlet and tile battens inside the air cavity of a pitched wooden roof. Finally, ***Paper 7*** includes new guidelines for pitched wooden roofs based on the results from ***Paper 5*** and ***6***.

List of Papers

4) Gullbrekken L, Kvande T, Time B (2017). Ventilated wooden roofs: Influence of local weather conditions – measurements, 11th Nordic Symposium on Building Physics, Trondheim, Norway, 11-14. June 2017. *Energy Procedia*, Vol. 132, p. 777-782.
5) Gullbrekken L, Uvsløkk S, Kvande T, Pettersson K, Time B. Wind pressure coefficients for roof venting purposes. *Journal of Wind Engineering and Industrial Aerodynamics.* Vol.175, pp. 144-152.
6) Gullbrekken L, Uvsløkk S, Geving S, Kvande T (2018). Local loss coefficients inside air cavity of pitched wooden roofs, *Journal of Building Physics*. Published online 1. December 2017.
7) Gullbrekken L, Uvsløkk S, Hygen HO, Kvande T, Time B. Air cavity design guidelines for pitched wooden roofs in cold climate. Submitted.

3 THEORETICAL FRAMEWORK

3.1 Roof design

The various design principles for wooden roofs are thoroughly discussed in Edvardsen and Ramstad (2014). There are two main types of structures treated, in this work named Type A (Bøhlerengen, 2007) and Type B (Bøhlerengen, 2012) and shown in Figures 6 and 7.

Type A. Pitched wooden roofs with separate wind barrier and underlayer roofing including a ventilated air cavity between the wind barrier and underlayer roof. Type A separates the rain and wind barrier with roofing directly on wooden counter battens or with the roofing and underlayer above a separate wind barrier. The roof is ventilated both between the wind barrier and rain barrier and between the rain barrier and the roofing. The guidelines of Bøhlerengen (2007) include detailed air cavity design specifications for roof length up to 7 m and roof angle larger than 10°-15°.

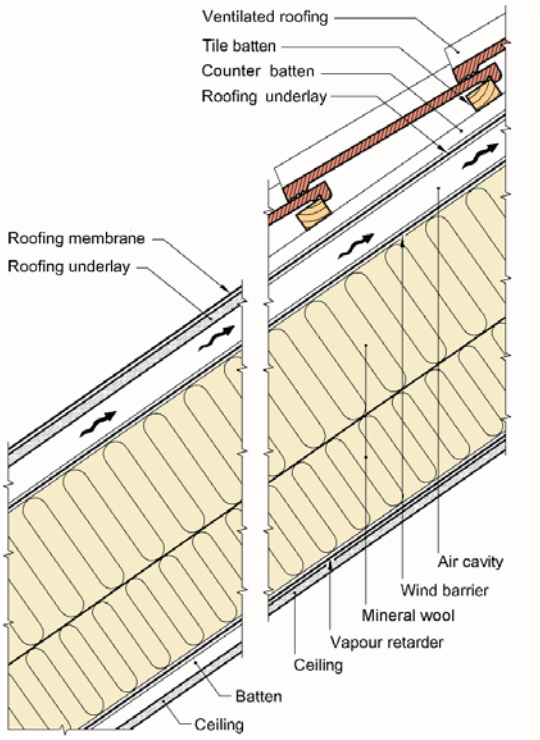

Figure 6. Pitched wooden roof Type A with separate wind barrier and underlayer roofing.

Type B. Pitched wooden roofs with combined underlayer roof and wind barrier (watertight vapour-open membrane). The main difference between Type A and Type B is that the drainage and ventilation of Type B are done directly under the roofing. The guidelines of Bøhlerengen (2012) include detailed air cavity design specifications for roof length up to 15 m and roof angle larger than 18°-22°.

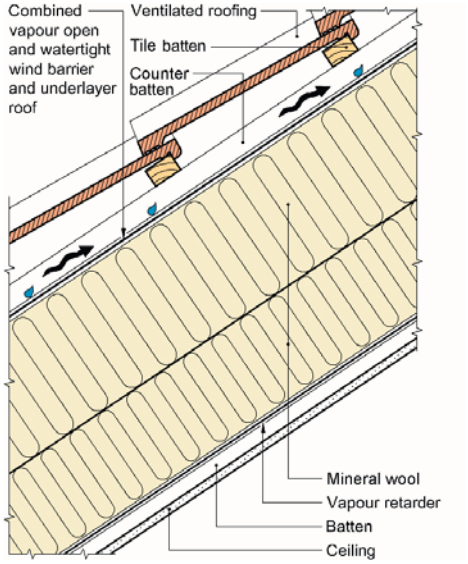

Figure 7. Pitched wooden roof Type B with combined underlayer roof and wind barrier.

3.2 Moisture and moisture redistribution

The typical wooden roof structure shown in Figure 7 is made up of the following from the cold- to warm- facing part of the structure:

- Roofing
- Ventilated air cavity
- Underlayer roof
- Wood frame structure with thermal insulation
- Vapour retarder
- Ceiling

The function of the vapour retarder is to stop diffusion of water vapour and air leakages from indoor air into the roof structure. The function of the underlayer roofing is to lead water leaking through the roofing away from the roof structure and to allow excessive moisture from built-in-moisture or other moisture sources to dry out. The driving force for this dry out mechanism is the partial water pressure difference. The moisture flow by diffusion is given by Fick's law:

$$g = -D_p \cdot \nabla p_v \qquad (1)$$

Where g is the amount of diffused moisture per time and area (kg/m²s), D_p is the water vapour diffusion coefficient based on vapour pressure (kg/(msPa)), ∇p_v is the vapour pressure gradient (Pa/m),

A newly built structure contains excessive moisture, even if it is produced in a factory and has not been exposed to moisture. Given a typical roof structure with a built-in moisture content of 20 %, Skogstad et al. (2011) estimate an excessive moisture amount of 1 kg per m² roof surface. Typically, the excessive moisture dries out during the first years of the structure's lifetime (Gullbrekken et al., 2015c). At low outdoor temperatures, typical during winter, the moisture will diffuse towards the wind barrier because of the temperature gradient and a corresponding decrease in the partial vapour pressure across the structure. The redistribution effect can be enhanced by natural convection, which is caused by temperature differences across cavities with air- permeable materials such as rockwool and glass wool (Geving and Uvsløkk, 2000; Økland, 1998). The latter occurs when water vapour is transported by air circulation inside the insulated cavities in the wall. Effects of natural and forced convection on the hygrothermal performance of highly insulated wall structures have been studied in laboratory measurements by Langmans et al. (2012), Kalamees and Kurnitski (2010) and Økland (1998). The results shows increased moisture levels at the upper cold part of the walls due to natural convection. It was also stated that an airtight vapour barrier on the warm side is required to obtain a moisture-safe structure.

3.3 Air gap physics, driving forces and pressure losses

The air flow through the air cavity system can be expressed by equation (2), where the air flow is proportional to the sum of the pressure difference along the air cavity system, Δp, and inversely proportional to the sum of flow resistances through the air cavity system, R. The solution of $\dot{V}$ is found by iteration because Δp and R are variables of $\dot{V}$.

$$\dot{V} = \frac{\sum \Delta p}{\sum R} \tag{2}$$

Driving forces are given by equations (3) to (5).

$$\sum \Delta p = \Delta p_e + \Delta p_v \tag{3}$$

$$\Delta p_e = \left(\rho_2 - \rho_1\right) g \cdot h \tag{4}$$

$$\Delta p_v = \frac{1}{2} \rho_1 \cdot u^2 \cdot \Delta c_p \tag{5}$$

Where Δp_e is the pressure difference because of buoyancy differences and Δp_v is the pressure difference because of driving forces of wind. ρ is the air density (kg/m³), g is

the gravity force (m/s²), h is the height difference between inlet and outlet (m) and u is the wind speed at 10 m in the upstream undisturbed flow (m/s). Δc_p is the wind pressure coefficient difference (-) which is defined in equations (8) and (9) (see Figure 8).

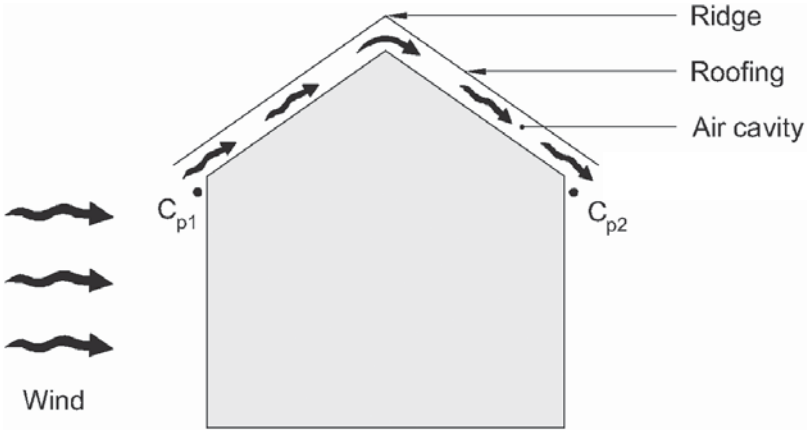

Figure 8. Cross section of a house showing the location of two pressure points for calculation of Δc_{px}.

$$c_{px} = \frac{P_x - P_0}{P_d} \quad (6)$$

$$P_d = \frac{\rho \cdot u^2}{2} \quad (7)$$

c_{px} is the wind pressure coefficient of a point (-), P_x is the static pressure at a point x on the building facade (Pa), P_0 is the static reference pressure (Pa)(at 10 m height), P_d is the dynamic pressure (Pa), ρ is the air density (kg/m³) and u is the wind speed at 10 m height(m/s).

Δc_p is defined by equations (8) and (9), where c_{px1} and c_{px2} are wind pressure coefficients at the positions shown in Figure 8.

$$\Delta c_{px} = c_{px1} - c_{px2} \quad (8)$$

$$\Delta c_p(\theta) = c_p(\theta) - c_p(180 - \theta) \quad (9)$$

Where θ is the wind approach angle.

The pressure losses through the air cavity system are given by:

$$\sum \Delta P = \sum \Delta P_f + \sum \Delta P_\xi \quad (10)$$

$$\Delta P_f = \frac{\lambda \cdot p_d}{D_h} \cdot L \quad (11)$$

$$\Delta P_\xi = \frac{\xi \cdot \rho \cdot u_m^2}{2} \cdot n \quad (12)$$

Where λ is the friction number (-), p_d is the dynamic pressure (Pa), L is the length of the channel (m).

$$D_h = \frac{2 \cdot a \cdot b}{a + b} \quad (13)$$

Where a and b are the side lengths of the rectangular air channel (m).
For laminar flow, the friction number λ (-) is inversely proportional with the Reynolds number, Re.

$$\lambda = \frac{64}{\mathrm{Re}} \quad (14)$$

Pressure losses in components like valves and bends are called local losses and are given by ΔP_ξ (Pa) and n, which is the number of obstacles. Where, ξ is the local loss coefficient (-), ρ is the density of the air (kg/m³), and u_m is the average velocity (m/s). u_m is given by airflow Q (m³/s) divided by the area of the smallest cross-section of the flow path A (m²).

4 METHODS

All the papers in this thesis involve a scoping literature review. In addition, the different papers involve reviews of the current state-of-the-art, the SINTEF Building Defects Archive, full-scale laboratory measurements, field measurements and numerical analysis. This section gives an overview and a short presentation of the different methods used in the thesis. The methods are more thoroughly presented in the different papers.

4.1 Scoping literature review

The articles started with a scoping literature review according to Arksey and O'Malley (2005). The focus of the literature review was to identify the main trends within the literature and to establish knowledge gaps. Any literature of interest was more closely read. Google Scholar and Oria were mainly used as search engines to find the relevant references.

4.2 SINTEF Building Defects Archive

For more than 60 years, SINTEF Building and Infrastructure (formerly the Norwegian Building Research Institute) has been mapping building damage. The work has been performed both through extensive field investigations and on behalf of the building sector. Detailed information about building defects has been collected and stored in an electronic archive. A thorough investigation into the process-induced building defects collected in this archive was performed by Kvande and Lisø (2009), Lisø et al. (2006) and Lisø et al. (2005). The study includes documents from the archive for the 10-year period from 1993 to 2002, which contains 2003 reports describing 2423 incidents or cases of defects. In the archive, the reports dealing with building defects are tagged "building defect". One of the advantages of the archive is the large number of cases collected over a long period of time. In addition, the archive contains thorough and detailed descriptions of the defects and possible causes of the defects, and the documents are prepared by experts within the field. Hence, the Building Defects Archive is particularly useful for the researcher to find typical building defects of different building constructions and the causes of these defects. The SINTEF Building Defect Archive is acknowledged as one of Norway's most important sources of knowledge about building defects and defect sources (Gullbrekken et al., 2016). However, an in-depth study of roof defects has not previously been conducted. Hence, ***Paper 1*** looks in more detail at the cases concerning roof defects covered by Lisø et al., (2006, 2005).

4.3 Laboratory measurements

Hot-Box

Laboratory measurements were performed using a rotatable guarded Hot-Box, see Figure 9 and ***Paper 3***. U-values are calculated on the basis of measured heat flow, metering area and temperature difference across the test specimen. The U-value is calculated according to NS-EN-ISO 8990 (1996) and is based on the mean value of between 12 and 24 one-hour measurement periods. The metering area of the Hot-Box is 2450 mm x 2450 mm. Surface thermal resistance coefficients were adjusted close to the standardised ones given in NS-EN-ISO 8990 (1996) prior to the tests by adjusting the air flow velocities adjacent to the surface on both the hot and the cold sides.

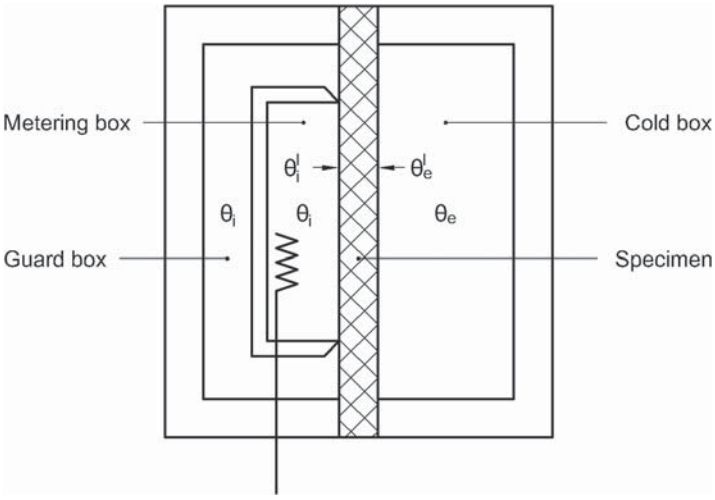

Figure 9. Principle sketch of the guarded Hot-Box-apparatus. θ_i is the temperature in the guard- and metering box. θ_e is the temperature in the cold box.

Air cavity model

A large-scale test model of the air gap of a pitched roof was built in the SINTEF and NTNU laboratory in Trondheim, and forms the basis of ***Paper 6***. The laboratory model of a pitched roof is shown in Figure 10. The purpose of constructing the model was to imitate the conditions below for example a roofing tile as shown in Figure 11 a). As Figure 11 b) shows the model consisted of an aluminium profile with a length of 3550 mm and an internal width of 552 mm. The width of the box corresponds to the air gap between two counter battens with a width of 48 mm and a centre-to-centre distance of 600 mm, which is a typical situation in a ventilated wooden roof.

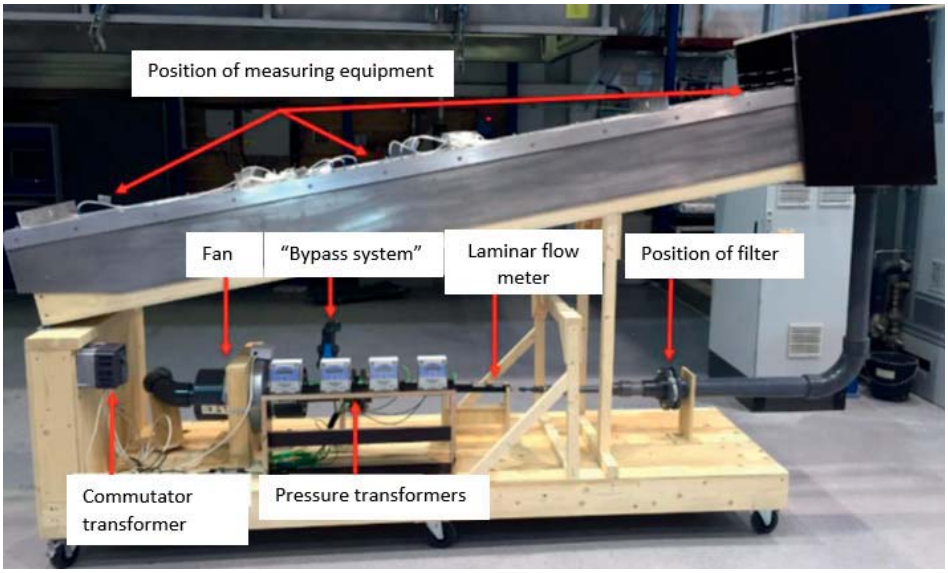

Figure 10. Large scale laboratory model of a pitched roof.

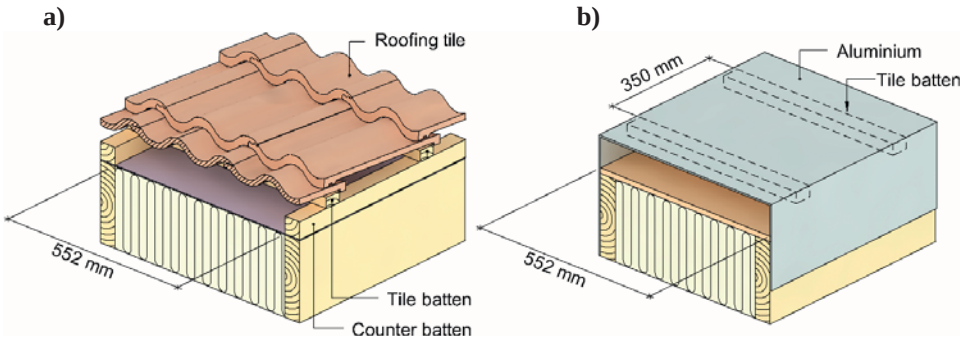

Figure 11. **a)** Cross-section of a typical Type B roof structure with roofing tiles. **b)** A cross-section of the test model consisting of an aluminium box corresponding to the air gap between two counter battens with a width of 48 mm and a centre-to-centre distance of 600 mm. The centre to centre distance of the tile battens is 350 mm.

In order to measure pressure drops, a fan sucked air through the air gap system. The airflow through the air gap was measured by a laminar flow meter. In order to measure the pressure differences, four pressure transmitters were used. The pressure difference was recorded with a data logger (Delphin Technology Expert Key 100C) with a measurement frequency of 1 Hz.

4.4 Field measurements

ZEB Test Cell Laboratory

The roof structure of a full-scale laboratory building (see Figure 12) located at NTNU campus in Trondheim, is the research object of ***Paper 4***. A cross section of the roof is shown in Figure 13.

Figure 12. The roof structure of ZEB Test Cell Laboratory located at the NTNU campus in Trondheim. The weather station is positioned 10 m above ground level, 1.5 m above the ridge of the roof.

The air cavities below the roofing have thermocouples positioned at the lower-facing surface of the roofing, in the middle of the air cavity and on the surface of the underlayer roofing as shown in Figure 13. Nine air cavities in parallel had nine thermocouples in each cavity, resulting in a total of 81 thermocouples. Two of the air cavities also had air pressure devices and omnidirectional remote air velocity probes.

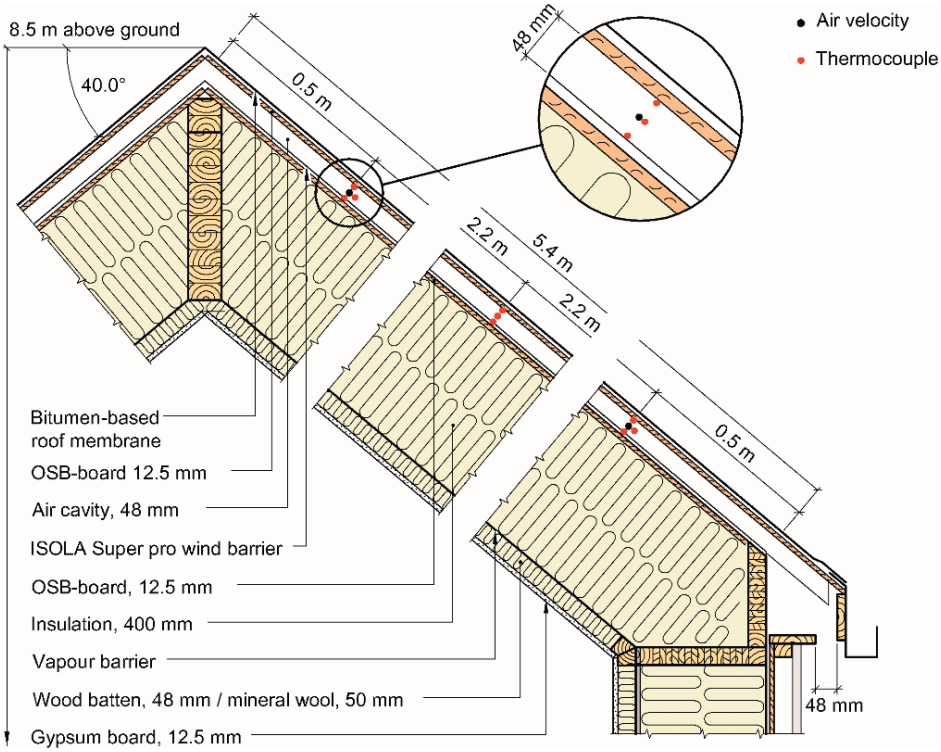

Figure 13. Roof structure of the ZEB Test Cell Laboratory had air velocity and temperature measurement equipment installed.

Tyholt test house

Measurements of wind pressure coefficients at the facade were conducted at a former test house located on a flat area in Tyholt in Trondheim, Norway by Uvsløkk (1996). The building was 8 m long, 5 m wide and 6 m high to the top of the roof, as Figure 14 shows. The ground at the test site was open with no trees or buildings within about 150 m in a sector from south-southeast to southwest, which was the dominating wind direction during the measurement periods. In order to measure wind approach angle, dynamic and static wind pressure measurement equipment was located 10 m above ground level i.e. 4 m above the ridge in the centre of the test house. Wind speed and global wind angle measurements were also taken 6 m above ground level in a mast positioned 40 m away in a west-northwest direction from the test house. By using an electrical motor, the test house could be rotated to measure different wind approach angles.

The measurements were performed in 1985 and reported in Uvsløkk (1996). However, the scope of Uvsløkk (1996) was limited to examining the wind pressure coefficients behind the cladding. In ***Paper 5***, the wind pressure coefficients measured at the facade of the test house have been analysed.

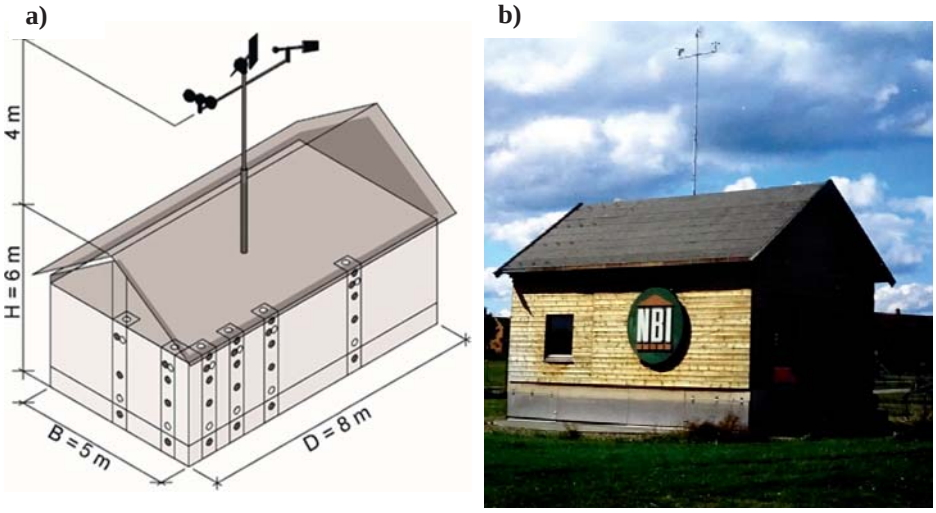

Figure 14. a) Dimensions of the test house and the wind pressure measurement positions shown as black circles. The wind approach angle, and dynamic and static wind pressure were measured 10 m above ground level, 4 m above the ridge of the test building. **b)** The rotatable test house located in Tyholt. Photo: Sivert Uvsløkk.

4.5 Numerical analysis

Laboratory measurements are expensive and take a lot of time. Compared to laboratory measurements, numerical calculations take less time and give the researchers the possibility to investigate a larger variety of designs. However, in order to trust calculations, it is necessary to validate laboratory measurements and/or field experiments.

COMSOL multiphysics

COMSOL multiphysics is a multiphysics simulation software that uses conventional physics-based user interfaces and coupled systems of partial differential equations. In the current work, the COMSOL multiphysics program has been used to model the air velocity distribution inside the air cavity. The simulation model has been used to calculate the loss in absolute pressure for different dynamic pressures inside the air channel and thereby calculate the local singular loss coefficients.

Analytical calculation model

An analytical calculation model has been developed at SINTEF Building and Infrastructure by Uvsløkk (2011). The model assumes an airflow through the air gap system given by the driving forces of wind and thermal buoyancy. It assumes a certain air cavity design with hydraulically smooth surfaces, a specific height of the counter batten and a specific number and height of tile battens. Furthermore, the model assumes snow on the roofing, which simplifies the physics of the roofing surface because radiation is neglected.

The model is very suitable for comparing different roof structures and in practical calculations of snow melt potential. In a practical design process, it is possible to investigate different designs of the air cavity and how they affect the snow melt potential.

The input in the calculation model of ***Paper 7*** is improved by the results of ***Paper 5*** and ***6***. The improvements include the driving forces by wind as well as improved local loss factors for sharp- and round- edged battens.

5 MAIN FINDINGS

5.1 Motivation, current state and future challenges (Paper 1 and 2)

Paper 1 includes a comprehensive study of the SINTEF Building Defects Archive. Process-induced building defect cases relating to the building envelope accounts for 66% of the investigated defect cases. Furthermore, 22% of the building defects are localised in roof structures. Of the 465 cases registered in the roof category, 40% are in the pitched wooden roof category for Types A, B, C, and D, (see Figure 15).

Moisture is found to be the main cause of defects, accounting for 76% of the 2423 cases. In pitched wooden roofs, 67% of the defects are caused by precipitation or indoor moisture. For thermally insulated pitched wooden roofs, the typical defects are summarised in Figure 16.

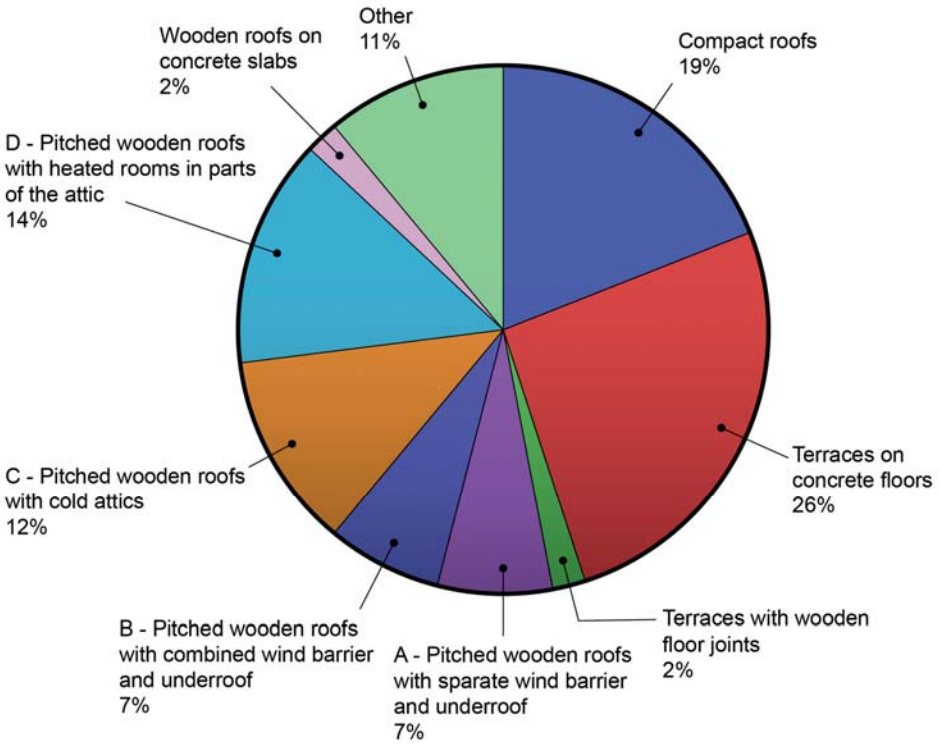

Figure 15. Defect cases for the 10-year period from 1993 to 2002 concerning roofs, distributed by type of roof (465 cases, 22% of the total amount of building defects) (Lisø et al., 2005). The defects sources are part of the study in ***Paper 1***.

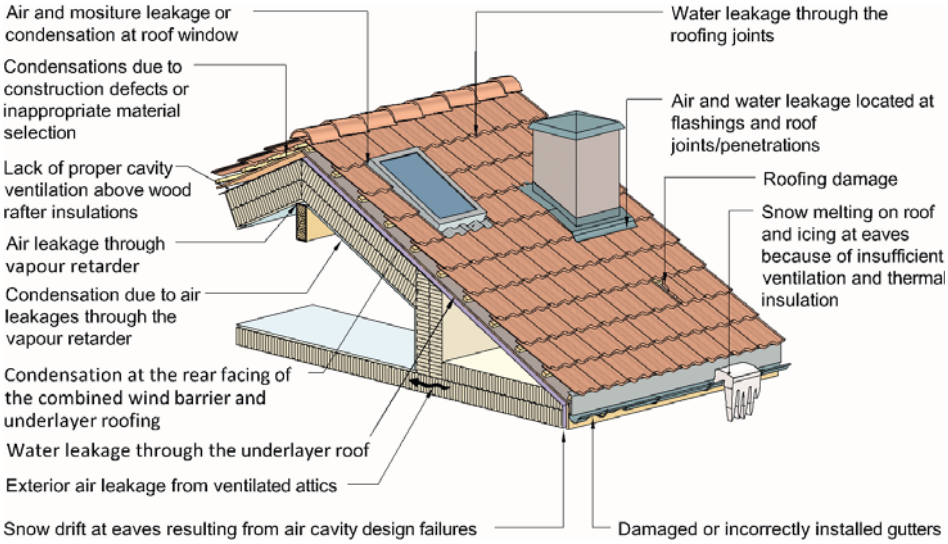

Figure 16. Typical defects in thermally insulated pitched wooden roofs according to findings from SINTEF Building Defect Archive.

Condensation in cold parts of the roof structure is often caused by air leakages through the vapour barrier, often in combination with poorly or insufficient indoor ventilation causing high moisture levels in the indoor air. As a result, an airtight vapour retarder and use of balanced ventilation systems are effective means to prevent moisture damage from internal air.

Paper 2 presents a thorough literature review of state-of-the-art experiences and challenges for building physical conditions related to the use of roof-integrated BIPV in the Nordic climate. The main findings include lack of practical guidelines for installation and ventilation of BIPV- systems and the need for preparation of BIPV- standards.

According to Ceron et al. (2013), almost 50% of the BIPV market is in roof applications. The primary function of the roof as a climate screen must still be fulfilled, even with BIPV- systems installed. The rain and air tightness of the roof must be intact. Joints between the BIPV panels and between the BIPV and roofing material must be rain-tight. BIPV-systems can cover the whole roof or they can cover parts of the roof. Systems covering part of the roof also demand rain-tight fittings. A sufficient level of ventilation of air beneath the roofing is necessary to prevent the growth of mould and moisture damage. In order to keep a high-performing BIPV- system, it might be necessary to increase the ventilation in order to lower the lower facing temperature of the BIPV.

There is a lack of practical guidelines for installation and ventilation of BIPV- systems. Misara and Pornimit (2011) points out the missing link between PV- and the construction-sector and lack of BIPV- standards based on building product requirements as obstacles for large-scale BIPV- application. BIPV- products that replace building components have to comply with conventional building regulations and PV-standards. Moreover, each

country has its own set of national regulations and standards, making it difficult for the PV manufacturers to address relevant documentation.

By introducing BIPV, the construction sector seems to choose "the previous traditional" way of building a roof structure (using a separate wind barrier and an underlayer roof). Experience both at the Multicomfort and ZEB Living Lab buildings has been that roof Type A has been a preferred solution (see Figure 17). From an environmental (less material) and a cost-effective point of view, it would be favourable to further develop systems and solutions which comply with the "modern more common" way of building roofs, i.e. Type B with a combined underlayer roof and wind barrier.

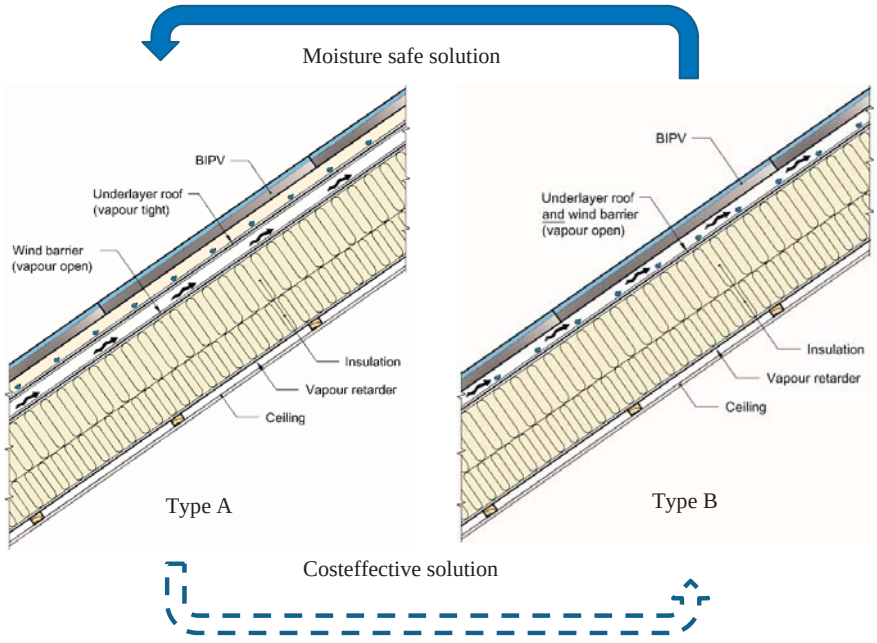

Figure 17. By introducing BIPV the construction sector seems to choose "the previous traditional" way of building a roof structure (Type A). Type B shows the roof construction using a combined underlayer roofing and wind barrier.

Snow covering and downfall of snow as well as sufficient rain-tightness of BIPV- systems were pointed out as areas where more research is necessary. The phenomenon of condensation on the exterior face of the roofing (PV-panel), typically occurring during the night with clear weather conditions, is also further examined in ***Paper 4***.

Part 1 of this thesis deals with the current state and further challenges of pitched wooden roofs and thereby the motivation for further work on climate adaptation of wooden roofs. The SINTEF Building Defects Archive was studied to get an overview of the current state and, typical defects and causes of the pitched roof structures in Norway. The study contributed to increased knowledge about the building defects of pitched wooden roofs.

Leakages from precipitation were found to be one of the main sources of defects. Hence, an air cavity design to increase moisture safety is crucial. A thorough literature review of state-of-the-art current and future challenges and possibilities by introduction of BIPV was conducted. The study revealed a lack of practical design guidelines for BIPV installation and insufficient standards regarding BIPV- products.
These studies formed a basis for the further studies of climate adaptation of pitched wooden roofs.

5.2 Increased insulation, moisture resilient structures (Paper 3)

Buildings that are designed to meet high energy-performance requirements, e.g. passive houses, require well-insulated building envelopes, with increased insulation thicknesses for roof, wall and floor structures. Increased insulation thicknesses may lead to increased risk of mould growth and moisture damage (Gullbrekken et al., 2015a; Økland, 1998). One reason for this is increased risk of natural convection in the insulated cavities causing moisture redistribution of, for example built-in- moisture in the timber frame.

Laboratory measurements of natural convection inside the insulation layer of highly insulated structures is presented in ***Paper 3***. Natural convection is air flow caused by temperature differences. The driving force is buoyancy caused by density differences in the air because of temperature differences. Natural convection causes increased heat transport and possible moisture redistribution inside air-permeable insulation materials of a structure. The laboratory measurements included measurements of heat transmittance of a 500 mm insulated timber frame structure in a Hot-Box apparatus. The novelty of these measurements was related to the study of angle of inclination. Different angles of inclination and temperature differences across the structure were tested. The measurements showed that the thermal transmittance affected both the temperature difference and the angle of inclination. The Nusselt number (Nu) shown in Figure 18 describes the ratio of the U-value with and without natural convection. A Nusselt number of 1.0 means that the thermal transmittance is not affected by the natural convection.

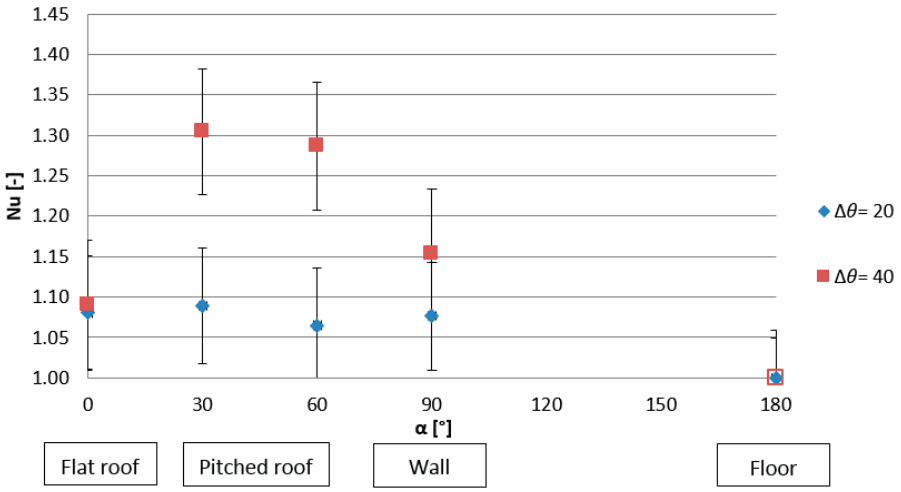

Figure 18. Thermal transmittance is affected both by the temperature difference and the angle of inclination.

The measurements show that the effect of natural convection was less given a flat roof or floor structure. Einstabland (2007) recommends a convection barrier in timber frame walls when insulation thickness exceeds 200 mm. Based on ***Paper 3***, a convection barrier is also recommended for pitched wooden roofs with the same insulation thickness (see Figure 19).

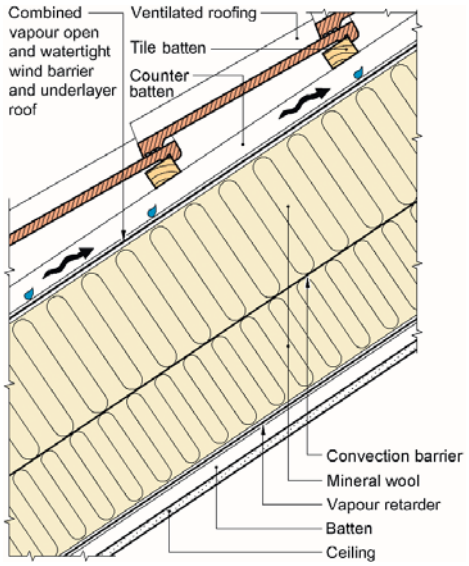

Figure 19. A convection barrier is recommended also for pitched wooden roofs when insulation thickness exceeds 200 mm.

5.3 Ventilating guideline knowledge base (Papers 4 to 7)

Paper 4 includes mapping of the risk of condensation on the interior surface of the ventilated cavity, as given in Zheng (2004), and a mapping of the air cavity velocity's dependence on the exterior wind speed. The mapping was done by means of a field experiment at the ZEB Test Cell Laboratory located on the NTNU campus in Trondheim.

The study included two ten-days periods during spring and summer as well as a one-week period during the autumn. The measurements show long periods with surface temperatures below the ambient temperature, especially during the spring and autumn periods.

During the spring and autumn periods, a strong correlation between the wind speed and air velocity inside the air cavity was found (see Figure 20). During summer, the correlation was less strong. A possible explanation could be lower wind speeds during the summer period as well as more natural convection inside the cavity because of high temperatures during sunny periods.

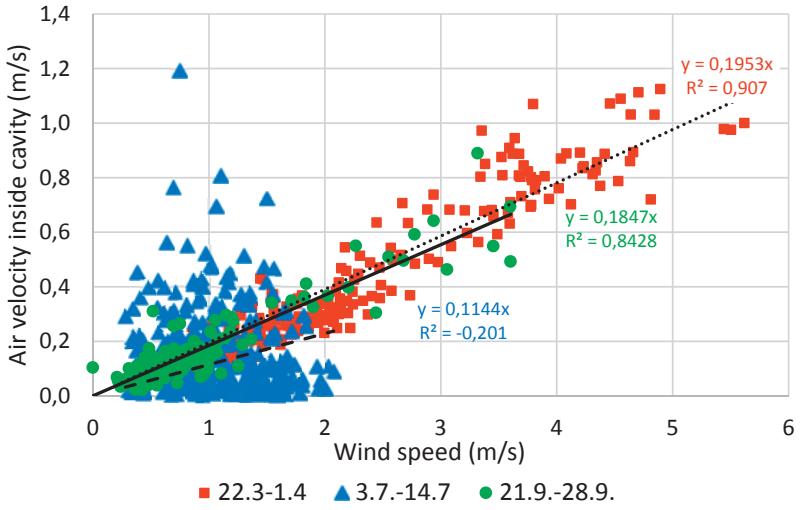

Figure 20. Wind speed and corresponding air cavity velocity during three measuring periods.

The driving forces of wind-driven ventilation of pitched wooden roofs are given by the wind speed, wind approach angle and the wind pressure coefficient. ***Paper 5*** focuses on the wind pressure coefficient and presents results from a full-scale test study performed in 1985 on a test house located in Tyholt in Trondheim, Norway. The test results are partly published by Uvsløkk (1996). However, the scope of Uvsløkk (1996) was limited to investigation of the wind pressure gradients in the air cavity behind the ventilated cladding. The aim of the current study was to investigate wind pressure coefficients at the wall surface close to the roof air cavity inlet and outlet. The wind pressure coefficients at

the air cavity openings of the pitched roof, together with the wind velocity and wind approach angle, define the driving forces of wind-driven ventilation. Knowledge about such parameters is necessary to more accurately calculate wind-driven ventilation of pitched roofs.

The results from the study show that the wind pressure coefficient at the surface of the cladding varied very much depending on the wind approach angle (see Figure 21). For practical engineering assessments and calculation, an average value is valuable. When calculating wind-driven ventilation of pitched wooden roofs, the difference of the wind pressure coefficient at the outlet and inlet of the air cavity is necessary (Δc_p). An average Δc_p of 0.7 was found. The value can be used when performing calculation estimates for the ventilation of air cavities of pitched wooden roofs. The value is applicable given eaves-to-eaves ventilation.

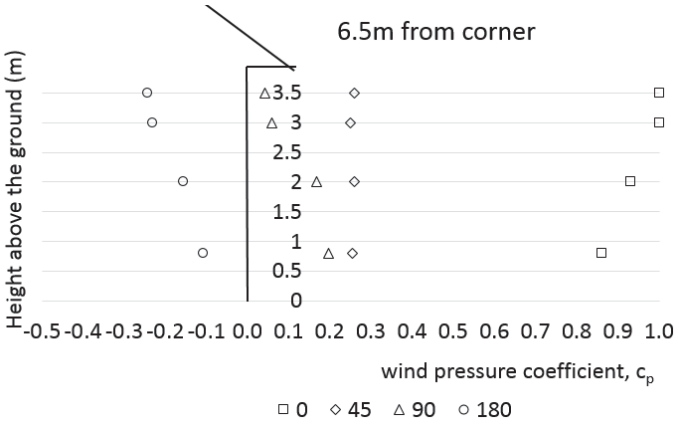

Figure 21. Wind pressure coefficient of different wind approach angles at the surface of the cladding in the middle of the long wall of the test house (see Figure 14).

In addition to the driving forces, examined in ***Paper 5***, the pressure losses inside the air cavity are essential when assessing the ventilation of pitched wooden roofs. Therefore, a full-scale laboratory model of a pitched wooden roof was built (see Figure 10). The roof model was used to measure local losses at the air cavity inlet and passing of battens, as presented in ***Paper 6***.

The local loss factors for different designs of the air cavity inlet were measured and compared to values from the literature and from a model developed in the COMSOL-multiphysics software. In addition, local loss factors for various designs of the counter-battens and tile- battens were calculated. An equation describing the local loss factors depending on the air cavity height, counter batten height and tile batten height was prepared. Measurements on round-edged battens were found to give lower local loss factors compared to sharp-edged battens, see Figure 22. In fact, a 40 % reduction in the local loss factor of round-edged battens compared to sharp edged battens was found. The

results for round-edged battens were found to be comparable to the existing literature by Hansen et al. (2013). Furthermore, by decreasing the height of the batten and increasing the height of the air cavity beneath the batten, a decrease in the local loss factor was found. The COMSOL- multiphysics software calculations showed a good correlation with the measured local loss factor for the 36 mm tile batten. The calculated local loss factor for the 30 mm tile batten was found to overestimate the measurements. For the 48 mm tile batten, the calculations underestimated the measured local loss factor.

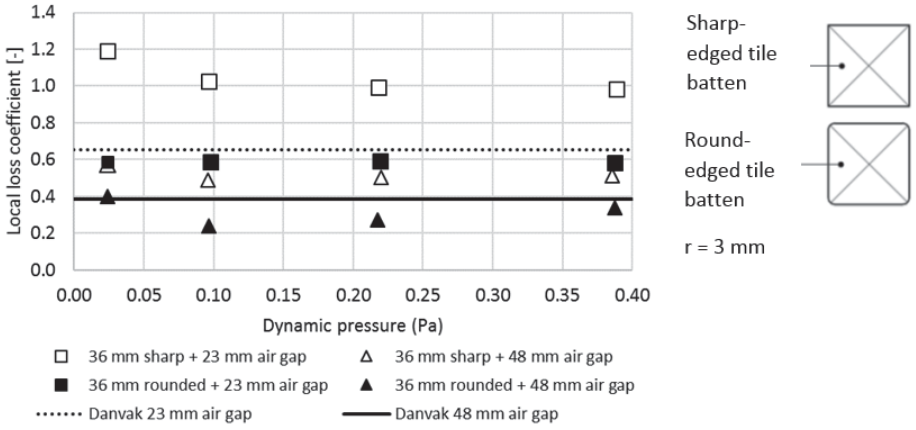

Figure 22. Local loss coefficient for sharp-edged and round-edged battens with different air gaps and dynamic air pressure of the airflow passing the tile batten. "Danvak" means values calculated from Hansen et al. (2013).

The purpose of ***Paper 7*** was to improve the practical guidelines for ventilation of pitched wooden roofs exceeding the guidelines of Bøhlerengen (2012;2007). The current guidelines in Norway were compared to other countries with more or less snow during the winter season. Similar ventilation requirements in the different countries with longer periods of snow on the ground were found. However, only the Norwegian requirements include a maximum length of the air cavity.

Uvsløkk (2011) assumed that a wind speed of 1 m/s is a conservative value and therefore could be used as a default value in calculations. According to Uvsløkk (2011) the wind speed in the heating season is larger than 1 m/s most locations in Norway. In ***Paper 7*** the subject is studied my means of a metrological investigation. The investigation indicated that the assumption of an average outdoor wind speed of 1 m/s was conservative, i.e. most geographical locations in Norway have more than 250 days with an average wind speed above 1 m/s (see Figure 23). However, the wind speed during the period with snow on the roof is of particular interest. Hence, the wind speed during a one month period during winter (January) was investigated. Most of the locations had an average wind speed above 1 m/s for more than 25- of the 31 days period. The results of ***Paper 7*** indicate that 1 m/s can serve as a conservative value.

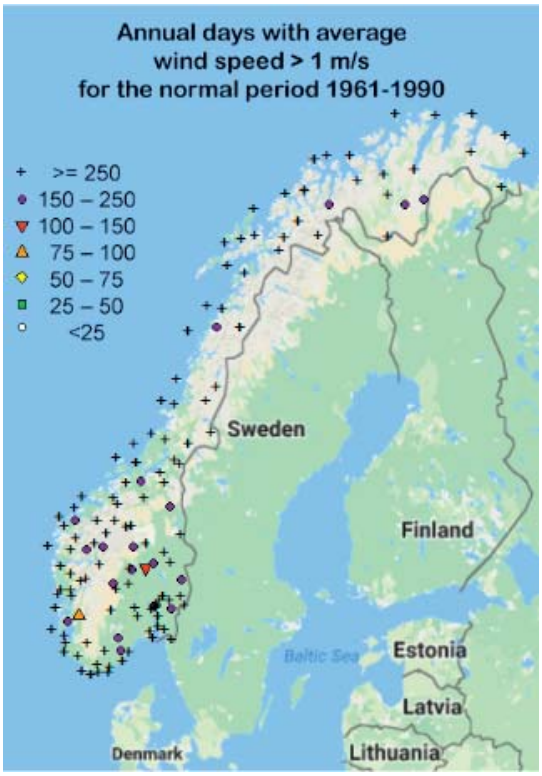

Figure 23. Number of days with daily average wind speeds above 1 m/s during a year for 217 Norwegian Metrological stations. Illustration: The Norwegian Meteorological Institute.

A large increase in the necessary height of the air cavity was found for roof lengths above 30 m. For a 30 m roof length a necessary height of approximately 160 mm was found. Higher air cavities will most likely not be applied in practice. Compact roof structures or ventilated roofs with interior ice-free drainpipes will serve as a more practical solution.

6 CONCLUSIONS

The presented work is a step towards more climate adapted wooden roofs. According to the SINTEF Building Defects Archive, moisture from both precipitation and indoor air is the dominant source of roof damage. This is especially critical when we bear in mind a 10-20 % increase in precipitation in the years to come and a slightly warmer climate. Hence, increased focus on risk reduction and moisture safety for building structures is needed.

Stricter building regulations and an increased focus on zero energy and zero emission-buildings make energy production on the building facades more relevant. Use of BIPV, especially on southern facing roofs can be a reasonable way to utilise roofs for energy production. However, the missing link between the PV and construction industry is a reason for the limited use of these systems. The main building physical challenges concerns rain-tightness of the BIPV- systems as well as snow covering and snow downfall hazards. There is also a need for development of roof structure with combined underlayer roof and wind barrier where the BIPV- panels serve as roofing. Guidelines for installation and construction build of BIPV systems in the Norwegian and Nordic climate are needed.

Natural convection inside highly insulated structures were found to significantly increase the heat transmission of roof structures. Natural convection may cause redistribution of moisture inside the insulation cavity. The effect causes higher moisture levels in the cold part of the structure. In order to reduce this risk, introduction of a vapour open convection barrier is recommended when the insulation thickness exceeds 200 mm, also for pitched roof structures.

The field measurements of the roof structure at the ZEB Test Cell Laboratory showed considerable under-temperature periods inside the air cavity. It was not clear whether the under-temperature caused condensation inside the air cavity. Ideally, ventilation of the roof structure should dry out the structure. During the long periods of under-temperature, the moisture content of the roof structure can increase. These findings raise the question of whether dynamic roof ventilation is a relevant solution. Valves positioned in the eaves structure could open and close depending on the conditions inside the air cavity and the exterior conditions and thereby increase the drying-out capacity of the structure.

Another measure to increase the ventilation of the air gap beneath the roofing is the design and dimensions of the counter- and tile battens. Increased counter batten height as well as use of round-edged tile battens was found to considerably lower the pressure loss. The study of local loss coefficients inside the air cavity of a roof and the study of wind pressure coefficients was performed in order to increase knowledge about the driving forces and resistances of ventilated roof structures. Given wind driven air flow through the air cavity beneath the roofing, an average $\overline{\Delta c_p}$ value of 0.7 is derived for practical engineering purposes.

The possibility to build longer ventilated pitched wooden roofs was investigated. Assuming an insulation thickness of 350 mm, an air gap height of 160 mm was found to be sufficient for lengths up to 30 m. The calculations are applicable for pitched wooden

roofs with a roof angle down to 1.4°. However, such low-pitched roofs bring along other building physical challenges related to: 1) water tightness of the roofing, 2) increased condense water dripping from the roofing, 3) evacuation of water entering the air cavity as rain, snow and condense water. Further, an air cavity height of 160 mm will mean that in practise it is not relevant to construct a long ventilated wooden roof in this way. In order to build longer ventilated roofs structures there is a need for practical solutions in order to include interior ice-free drainpipes.

7 FURTHER WORK

The scope of the thesis has been climate adaptation of pitched wooden roofs. Some possible approaches are proposed. However, further investigations are necessary. The main theme for further investigation is related to the design criteria for the air cavity. This relates to both Type A roofs, which have an increased complexity of the physics in a snow melt perspective because of two separate air cavities, and Type B roofs. Given a large, highly insulated, pitched roof, there might be situations where the ventilation needed for dry out of built in moisture is larger than the need for ventilation to avoid snow melt.

During periods with under-temperature, there is a risk of increased moisture level inside the air cavity and the roof structure. Investigation of the condensation potential of the air inside the air cavity is necessary to evaluate if condensation really occurs during the periods with under-temperature. The possibility to control the air flow through the air cavity by using adaptive valves should be further explored. The effect of using roofing materials that can hold water (hygroscopic) should also be further explored. A redesigning of the roof of the ZEB Test Cell Laboratory can be performed in order to better understand the physics inside a ventilated roof.

Periods with under-temperature is also highly challenging for BIPV in roofs. Further, there is a lack of practical guidelines for installation and structural build of BIPV that address recommendations regarding rain-tightness of the system including joints and fittings and necessary ventilation air gap beneath the PV panels. Development of standard methods to document these properties is required. In addition, BIPV products satisfying these demands need to be developed.

REFERENCES

Arksey H and O'Malley L. (2005) Scoping studies: towards a methodological framework. *International Journal of Social Research Methodology* 8: 19-32.

Bauer IH, Førland EJ, Haddeland I, Mayer S, Nesje A, Nilsen JEØ, Sandven S, Sandø AB, SortebergA, Ådlandsvik B. (2015) Klima i Norge 2100 [Climate in Norway 2100] *Norwegian Environment Agency*. Norway. (In Norwegian)

Blocken B and Carmeliet J. (2004) A review of wind-driven rain research in building science. *Journal of Wind Engineering and Industrial Aerodynamics* 92: 1079-1130.

Blocken B and Carmeliet J. (2012) A simplified numerical model for rainwater runoff on building facades: Possibilities and limitations. *Building and Environment* 53: 59-73.

Bøhlerengen T. (2007) Isolerte skrå tretak med lufting mellom vindsperre og undertak. (Insulated pitched wooden roofs with air cavity between the underlayer roofing and the wind barrier) Byggforskserien 525.101. SINTEF Building and Infrastructure. Norway. (In Norwegian)

Bøhlerengen T. (2012) Isolerte skrå tretak med kombinert undertak og vindsperre. [Insulated pitched wooden roofs with combined underlayer roofing and wind barrier] Byggforskserien 525.102. SINTEF Building and Infrastructure. Norway. (In Norwegian)

Bøhlerengen T and Thommesen JE. (2017) Takformer, taktyper og oppbygning. [Roof design and roof build up] Byggforskserien 525.002. SINTEF Building and Infrastructure. Norway. (In Norwegian)

Calonne N, Flin F, Morin S, Lesaffre B, Du Roscoat SR, Geindreau C. (2011) Numerical and experimental investigations of the effective thermal conductivity of snow. Geophysical Research Letters. 38: 1-6

Ceron I, Caamano-Martin E and Neila FJ. (2013) 'State-of-the-art' of building integrated photovoltaic products. *Renewable Energy* 58: 127-133.

Coléou, C., Xu, K., Lesaffre, B. and Brzoska, J.B. (1999) Capillary rise in snow. *Hydrological Processes*. 13: 1721-1732.

Edvardsen K and Ramstad T. (2007) *Trehus Håndbok 53.* [Wooden Houses Handbook 53]. SINTEF Building and Infrastructure. Norway. (In Norwegian)

Edvardsen K and Ramstad T. (2014) *Trehus Håndbok 5*. [Wooden Houses Handbook 5]. SINTEF Building and Infrastructure. Norway. (In Norwegian)

Einstabland H. (2007) Bindingsverk av tre. Varmeisolering og tetting. (Wood frame structures. Heat insulation and tightening). Byggforskserien 523.255. SINTEF Building and Infrastructure. Norway (In Norwegian)

Geving S. (2008) Yttervegger over terreng. Egenskaper og konstruksjonsprinsipper. Krav og anbefalinger. (Exterior wood frame walls. Properties and construction principles. Requirements and recommendations). Byggforskserien 523.002. SINTEF Building and Infrastructure. Norway (In Norwegian).

Geving S and Uvsløkk S. (2000) Moisture conditions in timber frame roof and wall structures. *Project report 273.* Norwegian Building Research Institute. Trondheim. Norway.

Gullbrekken L, Geving S, Time B and Andresen I. (2015a) Moisture conditions in well-insulated wood-frame walls. Simulations, laboratory measurements and field measurements. *Wood Material Science & Engineering* 10: 232-244.

Gullbrekken L, Kvande T, Jelle BP and Time B. (2016) Norwegian Pitched Roof Defects. *Buildings* 6 (2): 24.

Gullbrekken L, Kvande T and Time B. (2015b) Roof-integrated PV in Nordic Climate - Building Physical Challenges. *Energy Procedia* 78: 1962-1967.

Gullbrekken L, Time B and Andresen I. (2015c) Moisture conditions in passive house wall-and roof- constructions. *Energy Procedia* 78:219-224

Hansen HE, Kjerulf-Jensen P and Stampe OB. (2013) *Varme og klimateknik Danvak Grundbog*.[Heat and climate technic Danvak] Danvak ApS. Denmark

Jelle B. (2013) The challenge of removing snow downfall on photovoltaic solar cell roofs in order to maximize solar energy efficiency—Research opportunities for the future. *Energy and Buildings* 67: 334-351.

Kalamees T and Kurnitski J. (2010) Moisture Convection Performance of External Walls and Roofs. *Journal of Building Physics* 33: 225-247.

Kvande T and Lisø KR. (2009) Climate adapted design of masonry structures. *Building and Environment* 44: 2442-2450.

Langmans J, Klein R and Roels S. (2012) Hygrothermal risks of using exterior air barrier systems for highly insulated light weight walls: A laboratory investigation. *Building and Environment* 56: 192-202.

Lisø KR and Kvande T. (2007) Klimatilpasning av bygninger (Climate adaption of buildings). *SINTEF Building and Infrastructure*. Oslo. Norway

Lisø KR. (2006) Building envelope performance assessments in harsh climates: Methods for geographically dependent design. PhD-thesis 2006:187. Department of Civil and Transport Engineering. NTNU. Trondheim. Norway

Lisø KR, Kvande T and Thue JV. (2005) The Robustness of the Norwegian Building Stock - A Review of the Process Induced Building Defects. *7th symposium on building physics in the Nordic countries.* The Icelandic Building Research Institute. Reykjavik. Iceland. 1195-1202.

Lisø KR, Kvande T and Thue JV. (2006) Learning from experience–an analysis of process induced building defects in Norway. *Research in Building Physics and Building Engineering*: 425-432

Misara S and Pornnimit A. (2011) Mechanical characteristics of BIPV modules under different load scenarios and encapsulations. *International Solar Energy Society - ISES- 30th ISES Biennial Solar World Congress 2011.* Vol.3 Kassel, Germany.

O'Brien K, Sygna L and Haugen J. (2004) Vulnerable or Resilient? A Multi-Scale Assessment of Climate Impacts and Vulnerability in Norway. *Climatic Change* 64: 193-225.

Roels S and Langmans J. (2016) Highly insulated pitched roofs resilient to air flow patterns: Guidelines based on a literature review. *Energy and Buildings* 120: 10-18.

Rydock P, Lisø KR, Førland EJ, Nore K and Thue JV. (2005) A driving rain exposure index for Norway. *Building and Environment* 40: 1450-1458

Skogstad HB, Vågen M and Uvslokk S. (2011) Det drypper fra undertaket! (It is dripping from the underlayer roofing!). *Byggeindustrien* 03:2011. (In Norwegian)

Thue JV. (1993) *Report on Norwegian National Construction Leightweight roofs-wooden, sloped, ventilated (paralell roofs).* IEA Annex 24 HAMTIE Holzkirchen 27-28- October 1993.

Tilley Tajet HT and Hygen HO. (2017) Potential Risk of Wood Decay. MET Report 08:2017. *Norwegian Methrological Institute*. Oslo. Norway.

Time B. (Ed.). 2014 *Klima 2050 | Risk reduction through climate adaptation of buildings and infrastructure*, Project description for a Centre for Research-based Innovation (SFI), SINTEF Building and Infrastructure - 102009978, Norwegian Research Council 237859 (internal document).

Uvsløkk S. (1996) Importance of wind barriers for insulated timber frame constructions. *Journal of thermal insulation and building envelopes* 20: 40-62.

Uvsløkk S. (2011) Drying out capacity and snow melting risk for ventilated wooden roofs - a parameter study. *9th Nordic Symposium on Building Physics.* 29. May to 2. June 2011. Tampere. Finland. 441-448.

Uvsløkk S. (2011) Moisture and temperature conditions in cold lofts and risk of mould growth. *9th Nordic Symposium on Building Physics.* 29. May to 2. June 2011. Tampere. Finland.

Uvsløkk S, Skogstad HB. and Grynning S. (2010) How to prevent natural convection causing extra heat loss and moisture problems in thick insulation layers. *3rd Nordic Passive House Conference by Passivehus Norden.* Aalborg, Denmark.

ZEB (2017) Research Centre on Zero Emission Buildings (ZEB) (http://www.zeb.no/index.php/en/) (last accessed 24.11.2017)

Zheng R. (2004) Performance of highly insulated zinc roofs in moderate humid regions. PhD-thesis D/2004/7515/32. Katholieke Universiteit Leuven. Belgium

Økland Ø. (1998) Convection in Highly-Insulated Building Structures. PhD- thesis 1998:91. Department of Civil and Transport Engineering. NTNU. Trondheim. Norway.

INDIVIDUAL PAPERS

Part 1: Motivation, current state and future challenges (Papers 1 and 2)

List of Papers

1) Gullbrekken L, Kvande T, Time B (2016). Norwegian Pitched Roof Defects, *Buildings*, *6*(2), p. 24.
2) Gullbrekken L, Kvande T, Time B (2015). Roof-integrated PV in Nordic climate - Building physical challenges. The 6th International Building Physics Conference - IBPC 2015. *Energy Procedia*, Vol. 78, pp. 1962-1967.

Part 2: Increased insulation, moisture-resilient structures (Paper 3)

List of Paper

3) Gullbrekken L, Uvsløkk S, Kvande T, Time B (2017). Hot-Box measurements of highly insulated wall, roof and floor structures, *Journal of Building Physics*, Vol. 41(1), pp. 58–77.

Part 3: Ventilating guidelines, knowledge base (Papers 4 to 7)

List of Papers

4) Gullbrekken L, Kvande T, Time B (2017). Ventilated wooden roofs: Influence of local weather conditions – measurements, 11th Nordic Symposium on Building Physics, Trondheim, Norway, 11-14. June 2017. *Energy Procedia*, Vol. 132, p. 777-782.
5) Gullbrekken L, Uvsløkk S, Kvande T, Pettersson K, Time B. Wind pressure coefficients for roof venting purposes. *Journal of Wind Engineering and Industrial Aerodynamics.* Vol.175, pp. 144-152.
6) Gullbrekken L, Uvsløkk S, Geving S, Kvande T (2018). Local loss coefficients inside air cavity of pitched wooden roofs, *Journal of Building Physics*. Published online 1. December 2017.
7) Gullbrekken L, Uvsløkk S, Hygen HO, Kvande T, Time B. Air cavity design guidelines for pitched wooden roofs in cold climate. Submitted.

Paper I

Paper 1

L. Gullbrekken, T. Kvande, B. Time

Norwegian Pitched Roof Defects,

Buildings 6(2), 2016, page 24

buildings

MDPI

Article

Norwegian Pitched Roof Defects

Lars Gullbrekken [1,*], Tore Kvande [1], Bjørn Petter Jelle [1,2] and Berit Time [2]

[1] Department of Civil and Transport Engineering, Norwegian University of Science and Technology (NTNU), NO-7491 Trondheim, Norway; tore.kvande@ntnu.no (T.K.); bjorn.petter.jelle@sintef.no (B.P.J.)

[2] Department of Materials and Structures, SINTEF Building and Infrastructure, NO-7465 Trondheim, Norway; berit.time@sintef.no

* Correspondence: lars.gullbrekken@sintef.no; Tel.: +47-45474324

Academic Editor: Francisco López Almansa
Received: 1 April 2016; Accepted: 16 June 2016; Published: 21 June 2016

Abstract: The building constructions investigated in this work are pitched wooden roofs with exterior vertical drainpipes and wooden load-bearing system. The aim of this research is to further investigate the building defects of pitched wooden roofs and obtain an overview of typical roof defects. The work involves an analysis of the building defect archive from the research institute SINTEF Building and Infrastructure. The findings from the SINTEF archive show that moisture is a dominant exposure factor, especially in roof constructions. In pitched wooden roofs, more than half of the defects are caused by deficiencies in design, materials, or workmanship, where these deficiencies allow moisture from precipitation or indoor moisture into the structure. Hence, it is important to increase the focus on robust and durable solutions to avoid defects both from exterior and interior moisture sources in pitched wooden roofs. Proper design of interior ventilation and vapour retarders seem to be the main ways to control entry from interior moisture sources into attic and roof spaces.

Keywords: wood; roof; pitched; climate; robustness; moisture

1. Introduction

1.1. Wood Building Traditions and Climate Exposure

In the Nordic countries, many buildings have wooden frames. Such constructions are especially common for small houses. There is a well-developed tradition of using wood for exterior cladding, load-bearing systems, and interior cladding. In roof constructions, wood is mainly used for the load-bearing systems, which in the following paper are referred to as wooden roofs. The wood-based building tradition has developed due to easy access to high-quality raw materials. A favorable carbon footprint, a strong focus on CO_2 emissions from buildings, and consequent development of zero emission buildings make wooden roofs suitable for an increasing number of buildings. However, the use of wood in buildings may not always be favourable due to robustness issues and climate exposure (e.g., mould, rot, built-in moisture). This means a special focus is needed to develop wooden building technology.

Norway is characterized by an extremely varied climate, the rugged topography being one of the main reasons for large local differences over short distances and extreme seasonal variations [1]. The climate puts a great demand on the building envelope of Norwegian buildings. The building envelope and the roof in particular may be exposed to severe winds, snow loads, precipitation, freeze/thaw cycles, and rather large temperature fluctuations. The climate exposure strongly affects the durability of the roof materials and the long life performance of the roof constructions.

Measures to adapt the built environment to the anticipated climate changes were studied by [2]. They stress the immediate need for information and research both with respect to sensitivities in the built environment and technical solutions to prevent or minimize negative climatic impacts on

buildings. According to [3], the yearly Norwegian precipitation will increase 10%–20% depending on the climatic model used, which will put extra stress on roof constructions in particular.

1.2. Building Defects and Robustness

Building materials have to fulfil several demands during the lifetime of the various products. Consequently, it is important to select building materials which are proven to be durable [4]. This will also be important when utilizing new materials and technologies in the building envelope, like building integrated photovoltaics (BIPV) [5–7]. The lack of data on long-term durability can be compensated for by using accelerated ageing test methods [4].

A method to classify robustness of buildings and their components was studied by [8]. Their study recommends a framework for a robustness classification method for building materials, building assemblies and whole buildings taking into account service life and climate exposure. The robustness of a building or a building component will relate to the exposed climate as well as the intended service life. The study was general and the robustness of roof constructions was not treated in detail. Nevertheless, the suggested definition of robustness is also relevant for the work presented herein: "Materials and solutions having a high resistance against failure (e.g., moisture problems), and having a high probability of being constructed according to specifications. The service life of the materials and solutions will also be important" [8].

The yearly costs caused by process-induced building defects are about 4% ($\pm$2%) of the total yearly investments into new buildings (both residential and commercial) in Norway [9]. Process-induced building defects are defined as the "absence or reduction of presupposed quality which is observed after a construction project is finished and handed over to the owner, and which he demands to be repaired" [10]. Process-induced building defects therefore bring about exceptional maintenance and repair costs (*i.e.*, costs that should not have occurred). Many of these defects are located in the roofs. In the following discussions, the term "source of defect" is related to the exposure from the environment rather than material failure, improper design, and workmanship which is also causing the building defect.

In Norway, process-induced building defects have been studied by [11]. A comprehensive analysis of building defects was carried out by systematically investigating SINTEF's archive of building defect documents. The building defect documents are prepared both through extensive field investigations and on behalf of the construction and building industry. A total of 2423 cases described in 2003 reports were studied for the 10-year period from 1993 to 2002. Process-induced building defect cases relating to the building envelope accounted for 66% of the investigated defect cases. Moisture was the main cause of defects, accounting for 76% of the 2423 cases. This includes all types of construction defects, including roofs, which represented 22% of the total defects. However, a thorough study of roof defects has not previously been conducted. Hence, this study looks more thoroughly into the cases concerning roof defects covered by [11,12].

1.3. Objective and Scope

The aim of this research has been to further investigate the SINTEF building defects archive of pitched wooden roofs and obtain an overview of typical roof defects and common sources (critical exposure). The building defect analysis is adding to the study of [11,12] following the process induced building defects definition proposed by [10,11].

SINTEF's building defect archive classifies pitched roof constructions into the following four types: (A) pitched wooden roofs with separate wind barrier and underlayer roof (venting air cavity between wind barrier and underlayer roof), (B) pitched wooden roofs with combined underlayer roof and wind barrier, also known as watertight vapour open membrane, (C) pitched wooden roofs with cold attics, and (D) pitched wooden roofs with heated rooms in parts of the attic. "Wooden roof" is defined by the wood based load-bearing system of the roof according to [13]. Defects on roof construction types A, B, C, and D are compared with defects on compact roofs and terraces.

2. Pitched Wooden Roof Constructions

The constructions treated in this work are pitched roofs with exterior vertical drainpipes and wood based load bearing system. The various design principles for wooden roofs are thoroughly discussed in [13]. The principles below are presented in the order given in the SINTEF building defect archive.

2.1. Design Principles

The basic principle is that the roof construction must be ventilated in order to transport:

(1) moisture from the roof, and thus prevent mould growth and other moisture damage; and
(2) heat, and thus prevent unwanted melting of snow and ice at the eaves and gutters.

This work is limited to the following roof construction types (see also Figures 1–4):

A A Pitched wooden roofs with separate wind barrier and underlayer roof (ventilation air cavity between wind barrier and underlayer roof).
B Pitched wooden roofs with combined underlayer roof and wind barrier (watertight vapour open membrane).
C Pitched wooden roofs with cold attics.
D Pitched wooden roofs with heated rooms in parts of the attic.

2.2. Type A—Pitched Wooden Roof with Separate Wind Barrier and Underroof

Roof construction Type A is a typical roof built before the year 2000 (see Figure 1). The outer part of the roof consists of:

- raintight roofing;
- drainage and ventilation cavity;
- vapour-tight underlayer roof;
- ventilation cavity; and
- vapour open wind barrier.

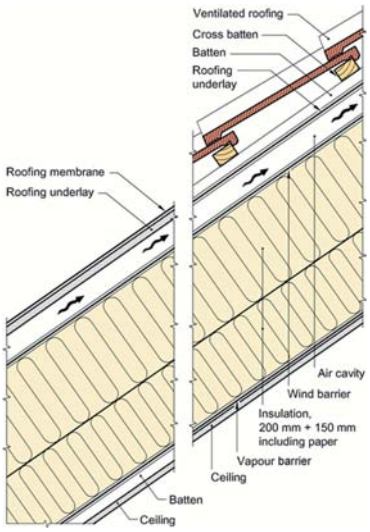

Figure 1. Roof Type A, which separates the rain and wind barrier [13]. Here shown with two common types of roofing.

Type A separates the rain and wind barrier with roofing directly on wooden sheets or with the roofing and underlayer above a separate wind barrier. The roof is ventilated both between the wind barrier and rain barrier and between the rain barrier and the roofing. The rain barrier can be vapour tight. This detail results in additional materials and often higher labour costs compared with the more developed and modern construction of Type B (see Figure 2).

2.3. Type B—Pitched Wooden Roofs with Combined Wind Barrier and Underlayer Roof

Type B is a development of Type A and an improved roof design (see Figure 2). The outer part of the roof construction consists of:

- raintight roofing;
- drainage and ventilation cavity; and
- combined vapour open and watertight wind barrier and underlayer roof.

The main difference between Type A and B is that the drainage and ventilation of Type B is performed directly under the roofing. Both roof types are thermally insulated between the wood rafters. However, the thermal insulation in roof Type B can be placed directly under the underlayer roof because the underlayer roof is a sufficiently vapour open and watertight wind barrier. A study done by [14] involved laboratory measurements of the performance of a combined wind barrier and underroof in driving rain. The measurements concluded that holes in the battens caused by fixing screws or nails are possible leakage locations in such roofs. The problem can be limited by use of special gaskets between the underlayer roofing and the batten [14].

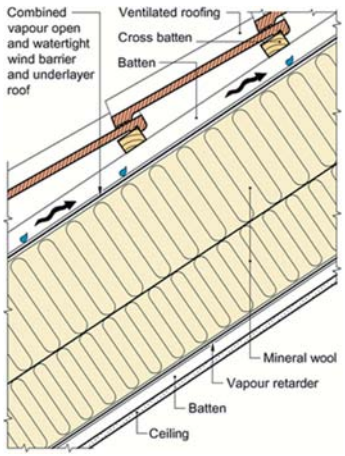

Figure 2. Roof Type B, which is an insulated pitched wooden roof with vapour open combined wind barrier and underlayer roof. All ventilation of the roof takes place in the air cavity below the roofing [13].

2.4. Type C—Pitched Wooden Roofs with Cold Attics

Type C consists of roofs with an air volume (attic) between the insulation and the roofing. During most of the year, the air temperature in the attic will be close to the ambient temperature, but during sunny summer days, the temperatures in the attic can be higher than the ambient temperature. The roof with cold attics can be built up in two different ways (see Figure 3):

(a) Cold, ventilated attic space with air stream flowing through the attic itself. The underlayer roof may be vapour tight. There are ventilation openings in the ridge and between the underlayer roof and the thermal insulation along the eaves of the building. Ventilation openings have to be

designed in order to avoid penetration of snow and rain into the attic. Only the vapour retarder contributes to the airtightness of the building (ceiling), making the solution vulnerable to holes and imperfections in the vapour retarder, which again can cause condensation because of air (containing moisture) leakages through the construction. Hagentoft *et al.* [15] found that the moisture level of cold ventilated lofts is improved if the attic floor is airtight, has low built-in moisture content, and has well-ventilated indoor air.

(b) Cold, unventilated attic space with all ventilation between the underlayer roof and roof covering. The construction is a further development of a) and an improved roof design. The underlayer roof is a vapour open and watertight wind barrier. Both the wind barrier and vapour retarder should be used continuously, thus making it easier to ensure airtightness of the building.

Figure 3. Roof Type C with cold attic. (**a**) Cold, ventilated attic space with air stream flowing through the attic itself. (**b**) Cold, unventilated attic space with all ventilation between the underlayer roof and the roof covering. Image further developed from [16].

2.5. Type D—Pitched Wooden Roofs with Heated Rooms in Part of the Attic

Type D consists of roofs with heated rooms in part of the attic and is thoroughly described by [13]. This type of construction is, according to Uvsløkk, particularly vulnerable to moisture damage and heat loss from air leakages because the vapour retarder is not continuous through the floor construction. The construction type can be built up in two different ways, or a combination of these:

(a) Thermally non-insulated ventilated attic. The underlayer roofing can be vapour tight. There are ventilation openings in the ridge and between the underlayer roof and the thermal insulation along the purlin of the building. Ventilation openings have to be designed in order to avoid penetration of snow and rain into the attic. The vapour retarder and wind barrier are not continuous through the floor construction and the roof is therefore particularly vulnerable to moisture damage due to air leakages.

(b) Thermally insulated non-ventilated attic. The underlayer roof has to be vapour open. The construction is a further development of a) and an improved solution. It is possible to make a continuous and airtight joint between the wind barrier on the wall and the underlayer roof, thus making the construction more resistant to moisture compared to a).

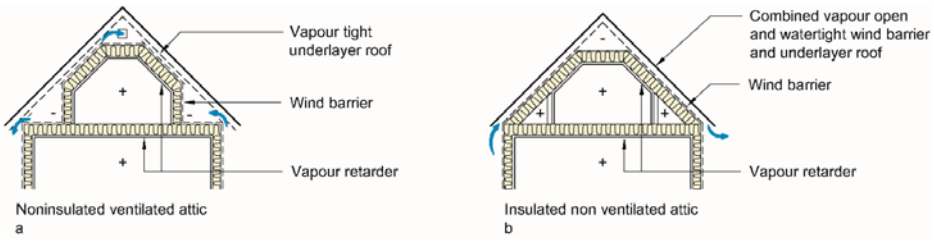

Figure 4. Roof Type D with heated rooms in part of the attic. Thermally insulated non-ventilated attic rooms (**a**) and thermally non-insulated, ventilated (from outside) attic rooms (**b**). Further developed from [13].

3. Analysis of Norwegian Roof Defects

3.1. SINTEF Building Defect Archive

For more than 60 years, SINTEF Building and Infrastructure (formerly the Norwegian Building Research Institute) has been mapping building damage. The work has been performed both through extensive field investigations and on behalf of the construction and building industry. Detailed information about building defects has been collected and stored in an electronic archive. A thorough investigation into the process-induced building defects collected in this archive was performed by [10–12]. The study includes documents from the archive for the 10-year period from 1993 to 2002, which contains 2003 reports describing 2423 incidents or cases of defects. However, a thorough study of roof defects has not previously been conducted. Hence, this study looks in more detail at the cases concerning roof defects covered by [11,12]. The cases with roof defects account for 465 incidents [11,12].

Although a large archive, due to a relatively limited number of specific cases, the building defect archive may not represent a satisfactory description of all building defects in Norway. A relatively high cost related to the engagement of SINTEF has led to professional customers being the dominant share of the cases in the archive (as compared to private householders). Furthermore, it is likely that the archive includes major and expensive cases of building defects rather than smaller-scale and more private issues. One of the advantages of the archive is the large number of cases collected over a long period of time. In addition, the archive contains thorough and detailed descriptions of the defects and possible causes of the defects, and the documents are prepared by experts within the field. Therefore the building defects archive is particularly well suited to find typical building defects of different building constructions and the causes of these defects. The SINTEF building defect archive is acknowledged as one of Norway's most important sources of knowledge about building defects and defect sources.

3.2. Building Defects Versus Source of Defect

As Figure 5 shows, 22% of the registered building defects are localized in roofs. Furthermore, 24% of the total building defects are caused by precipitation (see Table 1). It is worth noting that 75% of all defects are caused by moisture alone or as a consequence of moisture.

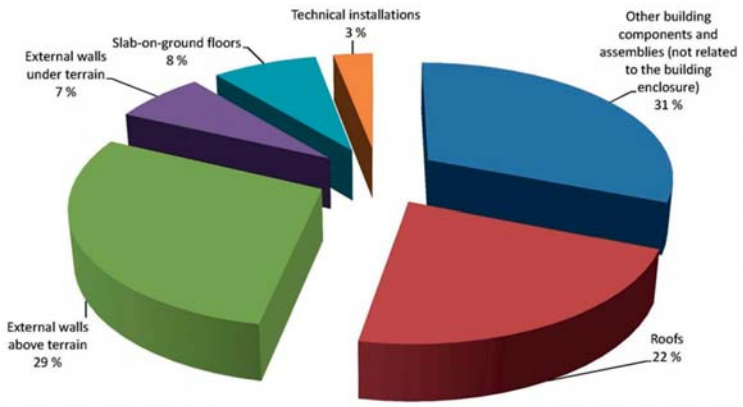

Figure 5. Process-induced building defect cases for the 10-year period from 1993–2002 (a total of 2423 building defect cases), distributed by localization of defects [12].

Table 1. Process-induced building defect cases for the 10-year period from 1993–2002, distributed by source of defects (critical exposure).

Selection	Total Number of Defect Cases	Precipitation (%)	Indoor Moisture (%)	Built-in Moisture (%)	Water in Soil (%)	Leakage Water (from e.g., Sanitary Installations) (%)	Combinations of Moisture Sources (%)	Sources of Moisture in Combination with Other sources (%)	Other Sources (not Moisture Related) (%) [2]
Total amount of building defects	2423	24	15	6	8	5	9	9	24
Total amount of roof cases	465	49	24	1	2	0	12	3	9
- Compact roof cases [1]	83	51	22	2	0	1	13	2	8
- Terrace on concrete floor cases	121	78	8	1	5	0	4	2	2
- Pitched wooden roof cases, total	186	33	34	1	1	0	16	3	12
○ Type A: Separate wind barrier and underlayer roof	33	33	42	0	0	0	12	3	9
○ Type B: Combined wind barrier and underlayer roof	32	50	28	0	0	0	19	0	3
○ Type C: Roofs with cold attics	58	34	24	0	1	0	16	5	19
○ Type D: Roofs with heated rooms in part of the attic	63	24	41	2	1	0	16	3	13

[1] A compact roof is a horizontal roof built up using inorganic insulation material and interior drainpipes. From the cold side of the construction, the roof is built up with a roofing membrane, insulation, a vapour retarder, and a load-bearing system; [2] Examples of non-moisture-related sources of damage are overloading, lack of capacity, vibrations, wear, wrong material composition, insufficient frost protection, noise problems, temperature load/movements, UV radiation, chemical exposure, and assembly errors.

Of the 465 cases registered in the roof category, 40% are in the pitched wooden roof category for Type A, B, C, and D (see Figure 6). The pitched wooden roof category is more thoroughly analysed in this study.

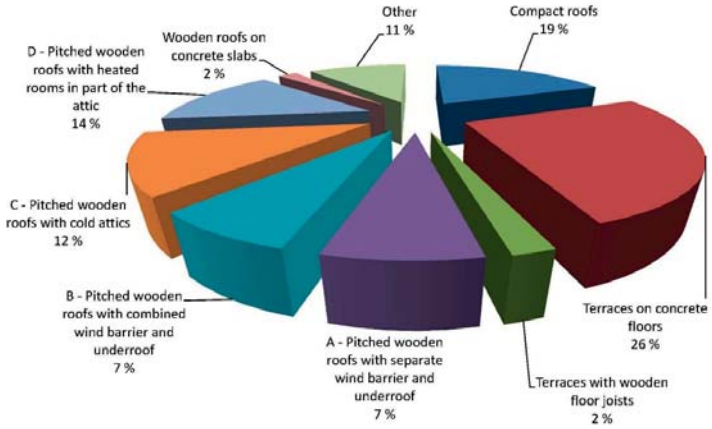

Figure 6. Defect cases for the 10-year period from 1993–2002 concerning roofs, distributed by type of roof (465 cases, 22% of the total amount of building defects) [12].

As much as 49% of the total roof defects are caused by precipitation and only 9% of the defects are not moisture related (see Table 1). Moisture from indoor air and precipitation are the dominating sources of defects in roofs (Table 1).

Table 1 also gives the defect source (critical exposure) distribution for each of the pitched wooden roof categories A, B, C, and D. Moisture from indoor air and precipitation account for 67% of the 186 cases with defects in pitched wooden roofs. Defects caused by indoor moisture are more frequent in the pitched wooden roof constructions.

Just over one-third (34%) of the defects in the pitched roof category are caused by moisture in indoor air compared to 22% and 8% for the categories of compact roofs and terraces on concrete floors, respectively. Most of the damages caused by moisture in indoor air are in the Type A and D categories (approximately 40% of the cases). It is most likely that the increased rate of defects in Type D roofs is caused by condensation in the roof construction due to hot, humid indoor air leaking through joints in the vapour retarder (see Figures 7 and 8).

The distribution by source (critical exposure) of building defects in the different pitched wooden roof constructions is the main focus in this study. There are approximately twice as many defect cases registered in the roof categories Type C and D as compared to Type A and B. This may indicate that Type A and B are more robust constructions than C and D, but note that the numbers are not related to the number of constructions built.

3.3. Typical Damage and Defects

Typical damage and mistakes in thermally insulated pitched wooden roofs, according to findings from SINTEF's building defect archive, are summarized in Figure 7.

Together with indoor moisture, precipitation is the dominant source of climate exposure defects. Typical defect mechanisms are leaky roofing or fittings which in turn can lead to leakages through the roof construction.

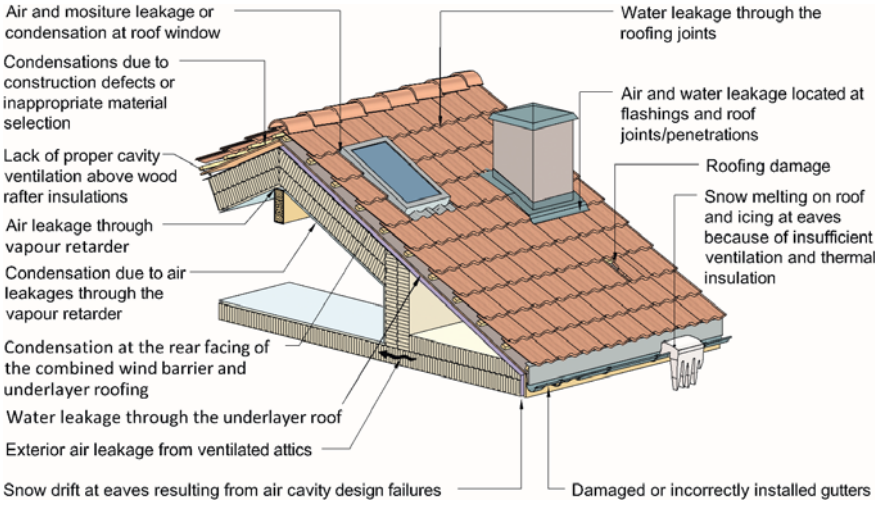

Figure 7. Typical defects in thermally insulated pitched wooden roofs according to findings from SINTEF's building defect archive.

Snow on the roofing creates an extra load that may be critical during snowy winters. In addition to the issue of how much snow is on the roof, the snow can melt and the water can freeze to ice. There can be different causes for the snowmelt (e.g., exterior climate such as rain and solar radiation exposure). Another cause can be lack of ventilation of the roofing in combination with a poorly insulated roof construction. Fresh snow has a relatively low thermal conductivity causing a temperature gradient through the snow [17]. The snow can therefore melt on the roofing even if the exterior temperature is significantly below 0 °C. The water is transported downwards and freezes on the cold unheated parts of the roof, for example, the eaves and gutters. When ice builds up, this can dam up the water and make it penetrate the roofing. Gutters and drains can also be broken by ice formation (see Figure 7). Ice formation may also deteriorate roofing materials when it spreads down the roof [18,19]. The problem with snowmelt on roofs is found to be reduced in modern and well-insulated roofs with well-ventilated roofing [20].

Wind can cause periodic vibrations of roofing materials and may thus lead to material fatigue and crack formation [21]. Requirements for fastening of roofing are dependent on the type of roofing and the geographical location (wind exposure) of the actual building.

Condensation in the cold parts of the roof construction is, according to [22], often caused by air leakages through the vapour retarder. Condensation damage can occur given air leakages in the vapour retarder and internal overpressure (see Figure 8). The chimney effect causes overpressure in the upper parts of a building through the heating season. Examples of typical air leakages are shown in Figure 8. Generally, air leakages in the vapour retarder are critical, but in order to get air leakages through the entire roof construction, there must also be air leakages in the underlayer roof. Note that the risk of condensation damage increases with high humidity levels in the indoor air, which is often caused by poor ventilation of the indoor air.

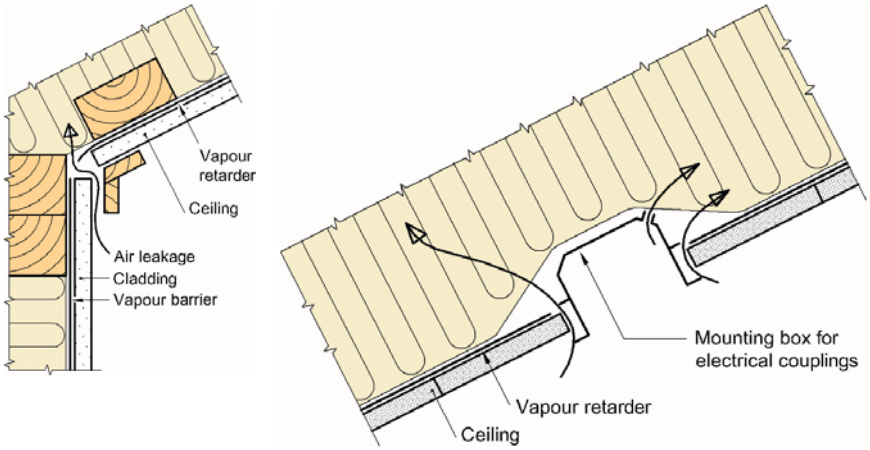

Figure 8. Examples of typical air leakage paths through the vapour retarder [20].

By securing a continuous airtight exterior wind barrier, the roof construction can be considered more moisture resistant. Air leakages through the vapour retarder may also be reduced when the exterior wind barrier is airtight.

4. Discussion

In the following section, the different roof constructions are discussed and compared.

4.1. Type A—Pitched Wooden Roofs with Separate Wind Barrier and Roofing Underlay

The study of the building defect archive shows that indoor moisture and moisture from precipitation are the main causes of defects. By comparing roof Type A with roof Type B, it seems that Type A has more damage from indoor moisture. A possible explanation for this is that Type B roofs are newer, possibly dating from the end of the 10-year period, while the instances of damage for Type A are registered in the beginning of the 10-year period. Towards the end of the 10-year period, the use of balanced indoor ventilation systems was more present, resulting in drier indoor air. Low moisture content in the indoor air helps to reduce the risk of building damage caused by moist indoor air. Towards the end of this 10-year period, there was also generally more focus in the construction industry on the importance of airtightness in the Norwegian building industry, resulting in reduced air leakage through the vapour retarder.

4.2. Type B—Pitched Wooden Roofs with Combined Wind Barrier and Roofing Underlay

Roof Type B is a more labour-efficient version of Type A because the wind barrier and the roofing underlay in roof Type A is replaced by one layer of vapour open and watertight membrane. Precipitation is a more frequent cause of damage compared to roof Type A. The single-layered solution of Type B can be considered more vulnerable to rain leakages compared to the two-layered solution in Type A. Type A therefore appears to be a better solution to avoid leakages from precipitation.

The Czech field investigations on roofing underlays performed by Dek [23] show low waterproof performance for combined underlayer roofs and wind barriers. A suggested explanation for the anticipated degradation of the underlayer roofs and the very poor results is the leaching of impregnation substances from the battens [23]. Low waterproof performance was also found in a field investigation performed by Brandt and Hansen [24]. If the waterproofing of the underlayer roofing is poor, the roof will be very vulnerable to water leakages through the roofing material. The watertightness of the roofing is dependent on the quality of both the roofing material and

the workmanship. The results from the Czech [23] and Danish [24] field investigations do not correspond to accelerated ageing laboratory tests performed by SINTEF on various underlayer roofing products. Accelerated ageing tests on different underlayer roofing products have been performed by SINTEF in the accelerated climate simulator according to Nordtest Method NT Build 495 [25]. The accelerated ageing is based on an assessment that precipitation or driving rain, solar radiation, elevated temperatures, and cyclic freezing and thawing are critical exposure factors. Most of the tested products performed well, including after the durability tests had been completed. However, laboratory measurements can only describe an ideal reality. In practice, it is impossible to include all the possible effects, for example, from leaching of impregnated battens. As a result of the mismatch between the European field experiences [23,24] and Norwegian laboratory findings, there is a need to perform further studies, and preferably a field investigation including various types of underlayer roofs in order to investigate the durability of underlayer roofs in the Norwegian climate.

4.3. Type C—Pitched Wooden Roofs with Cold Attics

Roof Type C can be built both with and without ventilation of the attic. A ventilated solution is more vulnerable to leakages in the vapour retarder at the ceiling of the roof compared to a non-ventilated solution which has a continuous exterior wind barrier. There are twice as many instances of damage in construction Type C compared to Type A and B. This could indicate that construction Type A and B are more robust compared to construction Type C and D, although we know that the number is not related to the number of constructions built. A large part of the damage (19%) is represented by other sources, with the common use of the attic as a storage area being an important reason for that.

4.4. Type D—Pitched Wooden Roofs with Heated Rooms in Part of the Attic

Roof Type D is rather common in Norwegian dwellings due to the efficient utilization of space. There are approximately 100% more building defect cases registered in this category compared to Type A and B. Many (41%) of the building defects are caused by indoor moisture. Type D has difficulties regarding airtightness of the floor construction; in particular, it is complicated to achieve a continuous and airtight joint of the vapour barrier in the floor construction (see Figure 4). As Figure 4 shows, the attic rooms can be ventilated, thus making the construction very vulnerable to air leakages from the inside.

Typical damage caused by indoor moisture include air leakages through the vapour barrier [20]. The driving force of the air leakage is internal overpressure caused by the stack (chimney) effect in the upper parts of the building. If the indoor ventilation is insufficient (*i.e.*, high moisture supply), there is a risk of condensation.

By securing a continuous airtight exterior wind barrier, the roof construction can be considered more protected from moisture. Air leakages through the vapour retarder may also be reduced when the exterior wind barrier is more airtight than the vapour barrier.

5. Conclusions

Findings derived from SINTEF's building defect archive show that moisture is a dominant source of defects, especially in roof constructions. In pitched wooden roofs, 67% of the defects are caused by precipitation or indoor moisture. An airtight vapour retarder and use of balanced ventilation systems are effective means to prevent moisture damage from internal air. Furthermore, a favourable carbon footprint, a strong focus on CO_2 emissions from buildings in general, and the development of zero emission buildings make wooden roofs suitable for an increasing number of large buildings. Thus, it is important to further increase the focus on robust solutions to avoid defects both from exterior and interior moisture sources in pitched wooden roofs.

Acknowledgments: The authors gratefully acknowledge the financial support by the Research Council of Norway and several partners through the Centre of Research-based Innovation "Klima 2050" (www.klima2050.no).

Author Contributions: Lars Gullbrekken was responsible for the literature review and has been the main author of the paper. Tore Kvande has served as the main supervisor during the provess and gave feedback to successive rough drafts made by Lars Gullbrekken. In addition, he was responsible for the analysis of the building defects archive. Bjørn Petter Jelle and Berit Time have contributed with their extensive experience within the field of building physics, especially related to building enclosure performance. They have also during the process provided comments on the prepared manuscript.

Conflicts of Interest: The authors declare no conflict of interest.

References

1. O'Brien, K.; Sygna, L.; Haugen, J. Vulnerable or resilient? A multi-scale assessment of climate impacts and vulnerability in Norway. *Clim. Change* **2004**, *64*, 193–225. [CrossRef]
2. Lisø, K.; Time, B.; Kvande, T. Building enclosure performance in a more severe climate. In *Research in Building Physics—Proceedings of the Second International Conference on Building Physics*; A.A. Balkema Publishers: Leuven, Belgium, 2003; pp. 309–317.
3. Bauer, I.H.; Førland, E.J.; Haddeland, I.; Mayer, S.; Nesje, A.; Nilsen, J.E.Ø.; Sandven, S.; Sandø, A.B.; Sorteberg, A.; Ådlandsvik, B. *Klima i Norge 2100 (Climate in Norway 2100)*; Norwegian environment Agency: Oslo, Norway, 2015. (In Norwegian)
4. Jelle, B.P. Accelerated climate ageing of building materials, components and structures in the laboratory. *J. Mater. Sci.* **2012**, *47*, 6475–6496. [CrossRef]
5. Jelle, B.P.; Breivik, C.; Røkenes, H.D. Building integrated photovoltaic products: A state-of-the-art review and future research opportunities. *Solar Energy Mater. Sol. Cells* **2012**, *100*, 69–96. [CrossRef]
6. Breivik, C.; Jelle, B.P.; Time, B.; Holmberget, Ø.; Nygård, J.; Bergheim, E. Large-scale experimental wind-driven rain exposure investigations of building integrated photovoltaics. *Sol. Energy* **2013**, *90*, 179–187. [CrossRef]
7. Gullbrekken, L.; Kvande, T.; Time, B. Roof-integrated PV in nordic climate—Building physical challenges. *Energy Proced.* **2015**, *78*, 1962–1967. [CrossRef]
8. Jelle, B.P.; Sveipe, E.; Wegger, E.; Gustavsen, A.; Grynning, S.; Thue, J.V.; Time, B.; Lisø, K.R. Robustness classification of materials, assemblies and buildings. *J. Build. Phys.* **2014**, *37*, 213–245. [CrossRef]
9. Ingvaldsen, T. *Byggskadeomfanget i Norge en Vurdering Basert På et Tidligere Arbeid og Nye Data (Building Defects in Norway an Assessment Based on Earlier Work and New Data)*; Prosjektrapport 17; SINTEF Byggforsk: Oslo, Norway, 2008. (In Norwegian)
10. Kvande, T.; Lisø, K.R. Climate adapted design of masonry structures. *Build. Environ.* **2009**, *44*, 2442–2450. [CrossRef]
11. Lisø, K.R.; Kvande, T.; Thue, J.V. *Research in Building Physics and Building Engineering*; Tyler & Francis: Oxford, UK, 2006; pp. 425–432.
12. Lisø, K.R.; Kvande, T.; Vincent, J.V. The Robustness of the Norwegian Building Stock—A Review of the Process Induced Building Defects. In Proceedings of the 7th Symposium on Building Physics in the Nordic Countries, Reykjavík, Iceland, 13–15 June 2005.
13. Edvardsen, K.; Ramstad, T. *Trehus Håndbok 5 (Wooden Houses Handbook No 5)*; SINTEF Building and Infrastructure: Oslo, Norway, 2014. (In Norwegian)
14. Pedersen, T.E.; Bakken, N.; Time, B. *Regntetthet for Kombinerte Undertak og Vindsperrer på Rull (Raintightness of Combined Underlayer Roofings and Wind Barriers)*; Prosjektrapport 23; SINTEF Building and Infrastructure: Trondheim, Norway, 2008. (In Norwegian)
15. Hagentoft, C.-E.; Sasic Kalagasidis, A. Moisture safe cold attics—Assessment based on risk analyses of performance and cost. In Proceedings of the 10th Nordic Symposium on Building Physics, Lund, Sweden, 15–19 June 2014.
16. Lisø, K.; Kvande, T. *Klimatilpassing av Bygninger (Climate Adaption of Buildings)*; SINTEF Building and Infrastructure: Oslo, Norway, 2007. (In Norwegian)
17. Calonne, N.; Flin, F.; Morin, S.; Lesaffre, B.; Du Roscoat, S.R.; Geindreau, C. Numerical and experimental investigations of the effective thermal conductivity of snow. *Geophys. Res. Lett.* **2011**, *38*, 1–6. [CrossRef]
18. Juul, H.; Bøhlerengen, T. *Ising på Tak En Studie av et Skadetilfelle (Ice Formation on Roofs—A Study of Damages)*; Norwegian Building Research Institute: Oslo, Norway, 1990. (In Norwegian)
19. Lossius, P.; Bøhlerengen, T. *Takstein Snø og Brekkasje (Concrete Roofing, Snow and Damage)*; Prosjektrapport 67; Norwegian Building Research Institute: Oslo, Norway, 1990. (In Norwegian)

20. Geving, S. *Fuktskader Årsaker, Utbedringer og Tiltak (Moisture Damage: Reasons, Improvements and Actions)*; SINTEF Building and Infrastructure: Oslo, Norway, 2011.
21. Mahendran, M. *Fatigue Behaviour of Corrugated Roofing under Cyclic Wind Loading*; James Cook University of North Queensland: Queensland, Australia, 1990.
22. Uvsløkk, S. Moisture and temperature conditions in cold lofts and risk of mould growth. In Proceedings of the Nordic Building Conference, Tampere, Finland, 29 May–2 June 2011.
23. Dek, A. *Research on the Lifetime of Membranes. DEKTIME Special 01*; Atelier Dek: Prague, Czech, 2012.
24. Brandt, E.; Hansen, E.J. Durability of roof underlays exposed to long time exposure under in-use conditions. In Proceedings of the XIII International Conference on Durability of Building Materials and Components, Sao Paulo, Brazil, 2–5 September 2014.
25. *Nordtest Method NT BUILD 495 Building Materials and Components in the Vertical Position: Exposure to Accelerated Climatic Strains*; Nordtest: Espoo, Finland, 2000.

Paper II

Paper 2

L. Gullbrekken, T. Kvande, B. Time

Roof-integrated PV in Nordic climate - Building physical challenges

The 6th International Building Physics Conference - IBPC 2015. Energy Procedia, Vol. 78, 2015, pages 1962-1967.

Full abstract:

Use of photovoltaics (PV) is key remedies in buildings where a large part of the energy supply should be based on renewable energy. PV in Nordic climate can be challenging because of snow, wind and temperatures below zero. The aim of this research work has been to provide a state-of-the art overview of recent experiences and challenges for building physical conditions related to the use of roof-integrated PV in Nordic climate. The study has identified practical guidelines for installation and ventilation of the roofing as challenges to be solved for extensive use of such systems in Nordic climate.

Larger Figures 1 A and B:

A

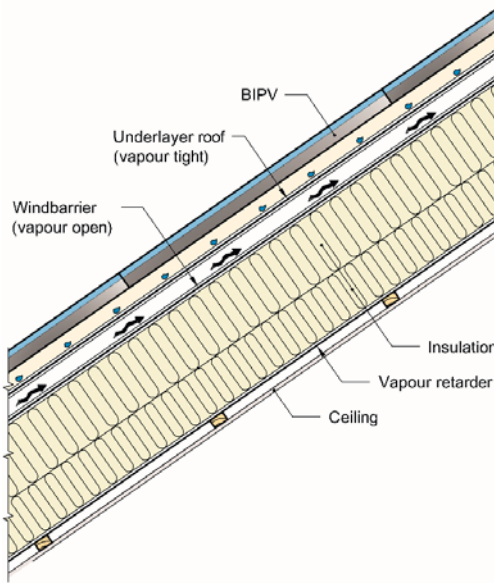

B

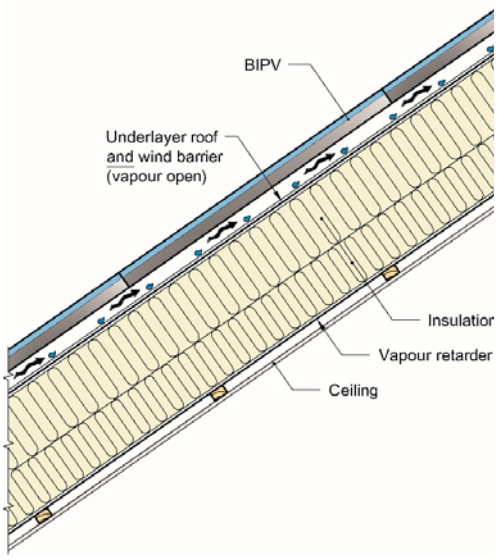

Available online at www.sciencedirect.com

ScienceDirect

Energy Procedia 78 (2015) 1962 – 1967

Energy Procedia

6th International Building Physics Conference, IBPC 2015

Roof-integrated PV in Nordic climate - Building physical challenges

Lars Gullbrekken[a]*, Tore Kvande[a], Berit Time[b]

[a]*NTNU, Norwegian University of Science and technology, Department of Civil and Transport Engineering , 7491 Trondheim, Norway*

[b]*SINTEF Building and infrastructure, Trondheim,*

Abstract

Use of photovoltaics (PV) is key remedies in buildings where a large part of the energy supply should be based on renewable energy. PV in Nordic climate can be challenging because of
and temperatures below zero. The aim of this research work has been to provide a state-of-the art overview of recent experiences and challenges for building physical conditions related to the use of roof-integrated PV in Nordic climate. The study has identified practical guidelines for installation and ventilation of the roofing as challenges to be solved for extensive use of such systems in Nordic climate.

Peer-review under responsibility of the CENTRO CONGRESSI INTERNAZIONALE SRL

Keywords:

1. Introduction

1.1. Building integrated photovoltaics (BIPVs)

Photovoltaic modules integrated into the building envelope, such as the roof or the façade, is commonly referred to as BIPV systems. Roof-integrated systems are preferred due to architectural design and an increasing focus on sustainability and embodied emissions[1]. The efficiency of devices is dependent on different factors; the building integrating technic/solution being one important factor.

* Corresponding author. Tel.: +47 45474324.
E-mail address: lars.gullbrekken@sintef.no

Peer-review under responsibility of the CENTRO CONGRESSI INTERNAZIONALE SRL
doi:10.1016/j.egypro.2015.11.382

BIPVs have dual functionality; replacing the conventional elements of construction and generating energy[2]. This implies that roof integrated PVs replace the conventional roofing, such as tiles, slate and metal roofing, which is favorable because of material saving.

BIPV products that replace building components have to comply with the conventional building regulations and PV-standards. There is a missing link between PV, and the construction sector and lack of BIPV standards based on building product requirement as obstacles for large scale BIPV application[3].

1.2. Nordic climate

Characteristic for Norway is the extremely varied climate, the rugged topography being one of the main reasons for large local differences over short distances and extreme seasonal variations. The climate is putting great demand on our building envelopes. The building envelope and the roof in particular may be exposed to severe wind, snow load, precipitation, freeze thaw cycles and rather large temperature fluctuations. Concerning BIPVs the climate may be extra challenging due to the fact most of the systems are developed for other climate conditions than the Nordic.

2. Objectives and Scope

The aim of this work has been to provide a state-of-the art overview of recent experiences and building physical challenges related to the use of BIPV in Nordic climate. The paper is based on a literature review focusing mainly on challenges of cold, pitched roofs. Flat, compact roofs are not a part of the study.

3. The principal roof construction

The construction treated in this work is pitched roofs. The various design principles for wooden roofs are thoroughly discussed in[4-6]. The basic principle is that the roof construction must be vented in order to transport:

1. Moisture from the roof and thus prevent the growth of mold and other moisture damage
2. Heat and thus prevent unwanted melting snow and icing at the eaves and gutters

The roof ventilation may be built up in two different ways as shown in Fig. 1. Traditionally the roof construction separates the underlay roof and the wind barrier (Fig. 1A). This was the traditional construction system until the development of materials that combine the wind barrier function and the underlay roofing function. The roof is vented between the wind barrier and the underlayer roof and may dependent of the roofing also be aerated between the underlayer roof and the roofing. The underlayer roof consists usually of a vapour tight material. Because of the vapour tightness an extra material layer is added compared to the more modern roof build up given in Fig. 1B. The roof built up is thus more material consuming and requires more labor cost compared to the more modern roof construction. The more modern roof build up as given in Fig. 1B consist of a rain tight roofing, a ventilation gap and a vapour open and watertight wind barrier as underlayer roof. The thermal insulation can be placed directly under the underlayer roof because the underlayer roof is sufficiently vapour open and watertight wind barrier.

By introducing BIPV the construction sector seems to choose the "previous traditional" way of building up a roof construction, due to robustness reasons. From an environmental (less material) and a cost effective point of view it would be favorable if we could further develop systems and solutions which comply with the "modern more common" way of doing it.

Fig. 1. A: The "previous traditional" way of building up a roof construction by a separate wind barrier and an underlayer roof.
B: The "modern more common" way with a combined wind barrier and underlayer roof.

4. Roof integration experiences and challenges

4.1. Roofing performance

According to[2] almost 50 % of the BIPV market is roof installations. The primary function of the roof as a climate screen must still be fulfilled also with BIPV-systems. The water and air tightness of the roof has to be intact which imply that the joints between the BIPV-panels and roofing material have to be water tight. BIPV-systems can cover the whole roof or they can cover part of the roof. Systems covering part of the roof also demand rain tight fittings. A sufficient level of ventilation of air beneath the roofing is necessary in order to prevent the growth of mold and moisture damage[7,8]. In order to keep a high performing BIPV system it may be necessary to increase the ventilation in order to lower the temperature of the BIPV[9,10].

4.2. Degradation of BIPV

Generally commercial available modules are highly reliable[11]. The operating life is determined by the durability of the encapsulation of the solar module[12]. Moisture penetration is causing the majority of the long term failures[13]. Field measurements performed by[11,14] indicate energy performance losses in the range of 0,5-1% due to degradation per year. There is however little experience regarding degradation and service life of BIPV in Nordic climate.

4.3. Raintightness of BIPV systems

Wind-driven rain is one of the most important moisture sources affecting the hygrothermal performance and the durability of building façades and roofs[15,16]. In particular the western coast of Norway is exposed to challenging rain conditions[17]. It is thus pity that hardly any literature reveals experience with driving rain performance of BIPV-systems. Newertheless a promising method was proposed by[18]. They performed a large scale testing of water run off capabilities and wind driven rain resistance of a specific commercial system. The system was tested at two different inclinations (15° and 30°). In order to control strains on the underlayer roof, it is recommended to choose BIPV-system with well documented driving rain performance preferably performed by the method given by[18].

4.4. Snow and ice on PVs

Traditional roofs have been designed to keep snow on the roof. This is contradicting to what is preferred for BIPVs. In order to maximize the PV energy production PV panels should have no snow cover. PV panels covered by snow during long periods in the winter will suffer a decrease in both energy and cost effectiveness. The Nordic winter months are however characterized by low solar insolation and therefore low potential for solar harvesting[19].

The annual loss in power production due to snow on a roof mounted PV system in Munich was estimated to 0,3-2,7%[20]. Comparing the reported number of snow days in Munich with snow data from the high populated cities in Norway shows similar or lower number of snow days for the Norwegian cities Trondheim, Bergen, Stavanger, Oslo[21]. Losses due to snowfall is dependent on technology and angle of the PV system[22]. Over the two years studied the losses ranged from 1-3,5% in sites in south-east Ontario (45°N). Another study performed by [23] including PV modules mounted in three different tilt angles (0°, 24°, 39°) near Lake Tahoe (California USA), a high altitude site with an average of 5m of snow per year showed annual power production losses in the range of 12-18%. It is hard to generalize the results to other locations as the area studied represents extreme cold and snow conditions, but it shows the snow covering challenges concerning power production.

Snow and ice melting or sliding down the BIPV may cause hazards such as snow and ice falling down representing a risk for people passing beneath the roof. One way of stopping downfall of snow is by installation of snow stoppers beneath the BIPV. The snow stoppers can cause the snow to accumulate on the BIPV giving a decrease in energy effectiveness. Snow sliding of PV can freeze on the roofing below the modules and the build up of ice can damage the roofing and the gutters.

The challenge with snow downfall on BIPV-systems mounted on walls and roofs was investigated by[24,25] in order to maximize the solar energy efficiency, with a special emphasis given on possible research opportunities for the future. Several solutions to the ice and snow problem were suggested. A special emphasis was given on different material surfaces like e.g. self-cleaning surfaces with origin in photo-catalytic hydrophilic surfaces, super-hydrophobic or ultra-hydrophobic surfaces and coarse micro structured or nanostructured surfaces without giving any clear design recommendation for preventing the problem. Since the Nordic climate includes snowrich locations, standard solutions adapted to Nordic climate are necessary in order to solve the challenges associated with snow.

4.5. Condensation on the rear side of a PV

If the temperature of the rear side of the BIPV is lower than the dew point of the surrounding, air condensation will occur on the modules. The phenomenon typical occurs during nights with clear weather conditions. If the temperature is below zero the condensation water will freeze. When the temperature rises above zero the water will thaw and might drip on the underlayer roof[26]. Hence, the underlayer system must be water proof and drain the water, and sufficient ventilation of the air gap between the modules and the underlayer roof is necessary in order to dry out the water. The situation with condensation is of special interest in Nordic climate due to frequently cold radiation situations. The problem of condensation is mentioned by[27], but no further studies have been performed.

4.6. Venting below the BIPV

In order to maximize the energy yield, to lower the degradation processes, and to improve the building physical properties ventilation below the BIPV is necessary[28].

The temperature of the PV module is dependent on the heat gains from the sun and the heat losses to the surrounding air and the wind velocity. The efficiency of the PV-panels is strongly dependent on the temperature of the PV-panel[29]. A efficiency drop by as much as 0,5% per °K increase in module temp. is suggested by[10]. A power output decrease by 0,4-0,5%K^{-1} for crystalline silicon modules and 0,1%K^{-1} for amorphous silicon is suggested by[30]. Assuming still air and attached to a building with good rear ventilation[27] suggests a 30°C panel temperature increase relative to ambient temperature at 1kW/m² insolation. For crystalline silicon modules this will give an efficiency decrease of 15%[31].

In order to dry out build in moisture and avoid snow melt a recommendation of a minimum ventilation gap of 48mm for roof lengths up to 7m is suggested by[4] for well insulated roofs. No ventilation recommendation for BIPV systems are specified by[32].

Heat transfer and air flow pattern created between two vertical parallel walls heated from one side was studied by [33]. The setup of the experiment was a mock-up of a façade with integrated PV-panels. Temperature distribution and mean velocities as a function of heat input was recorded inside the air gap. The laboratory study resulted in velocity profiles of the vented air gap behind the PV and mean velocities as a function of heat input onto the PV. The laboratory study was performed on a façade and did not include roof measurements[33]. Similar studies for roof ventilation in Nordic climate were not found.

Simulations of the effect of mounting type and mounting geometry on the temperature of a PV panel were performed by[29]. Both roof angle and height of the air cavity below the PV-panel effected the temperature and hence the efficiency of the PV-panel. The results confirm that larger angles and small aspect ratios are associated with higher efficiencies because of lower PV temperature. The aspect ratio is given by the length of the air gap divided by the height of the air gap.

Air change rate, temperatures and velocities in a roof mock up was also studied by[34]. Only ventilation by natural convection was taken into account. The inclination (25°, 45°, 70°, 90°) and the air gap of the roof was varied (0.23m, 0.115m and 0.06m). It was found that increased air gap and roof inclination resulted in higher flow rates inside the air gap. However the study did not end up in recommendations regarding size of the air gap[34].

A numerical study (CFD calculations) was performed by[35] in order to find the best cooling strategy for BIPV panels. A comparison analysis of different heights of the air gap for cooling of the roof was conducted. The results showed that an air gap height of 50mm was not sufficient to provide cooling of a 70m long BIPV roof. The developed model was considered a good starting point for further investigations.

In addition to reduced efficiencies, increased temperatures will cause thermal expansion and increased stress to the interconnections between the cells possibly leading to delamination[13].

The knowledge base regarding temperature profiles and ventilation below BIPV modules was found to be insuffi. Measurements of temperature profiles for the air gap below BIPV roofs in Nordic climate are lacking. Practical guidelines are needed regarding ventilation of BIPVs depending on size and inclination of the roof.

4.7. Underlayer roof

OSB- and plywood boards are the most common robust alternatives used as underlayer roofs. Unfortunately the water vapor permeability of such boards may be unfavorable in order to ensure drying out of built in moisture in the roof construction. The risk of degradation and mold growth in the roof construction is therefore higher compared to more vapour permeable roof underlay materials. Recommended values from SINTEF states that the s_d-value of a wind barrier should be less than 0,5m[36].

An extensive measurement campaign of s_d-value of OSB/3-boards was performed by[37] on boards from four major producers in Europe. Results showed higher s_d-values than the tabulated values in[38] for both wet- and dry-cup conditions. None of the investigated OSB-boards complied with the recommendations from SINTEF.

An improved solution is to apply vapour open wind barrier sheets such as porous wood fibre boards with asphalt coating in combination with a wind barrier foil. This solution is both robust and satisfies the recommended s_d-value. It is important that the underlayer roof system is documented regarding driving rain performance[39].

Currently, the installation of BIPV-systems implies a longer building period compared to traditional roofing methods, since the experience with this kind of roofing is limited. Therefore the underlayer roof must withstand a longer period of direct climate stresses before the roofing is completed and traffic (due to labor) on the roof. This also stresses the importance to use robust underlayer roof systems which has documented driving rain performance.

4.8. Penetrations

BIPV-systems imply penetrations of cables through the roof construction. In some cases the penetrations have to be performed both through the roofing and through the underlayer roof. The penetrations must be water- and airtight in order to avoid moisture problems in the construction. This requires that the penetrations through the roofing must be adapted to the roofing material used, and the penetrations through the underlayer roof must be adapted to the material used as underlayer roof. Penetration details and products tested in the laboratory according to[39] or similar method should be used. The test method implies testing of underlayer roofs with penetration details.

5. Conclusions

Large scale BIPV application on cold pitched roofs may be favorable in many cases, even in Nordic countries. However, there is a need for linking the PV- and construction sectors and preparing BIPV-standards. The literature review has identified several building physical challenges that have to be solved for extensive use of roof-integrated PV in Nordic climate. Practical guidelines for installation and ventilation of the roof integrated PV are considered to be key challenges. The guidelines need to include ventilation strategies depending on the size and inclination of the roof. More research is necessary in order to develop new solutions to cope with challenges such as snow on BIPVs possibly causing hazards such as snow and ice falling down and to develop BIPV systems with sufficient rain tightness.

Acknowledgements

The authors gratefully acknowledge the financial support by the Research Council of Norway and several partners through the SFI Klima 2050 (www.klima2050.no). Support is also given by FME ZEB (www.zeb.no).

References

[1] Dokka T, Wiberg A, Georges L, Mellegård S, Time B, Haase M, Maltha M, Lien A; *A zero emission consept analysis of a single family house*; ZEB Project report 9; SINTEF Byggforsk; 2013.
[2] Ceron I, Caamano-Martin E, Neila FJ; 'State-of-the-art' of building integrated photovoltaic products; *Renewable Energy*; 2013;58:127-133.
[3] Misara S, Pornnimit A; Mechanical characteristics of BIPV modules under different load scenarios and encaplsuations; *International Solar Energy Society -ISES- 30th ISES Biennial Solar World Congress 2011*;Kassel, Germany; 2011;3:2193-2203
[4] Byggforskserien; 525.101 Isolerte skrå tretak med lufting mellom vindsperre og undertak; SINTEF Byggforsk; 2007.
[5] Byggforskserien; 525.102 Isolerte skrå tretak med kombinert undertak og vindsperre; SINTEF Byggforsk; 2012.
[6] Edvardsen K, Ramstad T; *Trehus* Håndbok 5; SINTEF Byggforsk; 2014.
[7] Holme J; Mould growth on board-based wind-barrier products; In: *Energy Efficiency and New Approaches–Proceedings of the Fourth International Building Physics Conference*; Istanbul; 2009:75-82.
[8] Holme J; *Mould growth in buildings*: Doctoral thesis at NTNU; 2010:147.
[9] Skoplaki E, Palyvos J; On the temperature dependence of photovoltaic module electrical performance: A review of efficiency/power correlations; *Solar Energy*, 2009;835:614-624.
[10] Mattei M, Notton G, Cristofari C, Muselli M, Poggi P; Calculation of the polycrystalline PV module temperature using a simple method of energy balance; *Renewable Energy*, 2006;314:553-567.
[11] King D, Quintana M, Kratochvil J, Ellibee D, Hansen B; Photovoltaic module performance and durability following long-term field exposure; *Progress in Photovoltaics: Research and Applications*, 2000;82:241-256.
[12] Czanderna A, Pern F; Encapsulation of PV modules using ethylene vinyl acetate copolymer as pottant; *Solar Energy Materials and Solar cells*, 1996;43:101-181.
[13] Wenham S; *Applied photovoltaics*; Routledge; 2011.
[14] Vaaβen; Degradation von photovoltaik-modulen; *Erneuerbare Energien*, 2004, 6.
[15] Blocken B, Carmeliet J; A simplified numerical model for rainwater runoff on building facades: Possibilities and limitations; *Building and Environment*, 2012;530:59-73.
[16] Blocken B, Carmeliet J; A review of wind-driven rain research in building science; *Journal of Wind Engineering and Industrial Aerodynamics*, 2004; 9213:1079-1130.
[17] Lisø K, Kvande T; *Klimatilpassing av bygninger*; SINTEF Byggforsk; 2007.
[18] Breivik C, Jelle B, Time B, Holmberget Ø, Nygård J, Bergheim E, Dalehaug A; Large-scale experimental wind-driven rain exposure investigations of building integrated photovoltaics; *Solar Energy*, 2013;900:179-187.
[19] Byggforskserien; 552.455 Vannbaserte solfangere. Funksjon og energiutbytte; SINTEF Byggforsk; 2011.
[20] Becker G, Schiebelsberger B, Weber W, Vodermayer C, Zehner M, Kummerle G; An approach to the impact of snow on the yield of grid connected PV systems; *Proceedings of European PVSEC 2006*; Dresden; 2006, DOI: http://www.sev-bayern.de/content/snow.pdf
[21] Hygen H O*; Færre dager med snø på bakken i januar 2009*. DOI: http://met.no/?module=Articles;action=Article.publicShow;ID=1212.
[22] Andrews R, Pollard A, Pearce M; The effects of snowfall on solar photovoltaic performance; *Solar Energy*, 2013;920:84-97.
[23] Powers L, Newmiller J, Townsend T; Measuring and modeling the effect of snow on photovoltaic system performance; In: 35 IEEE Photovoltaic Specialists Conference – 2010; 2010:973-978.
[24] Jelle B; The challenge of removing snow downfall on photovoltaic solar cell roofs in order to maximize solar energy efficiency—Research opportunities for the future; Energy and Buildings, 2013; 670:334-351.
[25] Jelle B (Ed.); *Friction between Snow/Ice and roofing /Active Roof Installation Surfaces; in Euro-active roofer*; SINTEF; 2006.
[26] Geving S; *Fuktskader. Årsaker, utbedringer og tiltak*; Håndbok 3; SINTEF Byggforsk; 2011.
[27] Häberlin H; *Photovoltaics System Design and Practice*; Wiley; 2012.
[28] Earthscan; *Planning & Installing Photovoltaic Systems*; Eartscan; 2008.
[29] Wilson M, Paul M; Effect of mounting geometry on convection occurring under a photovoltaic panel and the corresponding efficiency using CFD; Solar Energy, 2011;8510:2540-2550.
[30] Norton B, Eames P, Mallick T, Huang M, Mccormack S, Mondol J, Yohanis Y; Enhancing the performance of building integrated photovoltaics; *Solar Energy*, 2011;858:1629-1664.
[31] Radziemska E,Klugmann E; Photovoltaic maximum power point varying with illumination and temperature; *Journal of solar energy engineering*, 2006;1281:34-39.
[32] SINTEF Building Reserch Design Guides; SINTEF Byggforsk; bks.byggforsk.no
[33] Sandberg M, Moshfegh B; Investigation of fluid flow and heat transfer in a vertical channel heated from one side by PV elements, part II - Experimental study; *Renewable Energy*, 1996;8 1–4:254-258.
[34] Sandberg M, Moshfegh B; Ventilated-solar roof air flow and heat transfer investigation; *Renewable Energy*, 1998;15 1–4:287-292.
[35] Misiopecki C, Gustavsen A, Time B; *Cooling of PV panels by natural convection*; ZEB Project report 6; SINTEF Byggforsk; 2012.
[36] Byggforskserien; 573.121 Materialer til luft- og damptetting; SINTEF Byggforsk; 2003.
[37] Korsnes S, Time B, Vågen M, Halstedt H, Geving S, Holme J; Moisture risk in prefabricated wooden wall elements (TES-elements) with a vapour retarder of OSB/3; In: Passivhus Norden 2013; Göteborg; 2013:336-348.
[38] NS-EN ISO 10456; *Building materials and products - Hygrothermal properties -Tabulated design values and procedures for determining declared and design thermal values;* Standard Norge; 2007.
[39] NT Build 421;*Watertightness under pulsating air pressure*; Nordtest; 1993.

Paper III

Paper 3

L. Gullbrekken, S. Uvsløkk, T. Kvande, B. Time

Hot-Box measurements of highly insulated wall, roof and floor structures

Journal of Building Physics, Vol. 41(1), 2017, pages 58–77.

Original Article

JOURNAL OF BUILDING PHYSICS

Journal of Building Physics
2017, Vol. 41(1) 58–77

DOI: 10.1177/1744259116669516
journals.sagepub.com/home/jen
SAGE

Hot-Box measurements of highly insulated wall, roof and floor structures

Lars Gullbrekken[1], Sivert Uvslokk[2], Tore Kvande[1] and Berit Time[2]

Abstract

The purpose of this study was to investigate how natural convection in air-permeable glass wool insulation affects the thermal transmittance in walls, roofs and floor structures. The results can be used to evaluate the need for a convection barrier in thick mineral wool layers. Natural convection is affected by several parameters. In this study, the angle of inclination, the heat flow direction and the temperature difference across the test section have been studied. Thermal transmittance and temperature distribution measured using thermocouples placed inside the insulation cavity clearly showed convection in the insulation when the test section was in pitched roof and wall positions. An efficient measure to reduce the natural convection is to divide the insulation layer into two thinner layers using a diffusion open convection barrier. A convection barrier is recommended by the authors both in wall and pitched roof structures if the insulation thickness exceeds 200 mm.

Keywords

Laboratory measurements, Hot-Box, natural convection, heat transfer, insulation

Introduction

Convection in building structures

Convection, or air flow, in building structures is caused by pressure differences from driving forces like fans, wind and temperature differences. Resulting air flow caused by temperature differences is called natural convection. The driving force is

[1]Norwegian University of Science and Technology (NTNU), Trondheim, Norway
[2]Stiftelsen for industriell og teknisk forskning (SINTEF) Building and Infrastructure, Trondheim, Norway

Corresponding author:
Lars Gullbrekken, Norwegian University of Science and Technology (NTNU), Høgskoleringen 7 A 7046, Trondheim, Norway.
Email: lars.gullbrekken@sintef.no

buoyancy caused by density differences in the air because of the temperature differences.

The risk of natural convection in an enclosure filled with a permeable material exposed to a given temperature difference may be described by the modified Rayleigh number Ra^*. Ra^* is defined in NS-EN ISO 10456:2007 (2007), see equation (1). According to NS-EN ISO 10456:2007 (2007), natural convection can be neglected when calculating U-values if $Ra^* < 2.5$

$$Ra^* = \frac{g\beta\rho c_p}{\nu} \cdot \frac{dk\Delta T}{\lambda_m} \tag{1}$$

The properties of the air are the heat expansion coefficient, β (1/K); kinematic viscosity, ν (m^2/s); density, ρ (kg/m^3); and specific heat capacity, c_p (J/kgK). The properties of the insulation material are air permeability k (m^2) and thermal conductivity λ_m(W/m^2 K). ΔT is the temperature difference across the specimen with insulation thickness, d (m).

The permeability of the mineral wool, k (m^2), given in equation (1) was calculated according to the following equation

$$k = \frac{L \cdot \nu \cdot dx}{A \cdot \Delta P} \tag{2}$$

where L is the air flow (m^3/s), ν is the kinematic viscosity (m^2/s), dx is the insulation thickness (m), A is the cross-sectional area from which air is flowing through (m^2) and ΔP is the pressure difference (Pa).

However, the fibre orientation in glass wool battens is not evenly distributed, but dominated by fibres parallel to the batten surface. Because of this, the permeability is usually substantially larger parallel ($\parallel$) rather than perpendicular ($\perp$) to the batten surface (Marmolet et al., 2012).To account for this, an equivalent permeability, k_e (m^2), representative for the air flow path, should be estimated and used in equation (1). According to Uvsløkk et al. (1996), k_e for walls can be calculated using equation (3). The equation takes into account the difference in permeability perpendicular to and parallel to the main fibre orientation, the cross-sectional area and length of a simplified flow path in the insulated cavities

$$k_e = \frac{\frac{h}{d} + \frac{d}{h}}{\frac{h}{d \cdot B_{\parallel}} + \frac{d}{h \cdot B_{\perp}}} \tag{3}$$

where h is the height of the insulated wall cavity (m), d is the depth (thickness) of the wall insulation (m), $B_{\parallel}$ is the permeability parallel to the fibres (m^2) and $B_{\perp}$ is the permeability perpendicular to the fibres (m^2).

Of interest, when evaluating the thermal performance of structural components, is also the ratio of the total heat transfer including convection to heat transfer without convection. The ratio is given by the Nusselt number, Nu, and has been calculated according to the following equation

$$Nu = \frac{U}{U_0} \tag{4}$$

where U is the U-value measured in the Hot-Box ($W/m^2 K$) and U_0 is the U-value when there is no convection ($W/m^2 K$). In the present Hot-Box measurement, the U_0 is the value of the tested structure in horizontal floor configuration, with heat flow direction downwards.

Challenges in structures with thick insulation

Buildings that are designed to meet high energy performance requirements, for example, passive houses, require well-insulated building envelopes, with increased insulation thicknesses for roof, wall and floor structures. Increased insulation thicknesses may lead to increased risk of mould growth and moisture damage (Gullbrekken et al., 2015; Økland, 1998). One reason for this is the increased risk of natural convection in the insulated cavities causing moisture redistribution in the timber frame.

Natural convection will cause the air to circulate in the cavity, rise on the warm side and drop on the cold side. The amount of natural convection depends on the driving forces and the flow resistance of the insulated cavities: (1) temperature difference across the wall, (2) equivalent air permeability of the insulated cavity and (3) insulation thickness.

In order to avoid convection, it is important that the insulation material fills the cavities completely, especially at the top and bottom of the cavities, in order to avoid air gaps. Gaps will decrease the flow resistance of the insulated cavity and hence increase the convection (Geving, 2011). If the insulation thickness exceeds 200 mm, Uvsløkk et al. (2010) recommend dividing the insulation into two parallel 'cavities' using an airtight and vapour-open barrier in the middle of two insulation layers. Using this approach, the driving force, the temperature difference across each layer, will be reduced by 50% and the total flow resistance in each layer will be nearly doubled (Uvsløkk et al., 2010).

Convection and the effect on thermal performance

Also previous studies have researched natural convection and effect on thermal performance for wall and roof structures.

Walls

Calculations and measurements performed by Bankvall (1972) indicated that natural convection did not have a significant effect on heat transfer in walls and roofs when glass wool insulation was used. However, the insulation thicknesses in Bankvall's studies varied from 50 to 145 mm and the temperature difference was

10–45 K. These insulation layers were rather thin compared with modern Nordic wooden frame structures.

Lecompte (1990) performed calculations of convection through the insulation and around the insulation in a cavity and compared it to Hot-Box measurements. The study only included a wall with 50-mm insulation in a cavity of 80 mm.

Brown et al. (1993) performed an extensive investigation on full-scale laboratory test walls in order to investigate how minor insulation defects affect the surface-averaged thermal resistance. In total, three different insulation densities and three different types of defects were tested. The study indicated that even though the defects were only located in the corners, it affected the natural convection of the entire test wall. Large temperature differences across the test walls and low insulation densities decreased the thermal resistance.

In the mid-1990s, several measurements of large-scale sections of timber frame walls insulated with glass wool were performed in the Hot-Box apparatus at SINTEF Building and Infrastructure/NTNU (Bjerkevoll, 1994; Johannessen, 1995; Jordanger, 1995). All the measurements were performed at standard conditions according to NS-EN-ISO 8990:1996 (1996). The work was performed in order to study natural convection in real timber frame walls. The wall thickness, type of glass wool and temperature conditions were varied. Some of the results were reported by Uvsløkk et al. (1996). The convection measurements in glass wool were summarized and supplemented by Janssen (1997). These measurements on full-size walls showed experimental Nusselt numbers between 1.07 and 1.12 for a wall with 200-mm glass wool insulation dependent on the temperature difference across the wall. A Nusselt number of 1.07 means that the *U*-value of a wall with convection is 7% higher than the *U*-value with no convection. The 300-mm insulated wall gave Nusselt numbers between 1.04 and 1.14. Calculations predicted insignificant amounts of additional heat loss by internal natural convection. A hypothesis of border regions of higher permeability was formulated. The existence of these regions was indicated by air flow measurements by Janssen (1997).

Roofs

Shankar and Hagentoft (2000) performed numerical calculations in order to predict the natural convection in horizontal roof structures. The Ra^* and Nusselt number were calculated given different insulation thicknesses and permeability of the insulation. It was found that an increase in insulation thickness, temperature difference and permeability of insulation material resulted in an increase in the natural convection and heat transfer. However, the calculations only included horizontally oriented insulation and the permeability was rather high ($>7.5 \times 10^{-9}\,m^2$).

Dyrbøl et al. (2002) performed measurements of convection in three different types of insulations. The test section was tested in both the vertical and horizontal positions. A distinct convection-induced heat flux was found, even at material thicknesses as low as 200 mm and a temperature difference across the insulation of

20 K. Furthermore, the risk of convection increasing the total heat flow was found to be related to highly permeable insulation materials. Given a certain level of permeability, convection was able to increase the total heat flow by more than 3% even under the most ideal conditions and at small temperature differences. However, the mean temperature of the insulation was not kept constant which affects the thermal conductivity of the materials.

Wahlgren (2007) presented a thorough literature review studying natural and forced convection in horizontal attic insulation. The study found large differences in reported critical modified Rayleigh numbers and hence the onset of convection. Variations in constructions, material properties, workmanship and boundary conditions were highlighted as reasons for the large differences.

A thorough literature review of convection in highly insulated pitched roofs was conducted by Roels and Langmans (2016) highlighting the use of high-density insulation ($>20\,kg/m^3$) and a continuous and wind tight vapour and wind barrier system in order to construct a well-performing and robust pitched wooden roof.

Convection and the effect on moisture transport

Natural convection in glass wool will not only affect the heat transmittance through the wall but also cause moisture redistribution in walls (Geving and Uvsløkk, 2000; Langmans et al., 2012). The latter occurs when water vapour is transported by the air circulation inside the insulated cavities in the wall. Effects of natural and forced convection on the hygrothermal performance of highly insulated building structures have been studied in laboratory measurements by Langmans et al. (2012), Kalamees and Kurnitski (2010) and Økland (1998). The results showed increased moisture levels at the upper cold part of the walls due to natural convection. It was also stated that an airtight vapour barrier on the warm side is required in order to obtain a moisture safe structure. However, roofs have not been part of these studies.

Objective and scope

The purpose of this study has been to investigate how the angle of inclination and the heat flow direction affect natural convection in thick timber frame structures with cavities filled with air-permeable insulation.

Experimental work

Methods

Natural convection has been studied by laboratory measurements using a rotatable guarded Hot-Box. *U*-value and temperature distribution in the insulation have been measured on a timber frame structure with 500-mm-thick cavities filled with battens of glass wool insulation. *U*-values are calculated on the bases of measured heat flow, metering area and temperature difference across the test section. The

U-value is calculated according to NS-EN-ISO 8990:1996 (1996) and based on the mean value between 12 and 24 one-hour measurement periods. The metering area of the Hot-Box is 2450 mm × 2450 mm. Surface thermal resistance coefficients were adjusted close to the standardized ones prior to the tests by adjusting the air flow velocities adjacent to the surface on both the hot and the cold sides. It is worth noting that during the measurements, the surface thermal resistances may differ slightly from the standardized values. Corrections to the values are made for these deviations so that all U-values are stated with normalized surface thermal resistance coefficients as specified in NS-EN-ISO 8990:1996 (1996). The standardized conditions are interior surface thermal resistance, $R_{si} = 0.13\,\mathrm{W/m^2\,K}$, and external surface resistance, $R_{se} = 0.04\,\mathrm{W/m^2\,K}$. The surface thermal resistances are kept constant for all the measurements.

Test section

The test section was composed of two timber frames of laminated wood. One frame had sills and studs of dimensions 48 mm × 298 mm and the other had sills and studs of dimensions 48 mm × 198 mm, in sum 48 mm × 496 mm. The two timber frames were fixed together using long construction screws and the longitudinal joint between the two timber frames was taped in order to avoid air leakages from one insulation cavity to another. Five of the screws were located within the metering area of the Hot-Box. The overall height of the test section was 2400 mm and the overall width was 3048 mm (see Figure 1). The test section had six vertical studs with centre-to-centre distance of 600 mm. The test section was insulated using glass wool insulation with a nominal heat conductivity of 0.035 W/m K and a density of $16\,\mathrm{kg/m^3}$. In total, four layers of insulation were installed into the cavity: two layers of 150 mm and two layers of 100 mm insulation. Gypsum boards with a thickness of 12.5 mm were fixed on both the cold and warm sides of the timber frame test section.

In order to study the effect of convection on the temperature profile, 39 thermocouples were installed inside and on the cold and warm sides of the test section. The thermocouples in the middle of the insulation layer were located 50, 100 and 150 mm away from the top and bottom sill as well as in the mid-height of the wall (see Figure 2). The thermocouples were of type T. The frames in Figure 2 indicate thermocouples included in Figures 9–12.

Boundary conditions and test sequence

Natural convection is affected by several parameters. In this study, the angle of inclination, the heat flow direction and the temperature difference across the test section have been varied. The measurements were performed at a temperature difference of 20 and 40 K across the test section and a constant mean temperature of 10°C. Measurements were performed with the test section in the following positions: wall, roof with pitch of 30° and 60° in addition to horizontal roof and floor.

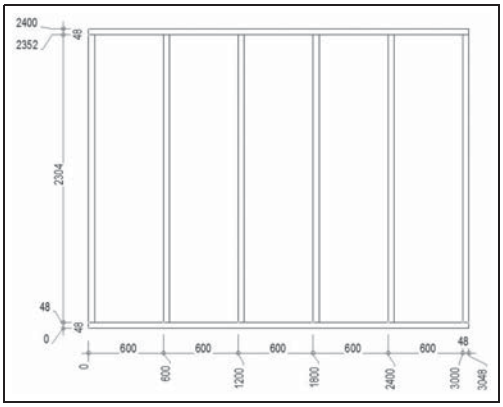

Figure 1. Cross section of the timber frame test section (dimensions in mm).

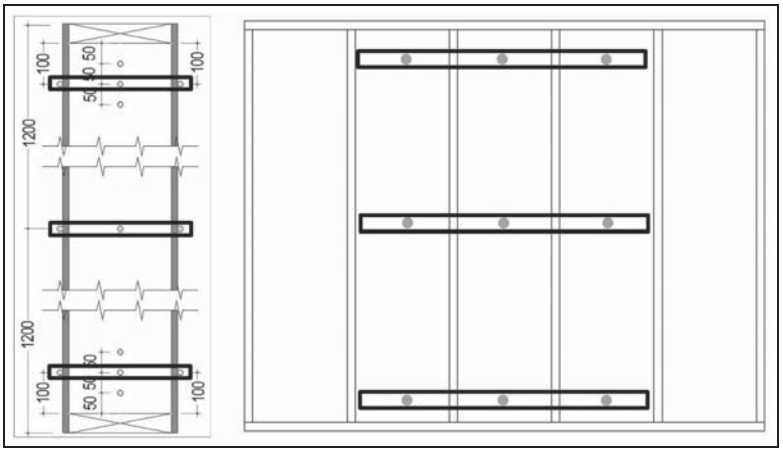

Figure 2. Positions of the 39 thermocouples, indicated by dots, inside (cross section to the left) and on the cold and warm surfaces of the test section (elevation view to the right). Frames indicate the position of the thermocouples included in Figures 9–12.

The tests were performed in steady-state conditions at temperature levels shown in Table 1. The test section was positioned between the hot and cold room of the guarded Hot-Box, as seen in Figure 3. In general, each test lasted for about 48 h in order to achieve a measurement period of at least 12 h with stable conditions.

Table 1. Overview of the variable tests and the conditions during the measurements.

Test variant	Angle of inclination (°)					Temperature cold room (°C)		Temperature warm room (°C)	
	90	60	30	0	180	0	−10	20	30
1	X					X		X	
2		X				X		X	
3			X			X		X	
4				X		X		X	
5					X	X		X	
6	X						X		X
7		X					X		X
8			X				X		X
9				X			X		X
10					X		X		X

Figure 3. The rotatable Hot-Box test facility. To the left, the test section is positioned as a floor (cold room below the test section). To the right, the angle of inclination of the test section is 30°.

Uncertainty assessment of Hot-Box measurements

Grynning et al. (2015) performed an assessment of the uncertainties associated with the Hot-Box measurements. The assessment was conducted with the identical Hot-Box as used in this study. The assessment was performed according to the procedure described in NS-EN-ISO 12567-1:2010 (2010). The uncertainties were stated with a coverage factor of two standard deviations and the corresponding 95%

confidence interval. The uncertainty assessment of this study is based on the work performed by Grynning et al. (2015).

As shown in equation (5) the root-mean-square (RMS) method is used to derive the uncertainty propagation of the measured U-value total uncertainty propagation $\Delta^P U_w/U_w$

$$\frac{\Delta^P U_w}{U_w} = \sqrt{\left[\frac{\Delta^P \Phi_w}{\Phi_w}\right]^2 + \left[\frac{\Delta^P A_w}{A_w}\right]^2 + \left[\frac{\Delta^P \delta\theta_{ie}}{\theta_{ie}}\right]^2} \tag{5}$$

where $\Delta^P \Phi_w/\Phi_w$ is the uncertainty of the sample heat flow (W), $\Delta^P A_w/A_w$ is the uncertainty in the measurement area and $\Delta^P \delta\theta_{ie}/\theta_{ie}$ is the uncertainty in the temperature difference between the cold and sides of the Hot-Box.

The uncertainty of the sample heat flow is based on the heat balance equation of the test chamber. Uncertainty of $\Delta^P \Phi_w/\Phi_w$ is expressed in equation (6)

$$\frac{\Delta^P \Phi_w}{\Phi_w} = \sqrt{\left[\frac{\Delta^P \Phi_{IN}}{\Phi_w}\right]^2 + \left[\frac{\Delta^P \Phi_{EXTR}}{\Phi_w}\right]^2 + \left[\frac{\Delta^P \Phi_{FL,w}}{\Phi_w}\right]} \tag{6}$$

where $\Delta^P \Phi_{IN}/\Phi_w$ is the uncertainty in power input to metering chamber (W), $\Delta^P \Phi_{EXTR}/\Phi_w$ is the uncertainty of the metering chamber heat flows and $\Delta^P \Phi_{FL,w}/\Phi_w$ is the uncertainty in the test sample flanking heat loss (W).

No correlation between the various terms of the balance equation was found. Using a temperature reference bath, Grynning et al. (2015) found that the relative scattering in measured temperatures was lower than 0.02 K.

Many uncertainties and systematic errors are avoided by conducting comparative measurements as done in this study. The test section is inserted only once into the Hot-Box apparatus. By comparing the results from different test conditions (angle and temperature), the uncertainties of metering area, heat conductivity of the materials and possible errors when inserting the test section into the apparatus are minimized. This is of course influencing the results of equations (5) and (6).

However, rotating the Hot-Box means introducing some new uncertainties compared to the measurements performed by Grynning et al. (2015). First of all, rotating the Hot-Box introduces a possibility that the measurement chamber can move in relation to the test section. To control this, the measurement chamber is equipped with actuators so that the position can be controlled outside the Hot-Box. Rotating the Hot-Box also affects the surface thermal resistance. By measuring the temperature on both the cold and the warm surfaces of the test section, in addition to the air temperature in the cold and the warm chambers, the interior surface thermal resistance and the external surface resistance are measured.

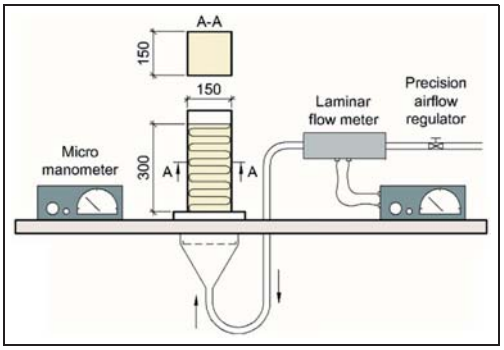

Figure 4. Principle of the apparatus used to measure the permeability of the glass wool.

Air permeability of the insulation material

Air permeability of the glass wool was measured according to NS-EN-ISO 9053:1993 (1993) using equation (2). The apparatus is shown in Figure 4. The air flow rate through the specimen is measured using a laminar flowmeter. The air pressure difference across the test specimen is measured using a micromanometer. The glass wool specimens were sawn with a band saw to fit the apparatus. The specimens were conditioned in laboratory climate (~20°C) and weighed before testing in order to calculate the density.

Three different test specimens both from the 150-mm insulation layer and the 100-mm insulation layer were taken from two different insulation batts. The specimen dimension perpendicular to the flow direction was oversized by 5 mm. Identical specimens were used to measure the permeability parallel and perpendicular to the fibre direction.

Equivalent air permeability of the insulated cavities

In order to measure the air flow resistance of the insulated cavities of the test section, an airtight box was constructed. The box had a length of 600 mm, width of 500 mm and a height of 200 mm. In order to secure an evenly distributed air flow, a perforated steel sheet was placed perpendicular to the air flow in the middle of the box.

When measuring the practical air permeability of the test section, the bottom and top sills of the test section were dismounted. The box was fixed to each insulated cavity to measure air flow resistance through the insulated cavity (see Figure 5). The box was fixed to a pair of studs and the perimeter of the box was

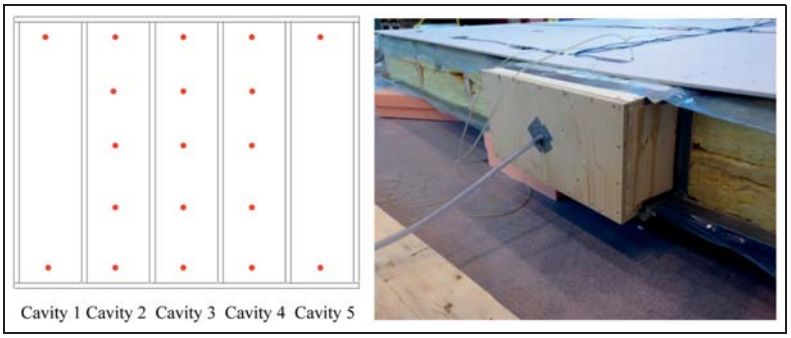

Figure 5. Equipment used for measuring equivalent air permeability of the insulated cavities of the test section. Red dots indicate positions of air pressure measurements (test section seen from the cold side).

sealed to the test section. A rotameter was attached to the box in order to measure the air flow. In order to calculate the air flow resistance and an equivalent permeability, the pressure drop inside the cavities with glass wool insulation was measured (see Figure 5). The equivalent permeability was calculated according to equation (2). In cavity numbers 2, 3 and 4 from the left-hand image, the pressure difference was measured for a 500-mm centre-to-centre distance. This was done in order to examine whether the air flow resistance of the insulated cavities was evenly distributed through the cavity. In cavity 1 and 5, the distance between the holes was 2000 mm. The pressure was measured at three different air flows: 5, 7 and 10 m^3/h.

Results

Hot-Box measurements

U-values derived from the Hot-Box measurements, surrounding conditions and the calculated modified Rayleigh number and Nusselt number for the different test variants are shown in Table 2. The modified Rayleigh number is calculated according to equations (1) and (3).

The Nusselt number is calculated by dividing each of the measured *U*-values by the measured *U*-value at a 180° angle assuming that there is no convection in the insulated cavities when the test section is in a floor position with the heat flow direction downwards.

The Nusselt number is increasing rapidly with increasing *Ra** for the 30° and 60° angles.

Table 2. Results from the Hot-Box measurements.

Test variant	Angle (°)	θ_e (°C)	θ_i (°C)	$\bar{\theta}$ (°C)	$\Delta\theta_{ie}$ (K)	*U*-value (W/m^2 K)	Modified Rayleigh number	Nusselt number
1	90	0	20	10	20	0.0845 ± 0.004	4.12	1.08 ± 0.077
2	60	0	20	10	20	0.0836 ± 0.004	4.12	1.06 ± 0.076
3	30	0	20	10	20	0.0855 ± 0.004	4.12	1.09 ± 0.078
4	0	0	20	10	20	0.0848 ± 0.004	4.12	1.08 ± 0.072
5	180	0	20	10	20	0.0785 ± 0.004	4.12	1.00 ± 0.049
6	90	−10	30	10	40	0.0906 ± 0.005	8.24	1.15 ± 0.092
7	60	−10	30	10	40	0.1010 ± 0.005	8.24	1.29 ± 0.100
8	30	−10	30	10	40	0.1024 ± 0.005	8.24	1.30 ± 0.103
9	0	−10	30	10	40	0.0860 ± 0.005	8.24	1.09 ± 0.087
10	180	−10	30	10	40	0.0780 ± 0.005	8.24	1.00 ± 0.059

Permeability of the insulation material

Figure 6 shows the measured permeability of the 100- and 150-mm-thick glass wool specimens as a function of the density of the glass wool. The average measured permeability perpendicular ($\perp$) and parallel ($\parallel$) to the main fibre direction was 1.62×10^{-9} m^2 and 4.25×10^{-9} m^2, respectively. The measured density of the different specimens varied from 16.3 to 19.0 kg/m^3.

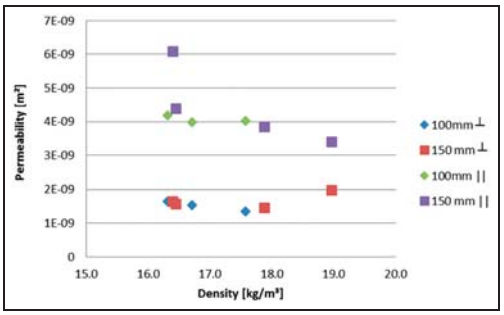

Figure 6. Permeability perpendicular and parallel to the main fibre direction as a function of the density of the glass wool specimen.

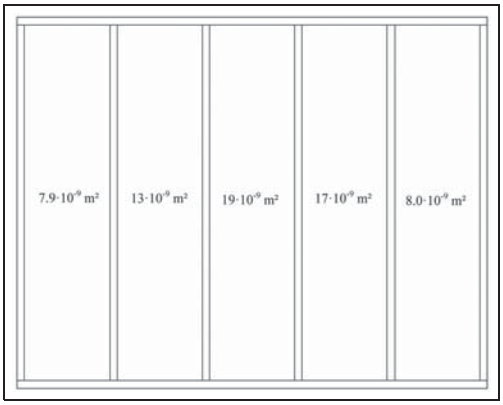

Figure 7. Measured equivalent permeability of the insulated cavities (test section seen from the warm side).

Figure 8. Air gaps in transition zones between the layers of insulation and between the insulation and the wood frame.

Measured equivalent permeability of the insulated cavities in the test section

Figure 7 shows the results from the air flow resistance measurements of each of the five cavities in the test section. The equivalent permeability was calculated using equation (2).

The average equivalent air permeability of the four cavities was $14 \times 10^{-9}\,\mathrm{m}^2$. In practice, with a total of four insulation layers, it is difficult to fill all the cavities precisely without any air gaps, as seen in Figure 8. The photo shows the bottom of the test section after the bottom beam has been removed. The tape which was used to seal the longitudinal joint in the bottom sill of the specimen was not removed before taking the picture.

Temperature distribution through the insulation layers

Figures 9–12 show the measured temperature profiles through the insulation layers in the three cavities, identified in Figure 2, at a temperature difference of 40 K

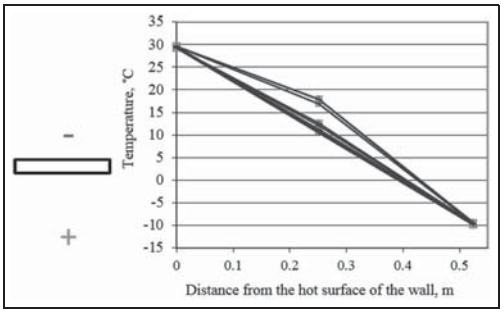

Figure 9. Temperature at the cold and warm surfaces of the test section and in the centre of the glass wool insulation, when oriented as a horizontal roof (see sectional drawing to the left).

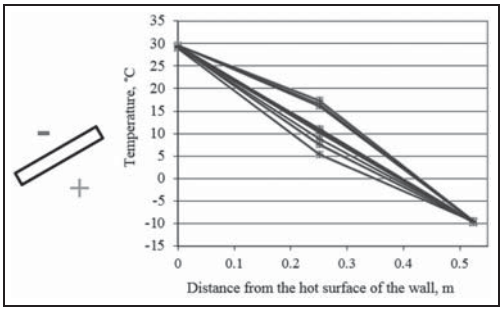

Figure 10. Temperature on the cold and warm surfaces of the test section and in the centre of the glass wool insulation at a 30° inclination (pitched roof).

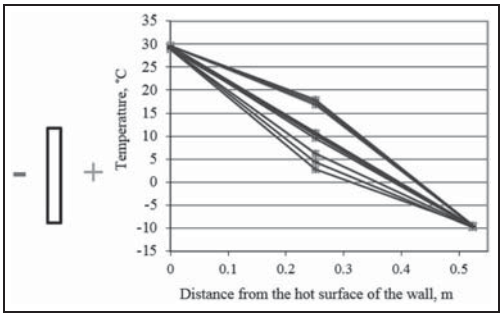

Figure 11. Temperature at the cold and warm surfaces of the test section and in the centre of the glass wool insulation, oriented as a wall.

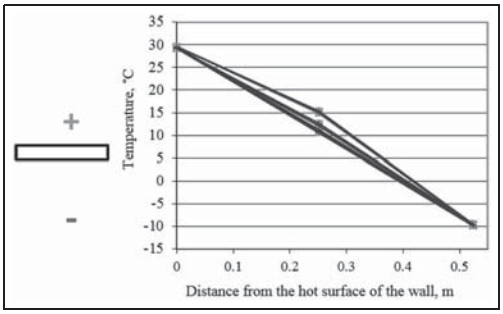

Figure 12. Temperature at the cold and warm surfaces of the test section and in the centre of the glass wool insulation, oriented as a floor.

across the test section. Figures 9–12 include three temperature profiles in each cavity, which means nine temperature profiles in total. Each profile consists of 24 hourly averaged values drawn on top of each other. The inclination of the test section is illustrated by a sectional drawing to the left. Only a range of the measurements is shown in this work. Temperature profiles that deviate from a straight line indicate convection in the insulation layer.

Discussion

Several laboratory studies have been performed prior to this study. However, these prior investigations have only included structures with insulation thicknesses up to 300 mm. A focus on energy efficiency in the building stock has made the building sector move towards more insulated structures. Therefore, it is highly relevant for the construction industry to increase its knowledge about convection in highly insulated structures, for example, >300 mm insulation thickness.

Angle of inclination

Given a temperature difference of 20 K, the Nusselt number is approximately equal for the angles 90°, 30° and 0°. By increasing the temperature difference to 40 K, the Nusselt number increases for all angles except for the horizontal roof configuration. Angles of 30° and 60° and a temperature difference of 40 K give the highest Nusselt number, showing that the pitched roof configuration gives the highest *U*-values for the test section. For the 30° and 60° inclinations, there is an approximately 25% increase in the Nusselt number when the temperature difference increases from 20 to 40 K.

According to NS-EN ISO 10456:2007 (2007), natural convection can be neglected if $Ra^* < 2.5$. The results from this study, given an insulation thickness of 500 mm, are in line with this. Previous studies by Bankvall (1972) indicate that there will be no convection in wall structures with Ra^* below 6 when the ratio is 5 between height and thickness of the cavities. The results of this study show that a Ra^* of 4 gives significant convection for all angles except for the floor configuration. Measurements performed by Uvsløkk et al. (2010) on a timber frame wall with a 300-mm glass wool insulation showed convection for Ra^* of 3.7. A literature review performed by Wahlgren (2007) shows that previous studies indicate no convection for a Ra^* below 10–30 for the horizontal roof configuration. This study of a timber frame structure with an insulation thickness of 500 mm shows that the onset of convection occurs at a lower Ra^* than the previous studies have shown. The main reason for this is most likely imperfections in the insulation layer in real timber frame structures giving a lower flow resistance than indicated by the permeability measurements of the insulation material.

Temperature difference over the test section

The results show that an increased temperature difference results in increased convection and hence increased practical *U*-values for the timber frame structures. The effect is largest for pitched roofs and wall configurations. The average temperature has been kept constant in this study. Janssen (1997) calculated a Nusselt number between 1.07 and 1.12 based on Hot-Box measurements on a full-size (2400 mm $\times$ 3048 mm) timber frame wall with 200 mm glass wool insulation dependent on the temperature difference over the wall. For a timber frame wall with 300-mm glass wool, the Nusselt number varied between 1.04 and 1.14. Janssen's measurements were carried out in the same Hot-Box apparatus as used in this study. The calculated Nusselt numbers based on measurements from this study of a timber frame structure with 500-mm glass wool varied from 1.08 ($\Delta\theta_{ie} = 20$) to 1.15 ($\Delta\theta_{ie} = 40$). The results of this study are in line with the former studies performed by Janssen (1997) and Uvsløkk (1996).

Given a horizontal roof structure and a permeability for the insulation material of $7.5 \times 10^{-9}\,m^2$, the calculations of Shankar and Hagentoft (2000) give a Nusselt number of approximately 1.3 for an insulation thickness of 500 mm and a temperature difference of 40 K. The comparable measured Nusselt number of this study is 1.09. The permeability of the glass wool used in this study for glass wool perpendicular and parallel to the main fibre direction was $1.62 \times 10^{-9}\,m^2$ and $4.25 \times 10^{-9}\,m^2$, respectively. It is difficult to compare the results when the permeabilities are so different. However, the rather large difference in the calculated and measured Nusselt number shows that low permeability is favourable considering natural convection.

This study also shows a big increase in the Nusselt number for the 30° and 60° inclinations when the temperature difference is raised from 20 to 40 K. A possible explanation is that an increased temperature difference and a larger driving force

imply formation of more convection loops inside the test section. However, formation of such loops cannot be seen from the temperature profiles in Figure 10.

Permeability of insulation material

The permeability is approximately twice as large parallel to the main fibre direction compared to when it is perpendicular to the main fibre direction. The measured permeability of the insulation material perpendicular and parallel to the main fibre direction was $1.62 \times 10^{-9}\,m^2$ and $4.25 \times 10^{-9}\,m^2$, respectively, for glass wool specimens from the same batch as used in the test section. This is in line with previous results from Økland (1998) and Dyrbøl et al. (2002). Uvsløkk et al. (2010) measured a permeability of $2.5 \times 10^{-9}\,m^2$ and $5.1 \times 10^{-9}\,m^2$ perpendicular and parallel to the main fibre direction, respectively. The higher permeability can be explained by a lower density of the glass wool of $13.2\,kg/m^3$. Generally, the permeability measurements performed in this study show approximately 10% greater permeability for the 150 mm batts compared to the 100 mm batts. The results cannot be explained by difference in density of the insulation. One main reason for the difference is that the 100-mm insulation was installed in three layers, while the 150-mm insulation was installed in two layers in the test apparatus. This could imply some differences in the installation of the specimens. Three layers of insulation also imply a possible lower permeability because of the surface resistance of the glass wool.

Equivalent permeability of insulated cavities

The average equivalent permeability, calculated on the basis of the air flow and pressure gradient measurements in the insulated cavities of the test section, was $14 \times 10^{-9}\,m^2$. This is nearly ten times larger than the measured permeability of the insulation material samples. This average equivalent permeability cannot be used for accurate estimation of Ra^*, but gives a good indication on the deviation between theoretical and practical flow resistance in insulated cavities. Note that there is a factor two ratio between the smallest and the largest equivalent air permeability numbers of the insulation cavities. Cavity 1 and 5 has considerable lower permeability compared to cavity 2, 3 and 4. A likely explanation is the differences in workmanship. As Figure 8 shows, there are some air gaps in the transition zones between the insulation layers and between the insulation and the timber frame. Large insulation thickness often means that for practical reasons, the insulation must be installed in several layers within the structure. This implies more transition zones and higher risk of imperfections and increased equivalent permeability of the insulated cavities. Even when the insulation is carefully installed as done in the experiments, there might be imperfections in transition zones between the insulation and the timber frame and between the different layers of insulation. In practice, with a total of four insulation layers, it is difficult to fill all the cavities precisely, as seen in Figure 8.

The air flow due to natural convection appears primarily in the zones near the cladding board on the exterior and interior sides of the test section where the pressure gradients are largest. Air gaps near the surfaces of the test section will increase the risk of convection while air gaps in the middle of the insulation will affect the natural convection to a smaller extent because of smaller driving forces.

Temperature profiles

The temperature profiles clearly show convection in the pitched roof and wall positions. In the floor situation, there is theoretically no potential for convection. Figure 12 shows the temperature profiles when there is no convection. As Figure 12 shows, there is some dissipation in the diagram, including where there is no theoretical potential for convection. When the insulation thickness is 500 mm, accurate positioning of the thermocouples in the middle of the insulation is challenging and a likely explanation is inaccurate positioning of the thermocouples.

Recommendations and measures to reduce the risk of convection

For practical application, natural convection can be reduced by dividing the insulation layer with a vapour-open convection barrier. Using this approach, the temperature gradient is reduced thus lowering the driving force.

Conclusion

Both the temperature difference across the test section and the angle of inclination of the test section affect the convection in the insulated cavities giving increased *U*-values and Nusselt numbers. Also, measured temperature profiles inside the insulation cavity clearly show convection in the test section for the pitched roof and wall configurations. For practical application, an efficient measure to reduce the natural convection is to divide the insulation layer into two thinner layers using a vapour-open convection barrier for walls and roof structures. Even though the insulation was carefully installed, insulation mistakes were discovered. The authors recommend use of a convection barrier in both wall and pitched roof structures if the insulation thickness exceeds 200 mm. A convection barrier will also reduce the impact of mistakes in the insulation. The use of a convection barrier is by that a simple means to reduce the risk of moisture problems and heat loss from a structure and thereby the energy use of buildings during operation.

Declaration of Conflicting Interests

The author(s) declared no potential conflicts of interest with respect to the research, authorship and/or publication of this article.

Funding

The author(s) disclosed receipt of the following financial support for the research, authorship, and/or publication of this article: The authors gratefully acknowledge the financial support by the Research Council of Norway and several partners through the Centre for Research-based Innovation Klima 2050 (HYPERLINK "http://www.klima2050.no" www.klima2050.no) and the Research Centre on Zero Emission Buildings (HYPERLINK "http://www.zeb.no" www.zeb.no).

References

Bankvall C (1972) *Natural convective heat transfer in insulated structures*, Report no. 38. Lund: Lund Institute of Technology (Division of Building and Technology), 1 January 1972.

Bjerkevoll GO (1994) *Hot-Box målinger på høyisolerte bygningskonstruksjoner* [Hot-Box measurements on highly insulated building constructions]. Master Thesis, Hovedoppgave, NTH, Trondheim (in Norwegian).

Brown WC, Bomberg MT, Ullett JM, et al. (1993) Measured thermal resistance of frame walls with defects in the installation of mineral fibre insulation. *Journal of Thermal Insulation and Building Envelopes* 16: 318–339.

Dyrbøl S, Svendsen S and Elmroth A (2002) Experimental investigation of the effect of natural convection on heat transfer in mineral wool. *Journal of Building Physics* 26: 153–164.

Geving S (2011) *Fuktskader Årsaker, Utbedringer og tiltak* [Moisture Damage, Causes, Repair]. Oslo: SINTEF Byggforsk (in Norwegian).

Geving S and Uvsløkk S (2000) *Moisture conditions in timber frame roof and wall structures*. Project report 273. Oslo: Norwegian Building Research Institute, 01 March 2000.

Grynning S, Misiopecki C, Uvsløkk S, et al. (2015) Thermal performance of in-between shading systems in multilayer glazing units: Hot-Box measurements and numerical simulations. *Journal of Building Physics* 39: 147–169.

Gullbrekken L, Geving S, Time B, et al. (2015) Moisture conditions in well-insulated wood-frame walls. Simulations, laboratory measurements and field measurements. *Wood Material Science & Engineering* 10(3): 232–244.

Janssen H (1997) *Thermal performance of highly insulated wood frame walls*. Master's Thesis, KUL NTNU, Trondheim.

Johannessen E (1995) *Hot-Box målinger på høyisolerte bygningskonstruksjoner* [Hot-Box measurements on highly insulated building constructions]. Master Thesis, Hovedoppgave, NTH, Trondheim (in Norwegian).

Jordanger GO (1995) *Naturlig konveksjon i vegger laboratorieforsøk* [*Natural convection in walls laboratory measurements*]. Master Thesis, Hovedoppgave, NTH, Trondheim (in Norwegian).

Kalamees T and Kurnitski J (2010) Moisture convection performance of external walls and roofs. *Journal of Building Physics* 33: 225–247.

Langmans J, Klein R and Roels S (2012) Hygrothermal risks of using exterior air barrier systems for highly insulated light weight walls: a laboratory investigation. *Building and Environment* 56: 192–202.

Lecompte J (1990) The influence of natural convection on the thermal quality of insulated cavity construction. *Building Research and Practice* 6: 346–354.

Marmolet L, Lewandowski M and Perwuelz A (2012) An air permeability study of anisotropic glass wool fibrous products. *Transport in Porous Media* 93: 79–97.

NS-EN-ISO 10456:2007 (2007) Hygrothermal properties – tabulated design values and procedures for determining declared and design thermal values.

NS-EN-ISO 12567-1:2010 (2010) Thermal performance of windows and doors – determination of thermal transmittance by the hot-box method – part 1: complete windows and doors.

NS-EN-ISO 8990:1996 (1996) Thermal insulation – determination of steady-state thermal transmission properties – calibrated and guarded hot box.

NS-EN-ISO 9053:1993 (1993) Acoustics materials for acoustical applications – determination of airflow resistance.

Økland Ø (1998) *Convection in highly-insulated building structures*. Doctoral Thesis 1998:86 NTNU, Norwegian University of Science and Technology (NTNU), Trondheim.

Roels S and Langmans J (2016) Highly insulated pitched roofs resilient to air flow patterns: guidelines based on a literature review. *Energy and Buildings*. Available at: http://dx.doi.org/10.1016/j.enbuild.2016.03.071

Shankar V and Hagentoft CE (2000) A numerical study of effect of natural convection on thermal properties of horizontal oriented porous insulation. *Journal of Building Physics* 24: 155–167.

Uvsløkk S, Skogstad HB and Aske IJ (1996) Natural convection in timber frame walls with thick thermal insulation layer. In: *Nordic building physics conference*, Espoo, 9–10 September.

Uvsløkk S, Skogstad HB and Grynning S (2010) How to prevent natural convection causing extra heat loss and moisture problems in thick insulation layers. In: *3rd Nordic passive house conference*, Aalborg, 7–8 October.

Wahlgren P (2007) Overview and literature survey of natural and forced convection in attic insulation. *Journal of Building Physics* 30: 351–370.

Paper IV

Paper 4

L. Gullbrekken, T. Kvande, B. Time

Ventilated wooden roofs:
Influence of local weather conditions – measurements

11th Nordic Symposium on Building Physics, Trondheim, Norway, 11-14. June 2017. Energy Procedia, Vol. 132, 2017, pages 777-782.

Available online at www.sciencedirect.com

ScienceDirect

Energy Procedia 132 (2017) 777–782

Energy Procedia

www.elsevier.com/locate/procedia

11th Nordic Symposium on Building Physics, NSB2017, 11-14 June 2017, Trondheim, Norway

Ventilated wooden roofs: Influence of local weather conditions - measurements

Lars Gullbrekken[a]*, Tore Kvande[a], Berit Time[b]

[a]*NTNU, Department of Civil and Environmental Engineering, Høgskoleringen 7A 7046 Trondheim, Norway*
[b]*SINTEF Building and Infrastructure, Department of Materials and Structures, Høgskoleringen 7B 7046 Trondheim, Norway*

Abstract

This study investigates the influence of temperature and air velocity conditions on ventilation and condensation in spring, summer and autumn periods inside a ventilated cavity in a full-scale wooden roof construction. The roof has 81 thermocouples, four air velocity measurement devices, and a weather station to record temperature and wind velocity. The temperature measurements show large periods of below-ambient temperature, especially during the spring and autumn. A strong correlation exists between the wind speed and air velocity inside the air cavity. Eave-to-eave ventilation was found to be effective, even with a roof angle of 40°.

Peer-review under responsibility of the organizing committee of the 11th Nordic Symposium on Building Physics.

Keywords: Roof; Pitched; Wooden; Field experiments; wind speed; air velocity

1. Main text

Pitched load-bearing wooden roof constructions with a ventilated air layer beneath the roofing is a typical construction in Central Europe [1] and Norway [2]. The purpose of the ventilated air layer is to 1) ventilate heat and prevent formation of ice on the eaves and gutters, 2) ventilate humidity from the roof construction and prevent formation of mould and rot inside the construction [3-5]. Hygrothermal conditions inside air cavities in roofs have been investigated by [5-7]. Measurements performed by [5] showed that a ventilation channel with a height between 48 mm and 98 mm was sufficient up to roof lengths of 7–8 m. Eaves-to-eaves ventilation was found to be very effective, given a low roof pitch. During a measuring period of 22 days, it was found that for 86 % of the time, the surface temperature of the roofing was lower than the air temperature. Hens and Janssens [6] found negative effects

* Corresponding author. Tel.: +47 454 74 324;
E-mail address: lars.gullbrekken@sintef.no

1876-6102
Peer-review under responsibility of the organizing committee of the 11th Nordic Symposium on Building Physics
10.1016/j.egypro.2017.10.029

due to air leakages and wind washing for the hygrothermal response and durability of insulated pitched wooden roofs. They stated that a ventilated air layer between the underlayer roofing and insulation was unnecessary [6] in roof constructions with vapour open underlayer roofing materials, as given by [4].

The purpose of this paper is to 1) map the risk of condensation on the interior surface of the ventilation cavity as given in [4] and 2) map the air cavity velocity dependency on the outside wind speed.

2. Method

The measurements were conducted on a full-scale experimental building, ZEB Test Cell Laboratory, located at the NTNU campus in Trondheim, 63°24'52.0"N 10°24'32.3"E, see Figure 1. The rectangular-shaped roof air cavity is 552 mm wide, 48 mm high and 10.8 m long. The roof angle was 40°. The lower surface in the ventilation gap consisted of a flexible underlayer roof on top of a 12.5 mm oriented strand board (OSB) board. The top of the air gap consists of an OSB board with a bitumen membrane roofing. As observed in Figure 2, there is no opening in the ridge of the roof; the roof is ventilated from eaves to eaves through a 48 mm wide opening in the eaves behind the gutter.

The building has a weather station located 10 m above ground level (see Figure 1). The exterior temperature, wind speed and direction were recorded at one-minute intervals.

In total, nine air cavities in parallel had nine thermocouples in each cavity, resulting in a total of 81 thermocouples. In each cavity, the sensors were distributed 0.5 m above the eaves, between the eave and the ridge, and 0.5 m below the ridge (see Figure 2). In the cross-section, the thermocouples were positioned on the lower-facing surface of the roofing, in the middle of the air cavity and on the surface of the underlayer roof. Two of the air cavities also had air pressure devices and omnidirectional remote air velocity probes (see Figure 1). The accuracy and measuring range of the applied devices are given in Table 1. The logger interval was set to one minute.

Table 1. Accuracy and measuring range of applied sensors

Sensor	Manufacturer	Type	Accuracy	Range
Thermocouple		Type T	±0.10 °C	-20–+60 °C
Pressure gauge	Kimo	SPI2-100	±0.2 % of reading	-100–+100 Pa
Air velocity	Kimo	SVO: omnidirectional	0.05 m/s or ±3 %	0.05–5 m/s

Fig. 1. Left: the omnidirectional air velocity measurement device. Right: the ZEB Test Cell Laboratory located at the NTNU campus in Trondheim. The weather station is positioned 10 m above ground level, 1.5 m above the ridge of the roof.

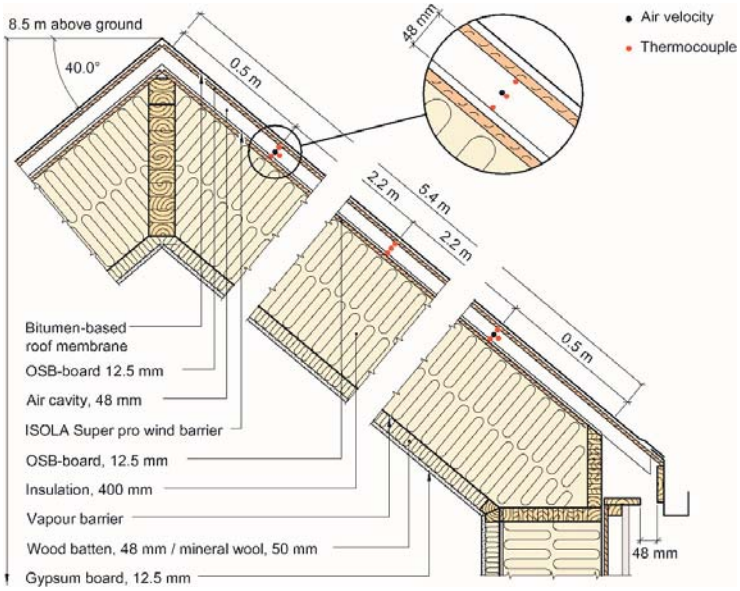

Fig.2. The roof structure in the ZEB Test Cell Laboratory and position of the thermocouples and the air velocity measuring device. The circle indicates the position from which the air velocity data is recorded.

3. Results

The results include temperature, air velocity and wind velocity during spring (March 22nd to March 31st), summer (July 3rd to 15th) and autumn (September 21st to 29th). Figure 3 and 4 shows the temperatures of the south side (160°) of the roof. The outdoor temperature, temperature on the underlayer roof, air temperature inside one of the air cavities and on the lower surface of the roofing during spring and summer are also given in Figure 3. Figure 4 shows the outdoor temperature and temperatures inside the air cavity during an autumn period. Table 2 gives the temperature conditions inside the air cavity.

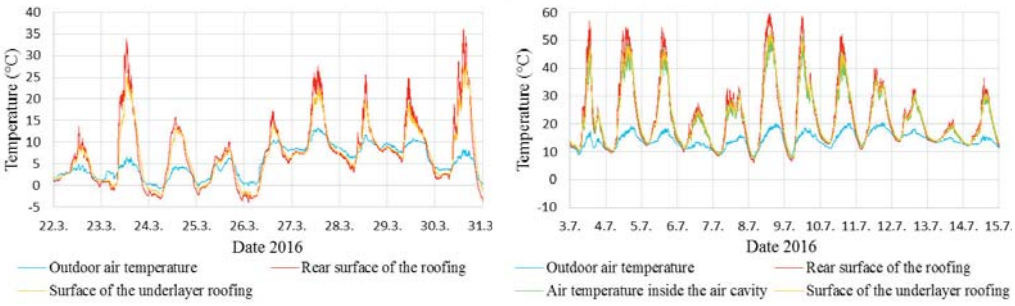

Fig. 3 Left: outdoor air temperature, temperature on the lower surface of the roofing, and temperature on the underlayer roof in the period from March 22nd to March 31st. Right: the air temperature inside the air cavity in the period from July 3rd to 15th. Recorded values are taken 2.2 m from the ridge.

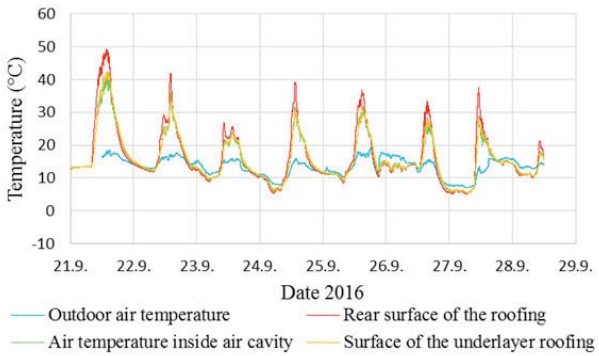

Figure 4: Outdoor air temperature, temperature on the lower surface of the roofing, and temperature on the underlayer roofing in the period from September 21st to 29th. Recorded values are taken 2.2 m from the ridge.

Table 2. Temperature conditions during the three periods inside the roof air cavity of the south side of the roof; measurements from the middle position of the roof.

	Lower surface of roofing			Top surface of the underlayer roofing		
Period	Share of period with temp. lower than outdoor air temp.	Largest temperature difference below ambient temperature	Maximum temperature	Share of period with temp. lower than outdoor air temp.	Largest temperature difference below ambient temperature	Maximum temperature
22.3–31.3	51 %	5 °C	36 °C	50 %	5 °C	28 °C
3.7–15.7	14 %	3 °C	60 °C	5 %	3 °C	57 °C
21.9–29.9	56 %	11 °C	49 °C	55 %	9 °C	47 °C

Figure 5 shows the air velocity inside the air cavity beneath the roofing as a function of the wind speed at 10 m above ground level. The air velocity device is positioned 0.5 m from the ridge at the north side of the roof.

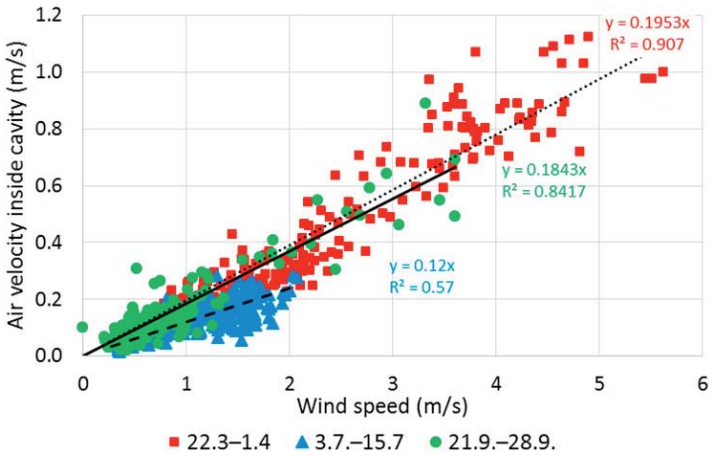

Fig. 5. Air velocity inside the air cavity for different seasons/periods as a function of wind speed at 10 m above ground level. The presented results are hourly averaged values calculated from raw data with a one-minute measuring interval.

4. Discussion

The measured temperatures presented in Figures 3 and 4 and Table 2 are results from the position between the ridge and the eave (mid-position) of the roof facing south. Figure 5 gives the measured air velocities in a position 0.5 m from the ridge in the air cavity for the roof slope facing north. Generally, the air velocity was higher lower down the roof (near the eaves) because of external wind fluctuations.

The measuring periods represent the conditions during a one-week period in the spring and autumn, and a twelve-day period during summer. The weather conditions during the start of the spring period included low temperatures around 0–5 °C, low wind speeds and periods of clear sky conditions, as recorded in Figure 3. At the end of the period, the temperature increased to around 5–10 °C and the wind speed was higher (typically a fresh breeze). During the summer period, the first three days had light sky cover, low wind speed and maximum temperatures of 15 °C. The next two days were cloudy and the last few days had long periods of clear sky and a maximum outdoor air temperature of 18 °C. The maximum temperature on the lower surface of the roofing during this period was close to 60 °C. The low temperatures in the roof structure on July 13th were caused by rainy conditions (see Figure 3). During the autumn period, the temperature ranged from 11 to 17 °C and there were generally low wind speeds. During the first two days, the sky cover was light with some sun (see Figure 4). On September 23rd, the sky was cloudy and for the rest of the period, the sky had a light cover. To summarize, the weather conditions during the measurement periods were quite typical for the seasonal climate in the location. The measuring periods do not include periods with snow on the roof.

The measurements show long periods where the temperature inside the air cavity is below the outdoor air temperature, also including periods of clear sky in the summer. Measurements performed by [5] showed surface temperatures below the ambient temperature for 86 % of the 22-day period with no snow on the roofing in the period from 14.1 to 24.3. An identical roof to the ZEB Test Cell Laboratory roof but with only 200 mm insulation showed surface temperatures below the ambient temperature on the underlayer roof 33 % of the time for a measurement period of 89 days [5].

The results from the ZEB Test Cell Laboratory roof during spring and autumn showed surface temperatures below the ambient temperatures for approximately half of the period. The measurements also show high temperatures in summer periods (up to 60 °C); note that the roofing color was dark. For this specific roof, there is a low risk of visible condensation droplets on the lower surface of the roofing due to the hygrothermal properties of the OSB board. However, high humidity levels increase the risk of mould growth on the OSB board. High summer temperatures, at least for the roof section oriented south, will terminate the mould growth [8]. Given a different roofing material, e.g. metal sheeting, the risk of condensation on the lower surface of the roofing is much larger. With metal sheeting, the condensation will represent an extra strain, and corrosion protection on the lower surface is therefore necessary. Condensation droplets on the underlayer roof also increase the risk of water leakages into the roof construction.

During the spring and autumn, a strong correlation was found between the wind velocity at 10 m above ground level and the air velocity inside the cavity below the roofing. These results are in line with the results from a similar roof construction reported by Blom [5]. However, the current study includes lower air velocities and wind speeds because devices with a higher resolution and better accuracy were used. During the summer, the correlation between the air velocity and the wind speed was less pronounced. A possible reason for this might be that the period only included days with low wind speeds.

Based on the measurements of air velocity, air change rates inside the air cavity were calculated. During the three measuring periods, the average air change rate varied from 38 to 133 h^{-1}. Fluctuating wind speed and air velocity means that the ratio between the air velocity and wind speed also fluctuates. Inside a ventilated air cavity, the air flow pattern is unstable and frequently alters between upward and downward air flows. Consequently, the air change rates estimated using omnidirectional anemometers are overestimated. A reduction factor for the air change rate of 5–40 % was proposed by [9]. The position of the air velocity measurement device is in the center of the air cavity. The middle air velocity is smaller than the air velocity measured at the center of the air cavity. Falk (2010) proposed a relationship between the middle velocity and maximum velocity, measured at the center of an air cavity, of ½ – ⅔ in an air cavity behind a wall cladding [10]. Given the above-mentioned reduction factors, the average air change rate of the three measuring periods can be estimated between 11 h^{-1} and 84 h^{-1}. This imply that eaves-to-eaves ventilation can be exploited effectively for ventilation of gabled roofs.

5. Conclusions

The measurements on the ZEB Test Cell Laboratory roof show long periods with surface temperatures below the ambient temperatures, especially during the spring and autumn periods. A strong correlation was found between the wind speed and air velocity inside the air cavity. The average air change rate of the three measuring periods can be estimated to 11 h^{-1} during periods with low wind speed and 84 h^{-1}during more windy periods. Eave-to-eave ventilation was found to be effective even though the roof angle was rather steep (40°).

Acknowledgements

The authors gratefully acknowledge the financial support by the Research Council of Norway and several partners through the Centre of Research-based Innovation "Klima 2050" (www.klima2050.no). Support is also given by FME ZEB (www.zeb.no).

References

[1] Roels S, Langmans J. Highly insulated pitched roofs resilient to air flow patterns: Guidelines based on a literature review. *Energy and Buildings* 2016;120:10-18.
[2] Gullbrekken L, Kvande T, Jelle B, Time B. Norwegian Pitched Roof Defects. *Buildings* 2016;6(2):24.
[3] Bøhlerengen T. *Isolerte skrå tretak med lufting mellom vindsperre og undertak. (Insulated pitched wooden roofs ventilated between the underlayer roof and the wind barrier) (In Norwegian)* SINTEF Building Research Design Guides 525.101. ISSN 2387-6328. SINTEF. Oslo. Norway. 2007
[4] Bøhlerengen T. *Isolerte skrå tretak med kombinert undertak og vindsperre. (Insulated pitched wooden roofs with combined underlayer roof and wind barrier) (In Norwegian)* SINTEF Building Research Design Guides 525.102. ISSN 2387-6328. SINTEF. Oslo. Norway.2012
[5] Blom P. *Ventilasjon av isolerte skrå tak (Ventilation of pitched roofs) (In Norwegian).* Doctoral thesis. NTH. Trondheim. Norway. 1990:39
[6] Hens H, Janssens A. *Cathedral ceilings: a test building evaluation in a cool, humid climate. Performance of exterior envelopes of whole buildings* IX International Conference Proceedings: ASHRAE Special Publications. 2004.
[7] Roels S, Deurinck M. The effect of a reflective underlay on the global thermal behaviour of pitched roofs. *Building and Environment* 2011;46(1):134-43.
[8] Holme J. *Mould growth in buildings*. Doctoral thesis. NTNU. Trondheim. Norway. 2010:147
[9] Falk J, Sandin K. Ventilated rainscreen cladding: Measurements of cavity air velocities, estimation of air change rates and evaluation of driving forces. *Building and Environment* 2013;59(0):164-76.
[10] Falk J. *Ventilarad luftspalt i yttervegg. (Ventilated air cavity in exterior walls) (In Swedish)* Doctoral thesis. TVBM-3155 Lunds Technical University. Lund. Sweden. 2010.

Paper 5

L. Gullbrekken, S. Uvsløkk, T. Kvande, K. Pettersson, B. Time

Wind pressure coefficients for roof ventilation purposes

Journal of Wind Engineering and Industrial Aerodynamics,
Vol 175, 2018, pages 144-152

Paper V

Journal of Wind Engineering & Industrial Aerodynamics 175 (2018) 144–152

Contents lists available at ScienceDirect

Journal of Wind Engineering & Industrial Aerodynamics

journal homepage: www.elsevier.com/locate/jweia

Wind pressure coefficients for roof ventilation purposes

Lars Gullbrekken [a,*], Sivert Uvsløkk [b], Tore Kvande [a], Kaj Pettersson [c], Berit Time [b]

[a] Department of Civil and Environmental Engineering, Norwegian University of Science and Technology (NTNU), Trondheim, Norway
[b] Department of Materials and Structures, SINTEF Building and Infrastructure, SINTEF, Trondheim, Norway
[c] Department of Architecture and Civil Engineering, Chalmers University of Technology, Gothenburg, Sweden

A B S T R A C T

Wind pressure coefficients (c_p) are important inputs for analytical calculations of wind load. The aim of this research is to investigate wind pressure coefficients on a test house located in Norway in order to pave the way for improved analysis of wind-driven roofing ventilation. The large-scale test measurements show that the wind pressure coefficient along the eaves of the house varies with different wind approach angles. Assuming wind-driven air flow through the air cavity beneath the roofing, an average $\overline{\Delta c_p}$ value of 0.7 is derived for practical engineering purposes. The results from the study are applicable for single or two-storey houses with pitched roofs at different roof angles.

1. Introduction

1.1. Background and scope

A load-bearing wooden roof is a proven and widely used type of construction in the Nordic countries. The various design principles for wooden roofs are thoroughly discussed by Edvardsen and Ramstad (2014). The basic principle is that the air cavity beneath the roofing must be ventilated to transport:

1. Moisture from the roof and thus prevent the growth of mould and moisture damage
2. Heat and thus prevent unwanted melting of snow and icing at the eaves and gutters

Roof ventilation guidelines for Norway are given by Bøhlerengen (2007, 2012) and are valid for roofs with a span less than 15 m and roof angle greater than 10° to 15°. A strong focus on CO_2-emissions from buildings most often favours wood-based materials and timber structures. Use of wood for the load-bearing system in roofs with increasingly longer spans and more complicated roof geometry is becoming more popular. In order to improve air cavity design guidelines for ventilated roofs it is necessary to increase the knowledge base for wind-driven ventilation of pitched roofs. The air change rate of the cavity is given by driving forces from wind and temperature differences (natural convection) together with pressure losses in the system. To calculate the wind-driven ventilation of such a roof it is necessary to calculate the difference in wind pressure coefficient, c_p, at the inlet and the exit of the air cavity. This difference is hereafter defined as Δc_p.

This work is based on measurements performed by Uvsløkk in 1985 and the work was previously partly published in Uvsløkk (1996). However, the scope of Uvsløkk (1996) was limited to examine the wind pressure gradients in the air cavity behind a ventilated cladding.

The aim of this research has been to investigate c_p at the wall surface of a test house located in Norway. In section 1.2–1.6 the theoretical framework for the wind pressure coefficient (c_p) and relevant past research on it are presented. In section 2 the experimental design and implementation used in this paper is presented. In sections 3 and 4 the results and a discussion of the implications are given, respectively. Section 5 consists of final thoughts and conclusions. The c_p at the air cavity openings of the roof, together with the wind velocity and wind approach angle, defines the driving forces of wind-driven air cavity ventilation. Therefore, knowledge about such parameters is necessary when calculating wind-driven air cavity ventilation of pitched roofs.

1.2. Wind pressure coefficient

The wind pressure coefficient at a point is defined as wind pressure at the point divided by the dynamic pressure in free wind at a reference height above ground, normally 10m (NS-EN, 1991-1-4:2005):

$$c_{px} = \frac{P_x - P_0}{P_d} \tag{1}$$

* Corresponding author.
E-mail address: lars.gullbrekken@sintef.no (L. Gullbrekken).

https://doi.org/10.1016/j.jweia.2018.01.026
Received 5 December 2016; Received in revised form 15 January 2018; Accepted 15 January 2018
Available online 20 February 2018

$$P_d = \frac{\rho \cdot U^2}{2} \quad (2)$$

c_{px} is the wind pressure coefficient of a point (−), P_x is the static pressure at point x on the building facade (Pa), P_0 is the static reference pressure (Pa)(at 10m height), P_d is the dynamic pressure (Pa), ρ is the air density (kg/m^3) and U is the wind speed at 10m (m/s).

Δc_p is defined by equations (3) and (4), where c_{px1} and c_{px2} are wind pressure coefficients at the positions shown in Fig. 1.

$$\Delta c_{px} = c_{px1} - c_{px2} \quad (3)$$

$$\Delta c_p(\theta) = c_p(\theta) - c_p(180 - \theta) \quad (4)$$

where θ is the wind approach angle (horizontal).

There are three methods to estimate c_p: full-scale test, a model test in a laboratory wind tunnel and by parametric equations derived from experiments. For a specific building, a fully accurate determination of c_p can only be done using a full-scale test (Bartko et al., 2016; Uvsløkk 1996) or a model test (Tominaga et al., 2015; Quan et al., 2011) of the specific building. Full-scale measurements are costly, difficult and require expertise, and consequently are only performed on complex and high rise buildings in order to develop parametric equations.

1.3. Full-scale tests

Wells and Hoxey (1980) performed full-scale wind coefficient measurements mainly on roofs of five different glasshouses situated in the UK. The measurements were done with the aim to increase knowledge about design values of wind coefficients of such buildings. Richardson and Surry (1991) performed comparisons of full-scale and model-scale measurements, focusing on mean wind pressure coefficients of four low-rise buildings. The mean pressure coefficients presented for four buildings suggested that a wind tunnel does not accurately model the separation of the flow on the windward roof. Full-scale measurements of side wall pressure coefficients reported for three buildings indicated a Δc_p across the air cavity of the roof of 0.6–1.0.

Wind pressure coefficients on a specific part of a building were calculated by Caracoglia and Jones (2009). The facade-measurements were performed close to a corner of the building which had a complex geometry. Wind-induced response on low-rise buildings by use of load cells in the foundation system of the building and in the wall/roof joint was investigated by Zisis and Stathopoulos (2012). For the mean wind pressure coefficient, the full-scale measurements showed excellent agreement with the model (wind tunnel) results given a suburban terrain. Given an open and light suburban terrain and a wind angle of 60° to the long wall of the test model, Fig. 6 in Zisis and Stathopoulos (2012) indicates a Δc_p across the air cavity of 0.5. Further, the results interpret a larger Δc_p in a more suburban terrain however it should be noted that the measurements only included one wind direction.

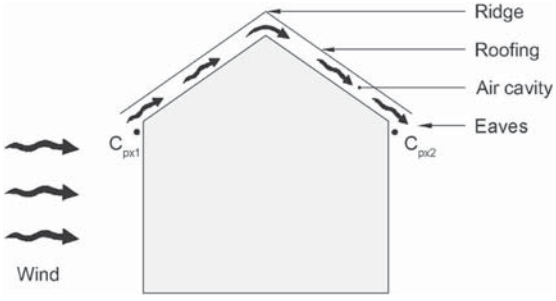

Fig. 1. Cross-section of a house showing the location of the two pressure points for calculation of Δc_{px}.

1.4. Model test

Kanda and Maruta (1993) performed model measurements of wind coefficients on a long low-rise building with a gable roof. On the windward wall they measured a wind pressure coefficient between 0.5 and 0.8 depending on the roof pitch. A thorough literature review of wind pressure measurements, using both field studies and model studies, was conducted by Uematsu and Isyumov (1999). They found a number of research efforts trying to determine wind loads on low-rise buildings. However, the authors still pinpointed the need for more measurement data to cover different variables.

Blom (1990) also performed model measurements using an identical downscaled model of the test house used in this study. However, the measurements were simplified and included, for example, only one wind approach angle.

Yang et al. (2008) performed model testing in a wind tunnel and compared the results to calculations, however, the measurements were only performed on a limited range of wind approach angles.

Tominaga et al. (2015) conducted wind tunnel experiments to examine air flow around building models and the results were used to validate a Computational Fluid Dynamics (CFD)-model. The model dimension were L x W = 6.6 × 6.6m and height from ground to eaves of 6m. Three different roof angles of 16.7, 26.6 and 36.9° with no roof overhang were tested. The model was oriented perpendicular to the flow. Although taking measurements of the driving forces for ventilation the air cavity beneath the roofing was not in the scope of the work, the study indicates a Δc_p across the air cavity of 1.1–1.4 for all the investigated roof angles (Fig. 2).

The c_p of the pitched roof is significantly influenced by the roof geometry of low-rise buildings (Xu and Reardon 1998; Blom 1990). Xu and Reardon (1998) performed wind tunnel measurements on a building model with 15°, 20° and 30° roof pitches and large overhangs. They found that a roof angle of 30° experienced the highest negative c_p at the roof corner compared to the 15°- and 20°- roof angle. Blom (1990) performed model measurements using an identical model of the test house used in the current study. He also concluded that the roof angle influences the distribution of c_p of a pitched roof.

Furthermore, Ahmad and Kumar (2002) studied the mean pressure coefficients on elevated and single-storey houses. By assuming the situation given in Fig. 1, the results from their study indicate a Δc_p across the air cavity of 0.6–1.3 depending on the height of the building.

1.5. Parametric equations

Muehleisen and Patrizi (2013) developed simplified parametric equations that more accurately describe the performance of isolated buildings. The study only included a flat roof configuration.

A thorough overview of pressure coefficient data and to what extent the data is currently implemented in building energy simulation and airflow network programs was performed by Cóstola et al. (2009). The following primary sources of data were mapped: full scale measurements, reduced scale measurements in wind tunnels and CFD (computational fluid dynamics) simulations. In addition, secondary sources such as databases and analytical models were studied. Cóstola et al. (2009) found that a wide range of parameters influence the pressure coefficients on building facades. A high uncertainty was also associated with pressure coefficients of buildings sheltered by neighbouring buildings.

The Eurocode 1 standard (NS-EN, 1991-1-4:2005) gives instructions for calculation of wind strains on building facades.

1.6. Knowledge gap

Several full-scale and model scale studies of c_p on facades and roofs have been conducted. However, to the authors' knowledge, there are few

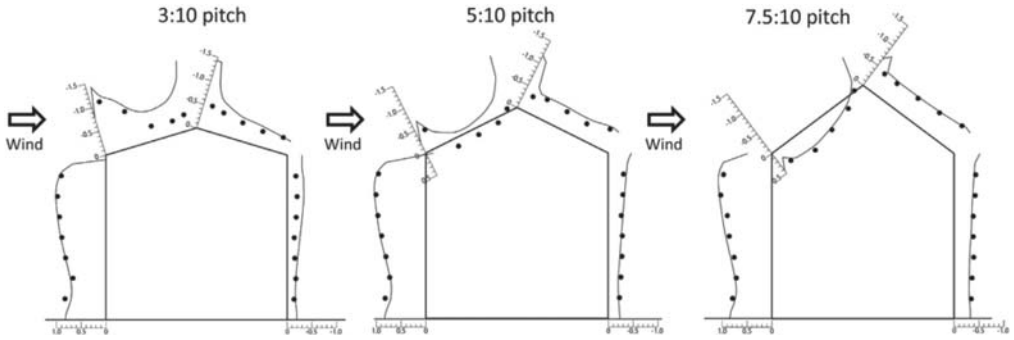

Fig. 2. Black dots represent measurements of c_p for a model house. Three different roof angles were studied. Figure from Tominaga et al. (2015).

studies of specific measurements of the c_p at the inlet and the outlet of the air cavity beneath the roofing of a pitched roof, defined by the authors as Δc_p. Analysis of the measurements by Tominaga et al. (2015), Zisis and Stathopoulos (2012) and Richardson and Surry (1991) indicates a Δc_p of 0.5–1.4, which represents a rather large span. This study is undertaken in order to more precisely derive a Δc_p applicable for an engineering evaluation of air cavity design.

2. Method

2.1. Test set-up

A test house located at an open field test station in Tyholt, Trondheim, (63.4222N, 10.4302E) 110m above sea level was equipped with instrumentation for wind pressure measurements (see Fig. 3). The building was 8m long, 5m wide and the height to the top of the roof was 6m. The roof angle was 38° and the attic space was ventilated through an opening along the eaves as shown in Figs. 3 and 4. The roof (ceiling), walls and floor were insulated. By use of an electric motor, the test house could be rotated making it possible to carry out wind pressure measurements for all parts of the walls at any wind approach angle. The ground at the test site was even and open with no trees or buildings within a distance of about 150m in a sector from south-southeast to southwest which was the dominating wind direction during the measurement periods. Wind speed was measured by a Lambrecht anemometer positioned 6m above ground level in a mast positioned 40m away in a west northwest direction from the test house, as Fig. 3 shows. Wind speed was also recorded by an identical anemometer located in the centre of the house, 4m above the ridge and 10m above ground level. This was to investigate the influence of the test house on the flow pattern of the wind.

Four groups of pressure measurement points were located on the long wall (see Fig. 4). In addition, two groups of pressure points were located on the short wall of the house. Eight pressure points in each group were distributed along a vertical line: four located in the air gap between the cladding and the wind barrier, and four on the exterior surface of the cladding. The wind pressure was measured using plastic tubes which were coupled to pressure transducers inside the test house. All the tubes were 10m long and had an interior diameter of 4 mm. At each exterior measuring point a plastic tube was coupled to a brass tube with the opening at the surface of the cladding. The brass tubes were 50 mm long and had an interior diameter of 3 mm. The 20 pressure transducers were Furnes Transducer FCO 40 (0–1000Pa) micro manometers. Of the 20 transducers, 16 were attached to the different pressure tubes. The remaining four were coupled to fixed measuring positions as follows: dynamic wind pressure at 10m above ground level, air pressure inside the house, wind pressure in the attic and wind pressure in a fixed position on

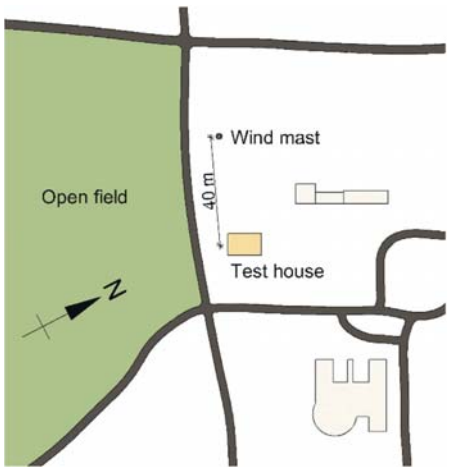

Fig. 3. Position of test house and wind mast at the field test station.

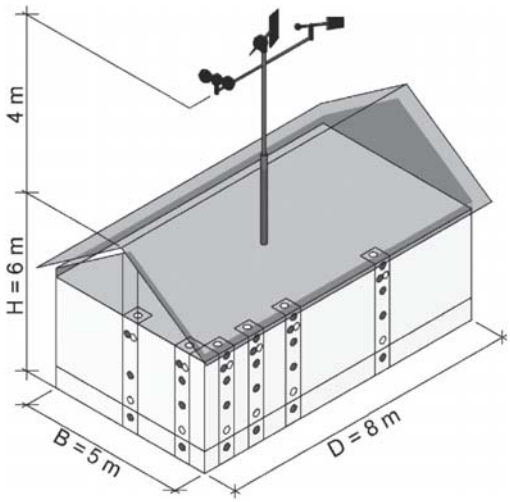

Fig. 4. The rotatable test house located in Tyholt in Trondheim used for wind pressure measurements.

the long wall. The pressure transducers reported the pressure difference between the wind pressure at the measuring point and the reference static pressure. Reference static pressure was measured in a mast 10m above ground, 4m above the ridge of the house and in the centre of the house (see Fig. 4). This was done by attaching all the pressure transducers to a plastic tube which ended at the surface of a vertical aluminium plate designed as a wind vane. Dynamic pressure and wind approach angle were also registered in this mast based on the principle presented in Hoxey and Wells (1974, 1977).

In advance of each measuring period, the tubes were cleaned by use of pressurised air. The pressure transducers were zeroed before and after each measurement series. Twenty values from each pressure transducer were recorded during the measurement period of ten seconds. Then, the test house was rotated to achieve a slightly different wind approach angle and the procedure was repeated. During stable wind all the measurements could be conducted within a couple of hours. Usually the measurements were repeated on another day in 15–25 different wind approach angles for all measuring positions.

Three construction variants have been investigated; two of these are shown in this paper in Fig. 5. The only difference between the construction variants is the horizontal wooden board. The main purpose of the board is to reduce rain and snow drifting into the attic. The horizontal part of the eaves was 100 mm. The third construction variant is not included because it was identical to variant 1 except for the design of the air cavity behind the cladding. In addition, the measurement data for this variant was limited. Accuracy and measuring range of applied sensors are given in Table 1.

Table 1
Accuracy and measuring range of applied sensors.

Sensor	Manufacturer	Type	Accuracy	Range
Pressure transmitter	Furness Control	FCO 40	±5% of reading	0–+1 000 Pa
Wind direction	Lambrecht	–	±2°	0–360°
Wind speed	Lambrecht	–	±5°	0.3–60 m/s

2.2. Uncertainty assessment

The root-mean-square (RMS) method was used to derive the uncertainty propagation of the measured c_p-values (equation (5)).

$$\frac{\Delta^P c_{px}}{c_{px}} = \sqrt{\left[\frac{\Delta^P P_\Delta}{P_\Delta}\right]^2 + \left[\frac{\Delta^P P_d}{P_d}\right]^2} \tag{5}$$

where $\frac{\Delta^P P_\Delta}{P_\Delta}$ is the uncertainty of P_Δ , which is defined as $P_\Delta = P_x - P_0$. $\frac{\Delta^P P_d}{P_d}$ is the uncertainty of P_d given by equation (2). No correlation between the terms of the balance equation was found.

Input data for this investigation was recorded wind speed measurements at 6m height above ground level of a wind mast and wind speed measurements at 10m above ground level. Identical anemometers to measure wind speed were used for the roof and wind mast measurements. NS-EN 1991-1-4:2005 + NA:2009 (section 4.3 and NA) was used to calculate the wind speed at a height of 10m from the data in the wind mast at 6m height.

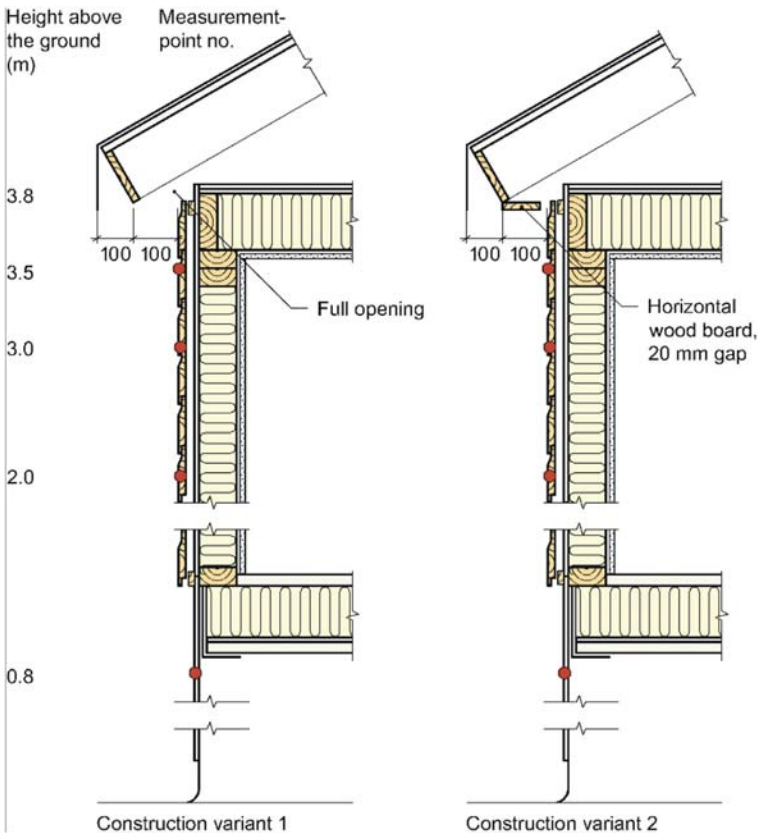

Fig. 5. Cross-section of the two wall sections studied in the field measurements. Red dots represent positions of the wind pressure measurements reported in the study. (For interpretation of the references to colour in this figure legend, the reader is referred to the Web version of this article.)

3. Results

The c_p of construction variant 2 at different positions on the cladding of the building is given in Fig. 6. The pressure measurements are positioned on the exterior surface of the cladding. Four different wind approach angles are included in Fig. 6: 0, 45, 90 and 180° ± 10°. An angle of 0° means that the wind approach angle is perpendicular to the wall.

The measured c_p at the surface of the cladding in different positions along the eaves of the house varies with different wind approach angles and position along the wall.

Fig. 7 gives the mean (time averaged) c_p for construction variant 1 at 3.5 metre height given different wind approach angles.

Tokyo Polytechnic University has released a large and very detailed database on wind tunnel tests on low-rise buildings (Tokyo Polytechnic University, 2007). Parts of the database are published in Muehleisen and Patrizi (2013). According to the current study the values D/H = 2.0 and D/B = 1.0 matches best with the geometry of the test house. The exact values for the test house are D/H = 8.0/3.8 = 2.11 and D/B = 8.0/5.0 = 1.6. D,H and B are defined in Fig. 4.

In Fig. 8 c_p -values from Muehleisen and Patrizi (2013) are plotted together with mean (time averaged) results from construction variant 2 at a height of 3.5m given different wind approach angles.

The c_p on the building facade according to NS-EN 1991-1-4:2005 together with the distribution of the measured c_p as a function of the wind approach angle is given in Fig. 9.

In general, the wind pressure difference between the inlet and the outlet of the air gap is the driving force for the wind-driven air change rate of the air gap beneath the roofing (see Fig. 1). For engineering evaluation purposes, a simple method to calculate the air flow in the air gap and a procedure to estimate the pressure difference is needed. An average wind pressure factor difference, $\overline{\Delta c_p}$, has been derived based on the wind pressure measurements near the roof eaves at a height of 3.5m above ground level. The calculation was performed by averaging the measurements of c_p at wind approach angles of 0, 30, 45, 60, 90, 120, 135, 150, 180 ± 10° at the different positions of the wall (0.4m, 1.7m, 3.5m from the corner). $\overline{\Delta c_p}$ was calculated using equation (4). Looking at Fig. 9 this means that for example, that:

$$\Delta c_p(0) = \text{cp (0)0.4m-cp(180)0.4m} = 0.75 - (-0.1) = 0.85$$

The resulting average value derived from all approach angles and positions was $\overline{\Delta c_p} = 0.7$.

The calculated wind speed at 10m in the wind mast was compared to the measured wind speed at 10m, 4m above the ridge and positioned in the centre of the test house. A ratio of the two wind speeds has been calculated by dividing the measured value by the calculated value. The results have been sorted into two categories (see Fig. 10). The global wind angle in the measurement period was 0–41°. Fig. 10 contains all available measurement data.

4. Discussion

4.1. Wind pressure coefficient

The largest positive c_p values were measured at the top of the middle section of the wall, given a wind approach angle perpendicular to the wall. The largest negative values were measured at the top of the wall, near the corner, at the wind approach angle of 90°, i.e. parallel to the wall. Both the distribution of the c_p on the building facade and the values of the c_p are in line with the investigations performed by Tominaga et al. (2015), Yang et al. (2008), Richardson and Blackmore (1995), Kanda and Maruta (1993) and Hoxey (1991). However, compared to the current study none of the previous field investigations includes the same amount of wind approach angles and measuring points on a building facade.

In general, a similar pressure distribution is found for c_p as a function of the wind approach angle for the measured c_p -values and the database from Tokyo shown in Fig. 8 (Tokyo Polytechnic University, 2007). Both investigations show largest c_p-values for the 0° wind approach angle. The

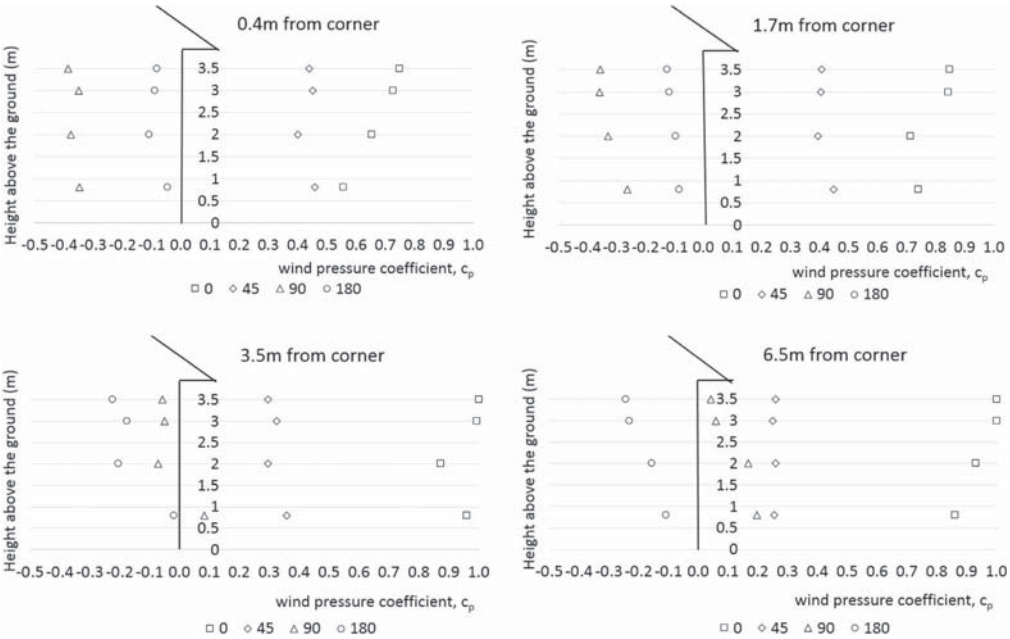

Fig. 6. Measured wind pressure coefficient, c_p, at positions 0.4m, 1.7m, 3.5m and 6.5 m from the corner; see black circle in Fig. 7. Results for the wind approach angles 0°, 45°, 90° and 180°. All results are for construction variant 2.

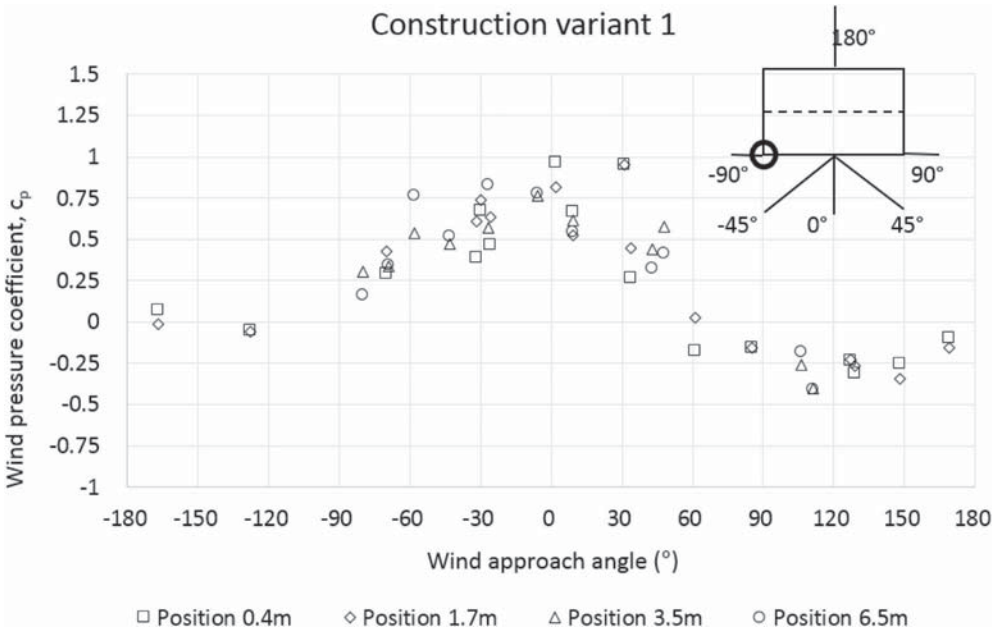

Fig. 7. Measured wind pressure coefficients, c_p, at four locations on the long wall, 3.5m above the ground and different wind approach angles (0° = perpendicular to the wall) for construction variant 1. Black circle in the upper-right corner of the diagram shows the corner from which the positions are measured.

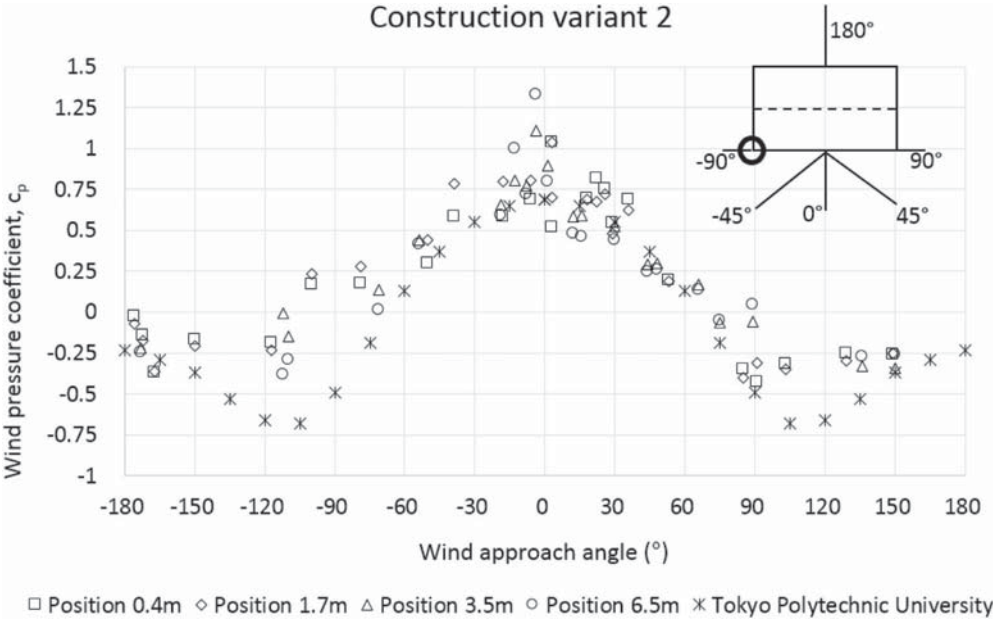

Fig. 8. Measured wind pressure coefficients, c_p, at four locations on the long wall 3.5m above the ground and different wind approach angles (0° = perpendicular to the wall) for construction variant 2. Black circle in the upper-right corner of the diagram shows the corner from which the positions are measured.

largest negative c_p-value was found for the wind approach angle of ±120°. For the wind approach angle of ±90–150° the calculated c_p values from the measurements differ somewhat compared to the Tokyo database values. One possible explanation is differences in the shape of the test building compared to the one used for the Tokyo database. The D/H value of the test building was 2.11 while the corresponding value from the database was 2.0. The D/B of the test house was 1.6 compared to 1.0 from the database. The values from the database show that both the

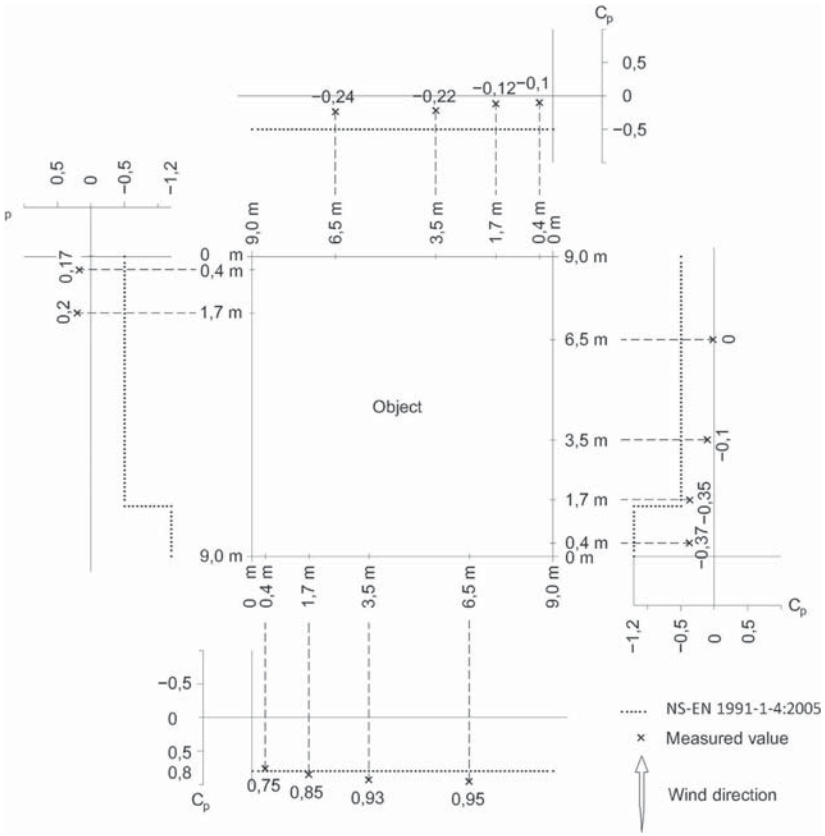

Fig. 9. Comparisons of c_p obtained by the measurements at 3.5m height above ground level, near the roof eave from this study and standard design values from NS-EN 1991-1-4:2005.

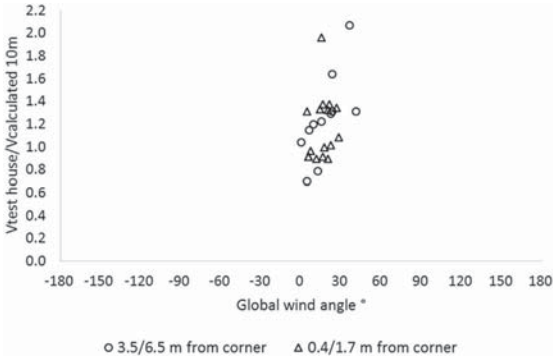

Fig. 10. Ratio of the wind speed measured on the test house compared to calculated wind speed in a mast at 10m above ground level as a function of the global wind approach angle. The wind mast was positioned 40m away from the test house (as per Fig. 3).

D/H-values and the D/B-values have a significant impact on the c_p, especially for the wind approach angles between ±60 and 180°. This is also the interval with the largest deviation between the measurements and the values from the Tokyo database.

The Tokyo database results are from model measurements performed in a wind tunnel. In a wind tunnel, it is of course easier to control both wind speed and direction compared to field measurements where both the wind speed and direction fluctuate. This might explain part of the difference between the model measurements and the field measurements. However, field measurements reproduce natural conditions to a greater extent than laboratory measurements.

At a wind approach angle of 0°, the measured and NS-EN 1991-1-4:2005 values correspond. However, for the additional approach angles the c_p is overestimated by the standard. Values in NS-EN 1991-1-4:2005 are typically used to obtain design values for wind loads on building components. Therefore, it can be anticipated that the values from the standard gives conservative values for the c_p.

4.2. Design variants

There are fewer measuring values for construction variant 1 compared to variant 2 because the measurements were taken during different periods as the roof overhang was redesigned between the two measurements. The c_p-values of construction variant 1 and 2 are rather similar, showing the largest positive c_p for the wind approach angle of 0°, and the largest negative c_p at ±120–150°. In particular, there are small differences in c_p for the wind approach angles 0–180°. However, the c_p for the wind approach angles -0- to −180° shows differing data points, especially for wind approach angles of −90 to −180°. Missing measurement data for these wind approach angles for variant 1 makes it difficult to draw conclusions. The results indicate that the design of the eaves affects the wind pressure coefficient at the upper part of the facade to a small extent.

4.3. Test set up

In order to evaluate the driving forces of the vented air cavity the wind pressure coefficients at the air cavity openings beneath the roofing are highly relevant. In this specific case the horizontal roof overhang is 0.2m and the pressure measuring points are positioned 0.25m below the horizontal part of the roof overhang. The position was chosen so as to produce as general values as possible. From a practical perspective, the dimension of the roof overhang is project specific, as is the position of the air inlets in the horizontal part of the roof overhang. A trend in Nordic architecture is for slim eaves resulting in the gutter being nearly at the surface of the cladding. Fig. 6 shows how the c_p varies with the height above the ground and the position along the wall. The roof overhang is identical for all the measurements. According to NS-EN 1991-1-4:2005 the c_p on the wall beneath the roof overhang is equal to the c_p at the top of the wall. Additionally, Blom (1990) states that the difference in the c_p of the upper part of the wall and beneath the roof overhang is rather small. Given no roof overhang, Fig. 2 indicates that the roof angle affects the c_p at the upper part of the wall to a small extent.

Previously, Caracoglia and Jones (2009) used a sampling period of 300 s, and Wells and Hoxey (1980) used a sampling period of 240 s. However, the purpose of the current study was to produce wind pressure coefficients at specific wind approach angles. By increasing the sampling period, the variance in the wind approach angle will also increase. This was also stated by Wells and Hoxey (1980) who developed a method to take this into account. However, both Caracoglia and Jones (2009) and Wells and Hoxey (1980) performed measurements on houses that could not be rotated. The current measurements were performed using a rotatable test house in order to achieve specific wind approach angles and therefore shorter measuring periods were chosen. The ten second measuring period was chosen to enable as many measurements as possible to be taken and to reduce the variations in wind approach angle.

The wind measurement location was chosen in order to get standardised static and dynamic pressures at a height of 10m. The wind pressure measurements were conducted by direct measurement of the pressure difference of the static pressure at 10m to the static pressure at the surface of the cladding. As there was only 4m between the ridge and the position of the static and the dynamic wind pressure measurement device the measurements can probably not be considered a free-stream wind field. However, direct measurements of pressure difference require a location close to or on the test house in order to ensure a close distance between the measuring points on the facade and the wind measurement. Therefore, the test set up minimises the time lag between the wind gust hitting the facade and the wind reference. This was also why an identical length of all plastic tubes for the different measuring positions was used.

The distance between the wind measuring device at the test house and in the wind mast was 40m. The calculated ratio of the measured wind speed at the test house and at the wind mast in Fig. 10 gives the instant wind speed difference. The global wind approach angle has a direct influence on this ratio. For some global wind approach angles there will be a significant time lag between the wind front hitting the test house and the wind mast. A global wind approach angle perpendicular to the line through the test house and the wind mast will lower the latter time lag as much as possible. Hence, a global wind approach angle of south-southwest (~20°) gives the smallest time lag. By analysing the data for this wind approach angle a ratio of 1.27 was calculated. That implies that on average the wind speed 4m above the ridge of the test house is 27% higher than the calculated wind speed at a height of 10m in the wind mast. In turn, this gives a reduced value of c_p according to equation (1). The difference in static pressure at the two locations was, however, not measured and therefore evaluation of the static pressure difference at the two locations is lacking.

According to NS-EN 1991-1-4:2005 and the previous results of Tominaga et al. (2015) and Ahmad and Kumar (2002) the results from the current study can be applicable for one to two-storey houses with pitched roof and different roof angles. The measurements from Ahmad and Kumar (2002) show increasing c_p -values with increasing building heights.

4.3.1. Uncertainty of wind pressure measurements

It has not been possible to evaluate the error in measured c_p. The following points indicate the possible sources and levels of error.

1) Each of the measured local loss coefficients consist of 20 measurements. The calculation of the wind pressure coefficient is based on the ratio of the pressure difference of the facade and the static pressure at a height of 10m and the dynamic pressure at a height of 10m. By assuming ±5% of reading accuracy the uncertainty of the measurements can be calculated to 7%.
2) The test house affects the dynamic wind pressure measurements performed in 4m height above the ridge. On average the wind speed 4m above the ridge of the test house is 27% higher than the calculated wind speed at a height of 10m in the wind mast. In turn, this gives a reduced value of c_p according to equation (1). However, the difference in static pressure at the two locations has not been measured.

4.4. Practical use

As previously stated Δc_p is essential when calculating the wind-driven ventilation of the air cavity below the roofing. When using Δc_p for ventilation purposes the Δc_p is calculated by equation (4) assuming that the roofing is ventilated by air flowing directly through the roof structure. However, in a real situation the air change rate of the air cavity beneath the roofing is strongly dynamic and affected by several parameters among them the design and position of the air cavity openings as well as the design of the air cavity beneath the roofing. As Cóstola et al. (2009) mentioned, the typical wind approach angle is also dependent on the location and orientation of the specific house. Calculations of ventilation of roofing in practice require simplifications regarding both wind approach angle and typical wind velocity.

In practical calculations of the ventilation of the air cavity beneath the roofing it is necessary to assume a conservative wind speed and -approach angle at the location of the roof structure. In such cases an average value of Δc_p is valuable for estimating the ventilation of the roof cavity.

In this work a $\overline{\Delta c_p}$ of 0.7 was derived by assuming that the roofing is ventilated by air flowing directly through the roof structure (see Fig. 1). By studying the results from Tominaga et al. (2015), Richardson and Surry (1991) and Zisis and Stathopoulos (2012) the authors found a Δc_p of 0.5–1.4. The results from the current study are in line with the results from these previous studies. Results from Zisis and Stathopoulos (2012) show a larger Δc_p given a more urban terrain. The impact from sheltering is not a part of this study, but might influence the c_p and therefore needs to be further investigated.

In practice, roofing materials might often have openings in the ridge of the roofing. Openings in the air cavity positioned at different heights introduces natural convection as a driving force of air change in the air cavity. The results from the study only apply to ventilation from eaves to eaves, as shown in Fig. 1. Wind pressure coefficients on different pitched roofs were measured by Ahmad and Kumar (2002) and Tominaga et al. (2015), see Fig. 2. As the results from these studies show, there is a negative wind pressure coefficient at the ridge depending on the height above ground and pitch of the roof. Given openings in the ridge, in practice the roofing will be ventilated both through the ventilation opening in the ridge and from eaves to eaves, as shown in Fig. 1. However, for a winter situation with snow on the roof the situation will be as shown in Fig. 1. The distribution between the air cavity ventilation through the eaves-ridge and eaves-eaves of the roof has not been part of the current study, but also needs to be further investigated.

5. Conclusion

The paper describes detailed full-scale measurements of wind pressure coefficients on a rotatable test house. The large-scale test measurements show that the wind pressure coefficient along the eaves of the house vary with different wind approach angles. Furthermore, the measurements show increasing c_p at the upper, middle part of the wall. Both the distribution of the c_p on the building facade and the values of the c_p are in line with previous field and laboratory investigations.

A $\overline{\Delta c_p}$ of 0.7, needed for engineering evaluations, was calculated by assuming that the roofing is ventilated by air flowing directly through the roof structure. The results from the study are applicable for one to two-storey buildings with pitched roof and different roof angles.

Acknowledgements

The authors gratefully acknowledge the financial support of the Research Council of Norway and several partners through the Centre of Research-based Innovation "Klima 2050" (www.klima2050.no) (p. nr.: 237859). A special thanks to CAD operator Bjørnar Nørstebø and Remy Eik. The authors also gratefully acknowledge the anonymous Journal of Wind Engineering & Industrial Aerodynamics referees for valuable comments on the text.

References

Ahmad, S., Kumar, K., 2002. Effect of geometry on wind pressures on low-rise hip roof buildings. J. Wind Eng. Ind. Aerod. 90, 755–779.
Bartko, M., Molleti, S., Baskaran, A., 2016. In situ measurements of wind pressures on low slope membrane roofs. J. Wind Eng. Ind. Aerod. 153, 78–91.
Blom, P., 1990. Ventilasjon Av Isolerte Skrå Tak. (Ventilation of Pitched Wooden Roofs)(In Norwegian). PhD thesis 1990:39. NTH, Norway.
Bøhlerengen, T., 2007. 525.101 Isolerte Skrå Tretak Med Lufting Mellom Vindsperre Og Undertak. (Pitched Wooden Roofs with Ventilation between the Wind Barrier and the Underlayer Roofing)(In Norwegian) SINTEF Building Design Guides. SINTEF, Oslo.
Bøhlerengen, T., 2012. 525.102 Isolerte Skrå Tretak Med Kombinert Undertak Og Vindsperre. (Pitched Wooden Roofs with Combined Underlayer Roof and Wind Barrier)(In Norwegian) SINTEF Building Design Guides. SINTEF, Oslo.
Caracoglia, L., Jones, N.P., 2009. Analysis of full-scale wind and pressure measurements on a low-rise building. J. Wind Eng. Ind. Aerod. 97, 157–173.
Cóstola, D., Blocken, B., Hensen, J.L.M., 2009. Overview of pressure coefficient data in building energy simulation and airflow network programs. Build. Environ. 44, 2027–2036.
Edvardsen, K., Ramstad, T., 2014. Trehus Håndbok 5. (Wood Buildings Handbook 5)(In Norwegian). SINTEF Building and Infrastructure, Oslo.
Hoxey, R.P., 1991. Structural response of a portal framed building under wind load. J. Wind Eng. Ind. Aerod. 38, 347–356.
Hoxey, R.P., Wells, D.A., 1974. Instrumentation for full-scale wind load measurement on glasshouses. J. Agric. Eng. Res. 19, 435–438.
Hoxey, R.P., Wells, D.A., 1977. Full-scale wind pressure measurements on a twin-span 12.2 × 12.2 m inflated roof greenhouse. J. Wind Eng. Ind. Aerod. 2, 211–221.
Kanda, M., Maruta, E., 1993. Characteristics of fluctuating wind pressure on long low-rise buildings with gable roofs. J. Wind Eng. Ind. Aerod. 50, 173–182.
Muehleisen, R.T., Patrizi, S., 2013. A new parametric equation for the wind pressure coefficient for low-rise buildings. Energy Build. 57, 245–249.
NS-EN 1991-1-4:2005. Eurocode 1: Actions on structures Part 1-4: General actions Wind actions. Standard Norge.
Quan, Y., Liang, Y., Wang, F., Gu, M., 2011. Wind tunnel test study on the wind pressure coefficient of claddings of high-rise buildings. Selected Publications from Chinese Universities, 5, 518–524.
Richardson, G.M., Blackmore, P.A., 1995. The Silsoe structures building: comparison of 1 : 100 model-scale data with full-scale data. J. Wind Eng. Ind. Aerod. 57, 191–201.
Richardson, G.M., Surry, D., 1991. Comparisons of wind-tunnel and full-scale surface pressure measurements on low-rise pitched-roof buildings. J. Wind Eng. Ind. Aerod. 38, 249–256.
Tokyo Polytechnic University, 2007. Aerodynamic Database of Low-rise Buildings. http://www.wind.arch.t-kougei.ac.jp/info_center/windpressure/lowrise/mainpage.html. (Accessed 16 November 2016).
Tominaga, Y., Akabayashi, S.-I., Kitahara, T., Arinami, Y., 2015. Air flow around isolated gable-roof buildings with different roof pitches: wind tunnel experiments and CFD simulations. Build. Environ. 84, 204.
Uematsu, Y., Isyumov, N., 1999. Wind pressures acting on low-rise buildings. J. Wind Eng. Ind. Aerod. 82, 1–25.
Uvsløkk, S., 1996. The importance of wind barriers for insulated timber frame constructions. J. Build. Phys. 20, 40–62.
Wells, D.A., Hoxey, R.P., 1980. Measurements of wind loads on full-scale glasshouses. J. Wind Eng. Ind. Aerod. 6, 139–167.
Xu, Y.L., Reardon, G.F., 1998. Variations of wind pressure on hip roofs with roof pitch. J. Wind Eng. Ind. Aerod. 73, 267–284.
Yang, W., Quan, Y., Jin, X., Tamura, Y., Gu, M., 2008. Influences of equilibrium atmosphere boundary layer and turbulence parameter on wind loads of low-rise buildings. J. Wind Eng. Ind. Aerod. 96, 2080–2092.
Zisis, I., Stathopoulos, T., 2012. Wind load transfer mechanisms on a low wood building using full-scale load data. J. Wind Eng. Ind. Aerod. 104-106, 65–75.

Paper 6

L. Gullbrekken, S. Uvsløkk, S. Geving, T. Kvande.

Local loss coefficients inside air cavity of pitched wooden roofs

Journal of Building Physics. Published online 1. December 2017.

Paper VI

JOURNAL OF BUILDING PHYSICS

Original Article

Journal of Building Physics
1–23

DOI: 10.1177/1744259117740506
journals.sagepub.com/home/jen
SAGE

Local loss coefficients inside air cavity of ventilated pitched roofs

Lars Gullbrekken[1], Sivert Uvsløkk[2], Stig Geving[1] and Tore Kvande[1]

Abstract

Pitched roofs with a ventilated air cavity to avoid snow melt and ensure dry conditions beneath the roofing are a widely used construction in northern parts of Europe and America. The purpose of this study has been to determine pressure losses at the inlet (eaves) and inside the air cavity consisting of friction losses and passing of tile battens. These results are necessary to increase the accuracy of ventilation calculations of pitched roofs. Laboratory measurements, numerical analysis as well as calculations by use of empirical expressions have been used in the study. A large difference in the local loss coefficients depending on the edge design and height of the tile batten was found. The local loss coefficients of the round-edged tile battens were approximately 40% lower than the local loss coefficients of the sharp-edged tile battens. Furthermore, the local loss factor increased by increasing height of the tile batten. The numerical analysis was found to reliably reproduce the results from the measurements.

Keywords

Laboratory measurements, local loss coefficients, COMSOL, roofing ventilation, air cavity, tile batten

Introduction

Ventilated pitched roofs are currently a widely used construction for residential and non-residential buildings in northern parts of Europe and America. The air cavity

[1]Department of Civil and Environmental Engineering, Norwegian University of Science and Technology (NTNU), Trondheim, Norway
[2]Department of Materials and Structures, SINTEF Building and Infrastructure, SINTEF, Trondheim, Norway

Corresponding author:
Lars Gullbrekken, Department of Civil and Environmental Engineering, Norwegian University of Science and Technology (NTNU), Høgskoleringen 7A, 7046 Trondheim, Norway.
Email: lars.gullbrekken@sintef.no

beneath the roofing is ventilated to ensure dry conditions for the roof construction and keep the roofing temperature low enough to avoid snow melt. The construction is of special interest regarding the dry-out capacity in roofs with load-bearing systems of wood. When built in line with the guidelines given by Roels and Langmans (2016), Edvardsen and Ramstad (2014) and Uvsløkk (1996), ventilated pitched wooden roofs can be considered a robust roof design. However, there are well-known degradation issues related to snow melt and mould growth. Tobiasson et al. (1994) studied icing problems in northern America, and they reported that the icing problems of several buildings in northern New York were reduced by increasing the ventilation of the attics so that the temperature inside the attics was below −1°C when the external temperature was −5.5°C. Measurements performed in Canada by Walker and Forest (1995) showed that attic ventilation was mainly driven by wind, and that the ventilation increased by increasing wind speeds. The problem with snow melt on roofs is reduced in modern well-insulated roofs with well-ventilated roofing (Geving, 2011).

In the Nordic countries, the moisture conditions inside cold ventilated attics have been studied. In Sweden, Samuelson (1998) found that a reduction in the ventilation of the attics caused a drier climate inside the attic. However, the calculations assumed a totally airtight ceiling structure beneath the attic. In Norway, Blom (2001) conducted field measurements and calculations of ventilation of pitched wooden roofs with cold attics. Blom found that a 48 mm high air cavity was appropriate in pitched, ventilated roofs of single-family houses. Blom also pointed out that a key factor in moisture-safe constructions is to ensure continuous thermal insulation and avoid air leakages through the insulation.

The current Norwegian guidelines for pitched roofs as given by Edvardsen and Ramstad (2014) are too simplified. In particular, there are no common guidelines for roof constructions with low angles, complicated roof design, roof spans longer than 15 m and roofs with building-integrated photovoltaics (BIPV).

The driving forces given by wind and temperature differences (natural convection) together with the calculated pressure losses in the air cavity below the roofing define the ventilation rate of pitched wooden roofs. Important input parameters required to calculate the wind-driven ventilation of pitched roofs include wind speed together with the difference in wind pressure coefficient, c_p, at the inlet and the outlet of the ventilation cavity (Figure 1). Pressure losses in the air cavity are calculated based on the input data and includes air passing (hereafter called "passing") the inlet and outlet, tile battens and friction losses. The accuracy of these calculations obviously depends on the accuracy of the local loss coefficients for the passing of the inlet, tile battens and outlet.

The purpose of this study has been to determine pressure losses at the inlet (eaves) and inside the air cavity consisting of friction losses and passing of tile battens.

Theoretical framework

The airflow through the air cavity system $\dot{V}\,(\mathrm{m}^3/\mathrm{h})$ can be expressed by equation (1), where the airflow is proportional to the driving forces of roof

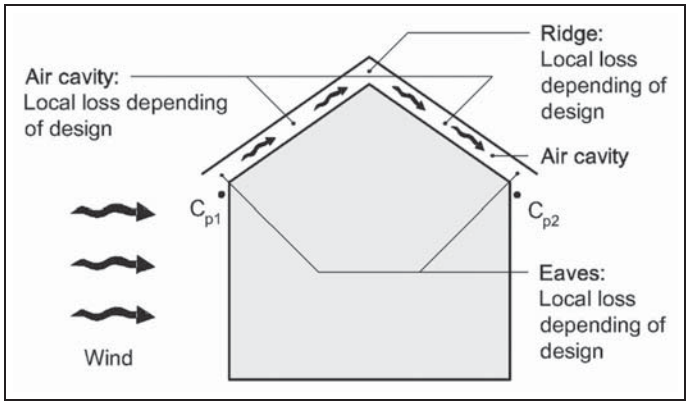

Figure 1. Important input parameters to calculate the wind-driven ventilation of pitched wooden roofs include wind speed together with the difference in wind pressure coefficient, c_p, at the inlet and outlet of the ventilation cavity as well as local losses inside the air cavity.

ventilation, Δp (Pa), given by the driving forces of wind and buoyancy. The airflow is inversely proportional to the sum of pressure losses through the air cavity system (Figure 1), R (Pa), in the following treated as friction loss and local losses.

$$\dot{V} = \sum \Delta p \cdot \frac{1}{\sum R} \tag{1}$$

Pressure losses and velocity profiles of pipes and air channels have previously been studied both theoretically and experimentally. Through these studies, empirical expressions have been developed for accurately calculating the pressure loss given well-defined flow situations (see Hansen et al., 2013).

The Reynolds number indicates whether a flow is laminar or turbulent: small Reynolds numbers give laminar flow, while large numbers give turbulent flow. The critical Reynolds number gives the value of the Reynolds number for the transition from laminar to turbulent flow. The size of the critical Reynolds number is dependent on the flow characteristics, sharp edges and change in velocity. For most flows, the critical Reynolds number is 2300 (Hansen et al., 2013)

$$\mathrm{Re} = \frac{u \cdot D_h}{\nu} \tag{2}$$

Re is the Reynolds number (–), u is the average velocity (m/s), D_h is the hydraulic diameter (m) of the flow channel and ν is the kinematic viscosity (m^2/s).

Friction loss. The pressure loss gradient (Pa/m) p_Δ inside a channel is dependent on the dynamic pressure p_d (Pa), the hydraulic diameter D_h (m) and the friction number λ (–)

$$p_\Delta = \lambda \frac{p_d}{D_h} \tag{3}$$

The dynamic pressure, p_d (Pa), is given by

$$p_d = \frac{1}{2} \cdot \rho \cdot {u_m}^2 \tag{4}$$

where ρ is the density of the air (kg/m^3) and u_m is the average air velocity (m/s).

The hydraulic diameter, D_h (m), is given by

$$D_h = \frac{2 \cdot a \cdot b}{a + b} \tag{5}$$

where a and b are the side lengths of the rectangular air channel (m).

For laminar flow, the friction number λ (–) is inversely proportional with the Reynolds number, Re

$$\lambda = \frac{64}{\mathrm{Re}} \tag{6}$$

Local losses. Pressure losses in components such as valves and bends are called local losses. Flow characteristics can be studied by applying established equations from fluid mechanics. Local pressure loss is given by the local loss coefficient, see equations (7) and (8). For $\xi = 0$, the local loss is zero and for $\xi = 1$ the local loss is equal to the dynamic pressure. At steady state, the driving forces are balanced by the pressure loss from friction and the pressure loss of the different minor losses along the flow path

$$\Delta P = \xi \cdot \frac{\rho \cdot u_m^2}{2} \tag{7}$$

$$\xi = \frac{2 \cdot \Delta P}{\rho \cdot u_m^2} \tag{8}$$

where ΔP is the pressure loss (Pa), ξ is the minor loss coefficient (–), ρ is the density of the air (kg/m^3) and u_m is the average velocity (m/s). u_m is given by the airflow Q (m^3/s) divided by the area of the smallest cross section of the flow path A (m^2).

Narrowing of the flow channel. The pressure loss in a narrowing cross-sectional flow area is caused by a contraction of the flow after the narrowing, given by the contraction factor α (see equation (10); Hansen et al., 2013; Figure 2)

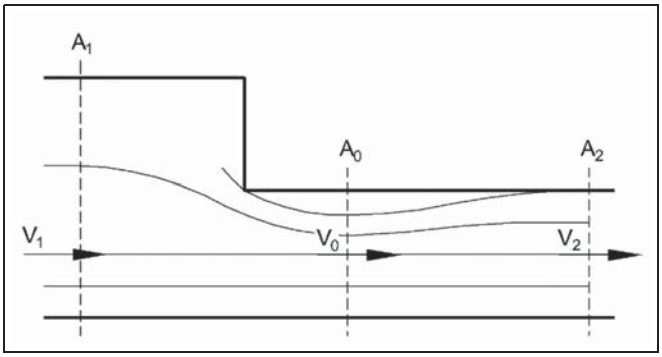

Figure 2. Pressure loss when there is a sharp decrease in the cross-sectional flow area.

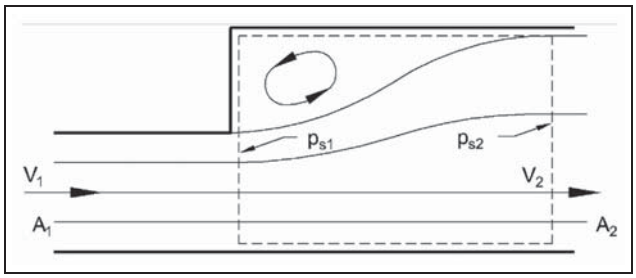

Figure 3. Pressure loss when there is a sharp increase in the cross-sectional flow area.

$$\xi_1 = \left(\frac{1}{\alpha} - 1\right)^2 \tag{9}$$

$$\alpha = \frac{A_0}{A_2} \tag{10}$$

Expansion of the flow channel. Pressure loss when there is a sharp increase in the cross-sectional flow area can be calculated using equation (11), giving the local pressure loss as a function of the cross-sectional area before and after the component (Hansen et al., 2013), see Figure 3

$$\xi_2 = \left(1 - \frac{A_1}{A_2}\right)^2 \tag{11}$$

The total local loss given by the expansion of the channel, ξ_1 (–), and narrowing of the channels, ξ_2(–), can be calculated using equation (12)

$$\xi = \xi_1 + \xi_2 \tag{12}$$

Previous research

In a laboratory study, Thiis et al. (2007) studied different roof eave designs and their inlet geometry to specify the ability to reduce snow penetration into the roof. The geometry and design of the ventilation openings was found to be the most important factor in reducing snow penetration. An inlet position close to the wall was found to give approximately five times more snow concentration of the air entering the roof cavity compared to a position close to the end of the eave. Idelchik (1994) contains a systematization and classification of data of hydraulic resistances from a large number of experimental studies carried out and published at different times in different countries.

Kronvall (1980) conducted measurements of airflow in building components and showed how the concept of fluid mechanics could be applied to airflow in building components. He also studied pressure losses at the entrance and bends in duct flows.

Later, Hofseth (2004) studied airflows in ventilated roof structures. As part of his work, he performed laboratory measurements of local losses of building components located inside the air cavity of the roof. He found that the local loss coefficient was dependent on the mass flow.

Falk and Sandin (2013) also performed laboratory measurements to estimate loss factors of metal battens inside ventilated wall cavities. They found that several of the loss factors were dependent on the air velocity.

Methods

The method includes both a laboratory investigation on a large-scale test model of a pitched wooden roof and numerical analysis using COMSOL software.

Laboratory test model

A large-scale test model of the ventilation air gap of a pitched roof was built in the SINTEF and NTNU laboratory in Trondheim, Norway. The model consisted of an aluminium profile with a length of 3550 mm and an internal width of 552 mm (Figure 4). As shown in Figure 4, the width of the box corresponds to the air gap between two counter battens with a width of 48 mm and a centre-to-centre distance of 600 mm, which is a typical situation in a ventilated wooden roof. As shown in Figures 5 and 6, the total length of the roof test model was 3550 mm and included a total of 11 tile battens with a centre-to-centre distance of 350 mm. Nine air pressure nipples were positioned in the top of the box, as shown in Figure 6.

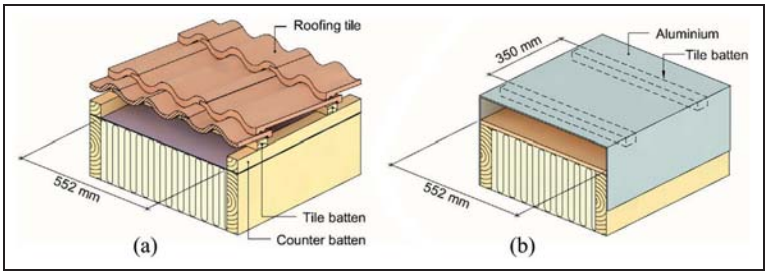

Figure 4. (a) Cross section of a typical roof construction with roofing tiles. (b) A cross section of the test model consisting of an aluminium box corresponding to the air gap between two counter battens with a width of 48 mm and a centre-to-centre distance of 600 mm. The centre-to-centre distance of the tile battens is 350 mm.

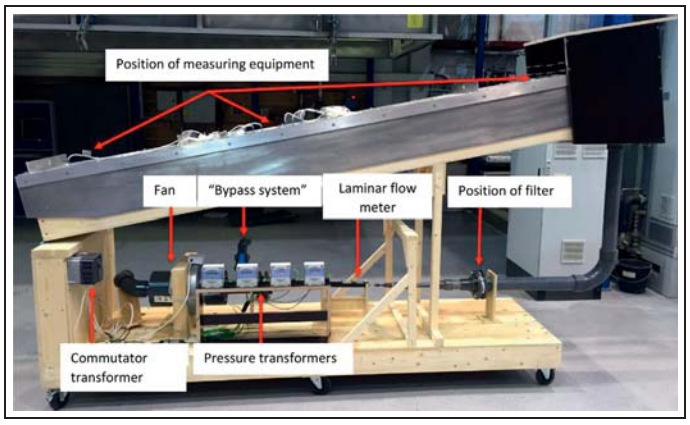

Figure 5. A large-scale test model of a pitched roof.

The airflow through the roof structure is measured by a laminar flow meter which is attached to a fan that sucks air through the ventilation gap system. To measure the pressure differences, four pressure transmitters (Furness Controls FCO 352 Model 1) were used. The pressure difference was recorded with a data logger (Delphin Technology Expert Key 100C) with a logger interval of 1 Hz (Figure 5). Each measuring step lasted approximately 120 s. The accuracy and measuring range of the applied instruments are given in Table 1.

Table 1. Accuracy and measuring range of applied sensors.

Sensor	Manufacturer	Type	Accuracy	Range
Thermocouple		Type T	±0.10°C	−20 to +60°C
Pressure transmitter	Furness control	FCO 352 Model 1	±0.25% of reading	0 to +50 Pa
Folding rule			±0.5 mm	0–2000 mm

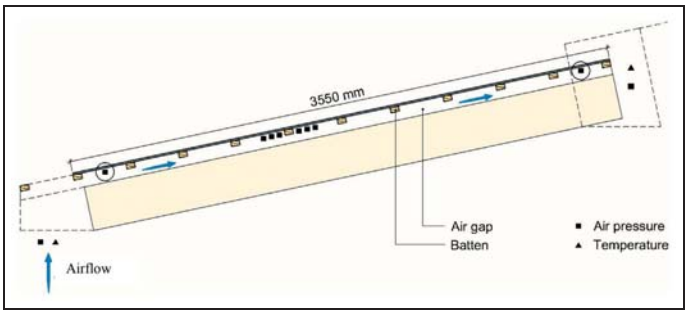

Figure 6. Cross section of the test model, with 10 air pressure monitor positions. The figures for the air pressure difference of the two points with circles, divided by the number of tile batten passings, which is nine, are used as input in equation (8).

Test procedure. The range of the air gap, height of the air cavity and centre-to-centre distance of the tile batten were determined by an investigation into the Norwegian building traditions described in Edvardsen and Ramstad (2014). To obtain as realistic measurements as possible the results, a field investigation of air velocity inside the air cavity of a roof was studied (Gullbrekken, 2017). He reported air velocity inside the air cavity for different seasons/periods as a function of wind speed at 10 m above ground level. The reported air velocity inside the air cavity was 0–1.2 m/s. The results were in line with a previous and corresponding investigation reported by Blom (1990). In addition, an important aspect was to choose air velocities that produced measurable static air pressure difference when passing battens. Simple calculations using equations (9) to (12) were performed to predict the pressure difference.

The test procedure was performed by installation of tile battens in the measuring rig, as shown in Figure 6. Then, the correct height of the air cavity beneath the tile batten was adjusted (23, 36 or 48 mm). The airflow was adjusted to fit the dynamic pressures of 0.05, 0.10, 0.20 and 0.40 Pa. This implies an increasing airflow by increasing height of the air cavity beneath the tile battens. A specific airflow was held constant in 120 s and the data were logged with 1 Hz logging interval. Then, a new airflow was set and held constant in 120 s and so on (Table 2).

Table 2. Test parameters, the chosen parameters and the reference to the chosen parameters.

Test parameters	Chosen parameters	Reference
Height of the air gap	23, 36, 48 (mm)	Edvardsen and Ramstad (2014)
Height of tile battens	30, 36, 48 (mm)	Edvardsen and Ramstad (2014)
Centre-to-centre distance tile battens	350 (mm)	Edvardsen and Ramstad (2014)
Air velocity below tile battens (corresponding dynamic pressure) (Pa)	0.20, 0.40, 0.60, 0.80 (m/s)	Gullbrekken (2017), Blom (1990)

Different design of the eave. To study the local pressure loss coefficient at the inlet of the ventilation cavity, we studied two different eave design solutions.

Classic design. A classic air inlet design in Norway has one or several air gaps in the horizontal part of the eave construction (Figure 7(a)). The laboratory investigation included measurements of local loss coefficients given one air gap with a width of 50 mm with and without installation of a fly net with an opening area of 67% covering the gap opening.

Modern design. Stricter requirements regarding airtightness of buildings necessitate a continuous wind barrier between wall and roof, as seen in Figure 7(b). In this case, the air inlet of the roof ventilation system is a 25 mm wide air gap behind the gutter. The laboratory investigation included measurements of local loss coefficients with and without a fly net covering the gap opening. The fly net had an opening area of 67%.

Airtightness of the laboratory test model. Initially, the airtightness of the test model was measured. The joints between the aluminium box and the rest of the test rig were sealed using tape. In addition, the inlet of the test rig was sealed. The measurements showed that the airflow through the sealed test model was less than 0.6% of the smallest tested airflow. By adding the rafter detail, the airflow through the sealed test model increased to 2.5% compared to the smallest tested airflow.

Uncertainty assessment of the laboratory measurements. The root mean square (RMS) method was used to derive the total uncertainty propagation of the measured local loss coefficients, $\Delta^p\xi/\xi$, see equations (17) and (18)

$$\xi = \frac{2 \cdot \Delta P}{\rho \cdot {u_m}^2} \tag{13}$$

$$\Delta P = P_1 - P_2 \tag{14}$$

$$\rho_{cavity} = \frac{\theta_{293.15K} \cdot \rho_{293.15K}}{\theta_{cavity}} = \frac{a}{T} \tag{15}$$

$$u_m^2 = \left(\frac{q}{A}\right)^2 \tag{16}$$

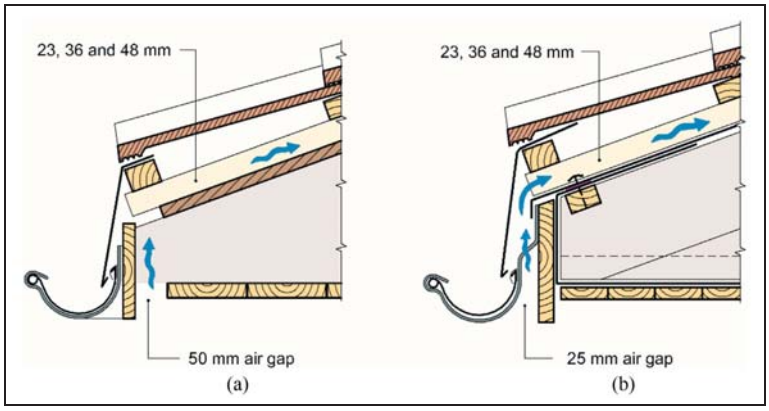

Figure 7. The two different eaves designs: (a) a classic solution with one air gap behind the gutter board and (b) a newer design with the air gap located between the gutter and the gutter board.

$$\xi = \frac{2 \cdot \Delta P \cdot T \cdot A^2 \cdot 60,000^2}{a \cdot q^2} \tag{17}$$

$$\frac{\Delta^p \xi}{\xi} = \sqrt{\left[\frac{\Delta^p(\Delta P)}{(\Delta P)}\right]^2 + \left[\frac{\Delta^p T}{T}\right]^2 + \left[\frac{\Delta^p A}{A}\right]^2 + \left[\frac{\Delta^p q}{q}\right]^2} \tag{18}$$

where P_1 (Pa) and P_2 (Pa) are the static air pressures at the particular measuring positions. u_m (m/s) is the average air velocity in the smallest cross section of the particular cross section. ρ is the density of the air (kg/m^3), θ is the temperature (K), q is the airflow (m^3/h) and A is the area of the smallest cross section of the air cavity of the particular cross section, where $(\Delta^p(\Delta P))/(\Delta P)$ is the uncertainty in the measured air pressure differences, $\Delta^p T/T$ is the uncertainty in the air temperature measurements, $\Delta^p A/A$ is the uncertainty in the cross-sectional area of the air cavity and the tile batten and $\Delta^p q/q$ is the uncertainty of the measured airflow through the air cavity.

No correlation between the various terms of the equation was found. The accuracy and measuring range of the applied instruments are given in Table 1.

Numerical analysis

Laboratory measurements are expensive and time-consuming. Compared to laboratory measurements, numerical analysis implies a large reduction of time and the possibility to investigate a larger span of design variation. Therefore, it is valuable to compare measurements with simulations of this study. In this study,

numerical analysis includes simulation of airflow inside the air cavity between the underlayer roofing and the roofing material. Conservation of mass, momentum and energy are based on the assumption of a flowing media with constant properties. In the laminar regime, the flow of the media can be predicted by solving the steady-state Navier–Stokes equations given in equation (19)

$$\rho\left[\frac{dv}{dt} + u + \nabla u\right] = \nabla \cdot \sigma + f \tag{19}$$

where ρ denotes the density of the fluid (kg/m^3), u is the velocity (m/s), $\nabla \cdot \sigma$ denotes shear stress and f being all other forces.

This can be rewritten assuming a Newtonian fluid

$$\rho\left[\frac{dv}{dt} + u + \nabla u\right] = -\nabla p + \mu\nabla^2 u + f \tag{20}$$

where p is the pressure (Pa) and μ (Pa s) is the dynamic viscosity

$$\nabla p = \mu\nabla^2 u + f - \rho\left[\frac{dv}{dt} + u + \nabla u\right] \tag{21}$$

COMSOL Multiphysics software has been used for mesh generation and to solve the system of partial differential equations. The COMSOL Multiphysics software includes eight built-in turbulence models. They differ how they model the flow close to the wall, number of additional variables solved for and what these variables represent. Among them are the low Re k–ε model and low Re k–ω model. The term 'Low Reynolds number' does not refer to the flow on a global scale, but in the region close to the wall where viscous effects dominate. A low Reynolds number model therefore more correctly reproduces the behaviour of different flows at small distances from the wall. The low Re k–ε model solves for two variables: k, the turbulence kinetic energy and ε, the rate of dissipation of turbulence energy. A wall function is used in the model. In that way, the flow close to the surfaces is not simulated. The low Re k–ω model is a model similar to the k–ε model, but it solves for ω, the specific rate of dissipation of kinetic energy. The model is more nonlinear and therefore somewhat more difficult to converge. The model is useful in many cases when the k–ε model is not accurate. In this work, we have used both models. The k–ε model that is more easily converging is used to find a preliminary solution. Based on the solution, the k–ω model is used to increase the accuracy of the solution. A coarse grid is used in the solver to lower the period to perform the simulations. Even so one calculation including four air velocities took several hours!

Calculation of the minor losses was performed according to equation (8). The static pressures of the simulations were read from the simulation model according to the laboratory measurements. The position of the static pressure of the model is indicated by red dots in Figure 8.

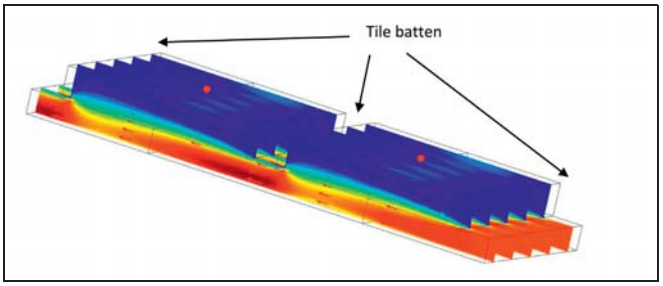

Figure 8. Five cross sections of the air velocity distribution inside the air cavity given by the COMSOL software. Higher air velocities are indicated in red colour. Red dots indicate the position of the static pressure measurements used in the calculations of the minor losses.

Simulation model. To simplify the model and thereby reduce the time needed for calculations, the model only included passing of one tile batten (Figure 8). The simulation model has been used to calculate the loss in absolute pressure at different dynamic pressures inside the air channel, thereby calculating the local singular loss coefficients according to equation (8). A parameter study including different dynamic pressures, dimensions of the tile batten and height of the air channel below the tile batten was conducted.

Results

Friction loss

Calculated and measured friction coefficients of the air cavity as a function of the Reynolds number are shown in Figure 9. The theoretical friction coefficient is calculated according to equation (6) assuming that airflow inside the air channel is laminar.

Sharp-edged and round-edged tile battens

The local loss coefficients for 36 mm sharp-edged and 36 mm round-edged tile battens for 23 mm and 48 mm air gaps are shown in Figure 10 along with theoretical values as given in the 'Danvak' handbook by Hansen et al. (2013).

Different dimensions of tile and counter battens

Figure 11 shows the local loss coefficients for tile battens that are 30, 36 and 48 mm high and air cavity heights of 23, 36 and 48 mm below the tile batten as a function of the dynamic pressure given by equation (4). The width of the tile batten is kept

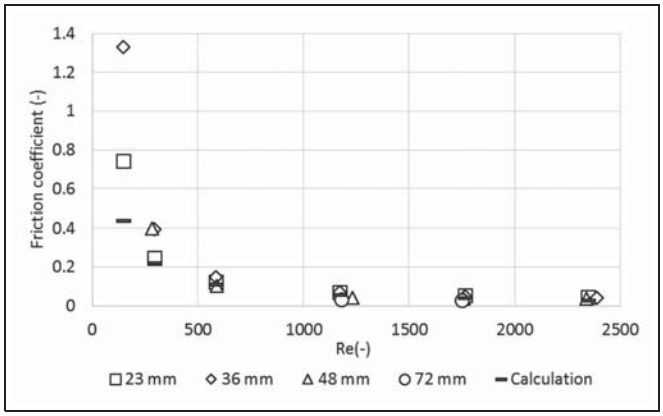

Figure 9. Calculated and measured friction coefficients in the air channel at different Reynolds numbers and counter batten thickness.

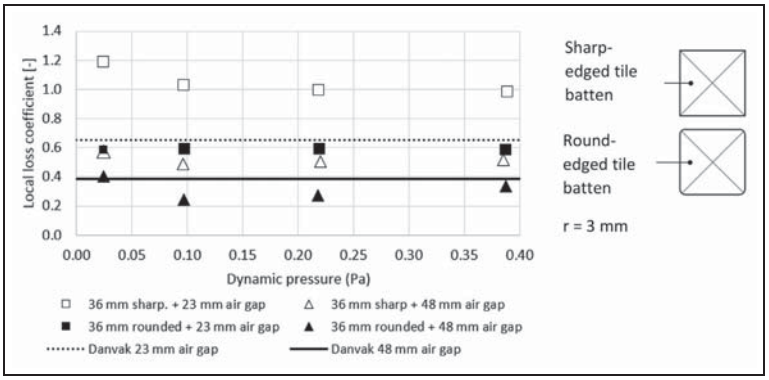

Figure 10. Local loss coefficient for sharp-edged and rounded battens with different air gaps and dynamic air pressure of the airflow passing the tile batten. 'Danvak' means values calculated from Hansen et al. (2013).

constant at 48 mm. The open symbols represent the results of the measurements, the filled symbols represent results from the COMSOL calculations and the straight lines represent calculated values according to equations (10) to (12) given in the 'Danvak' handbook (Hansen et al., 2013).

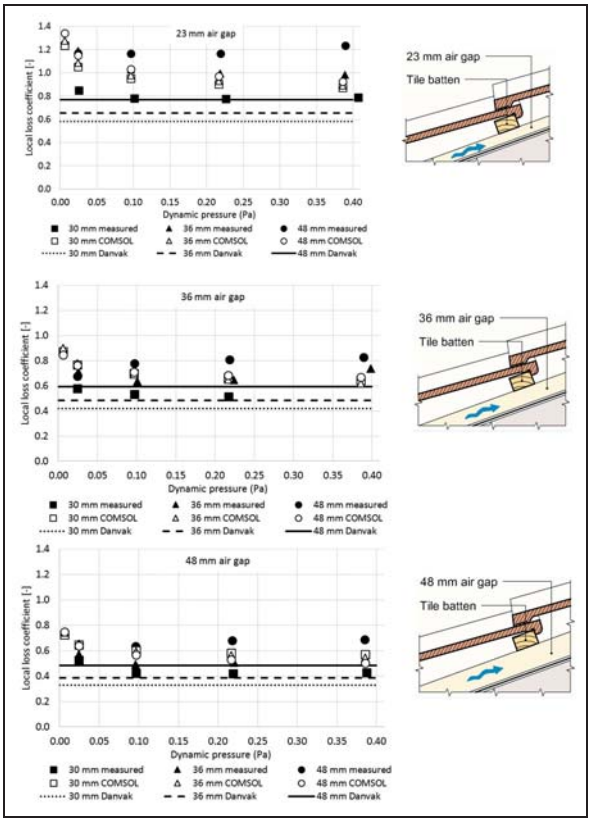

Figure 11. Local loss coefficient as a function of dynamic pressure for tile battens that are 30, 36 and 48 mm high. The filled symbols represent the results of the measurements, the open symbols represent results from the COMSOL calculations and the straight lines represent theoretical values according to equations (10) to (12) given in 'Danvak' handbook (Hansen et al., 2013).

To simplify the measuring results, equations (22) and (23) describe the local loss coefficient by passing of one sharp-edged batten. β in equation (23) is given by A_1 and A_2 in Figure 2. Equation (22) is derived by regression analysis and least square method. With a starting point in equation (9), the formulae were adjusted to obtain as small deviation between the measuring results and the equation as possible.

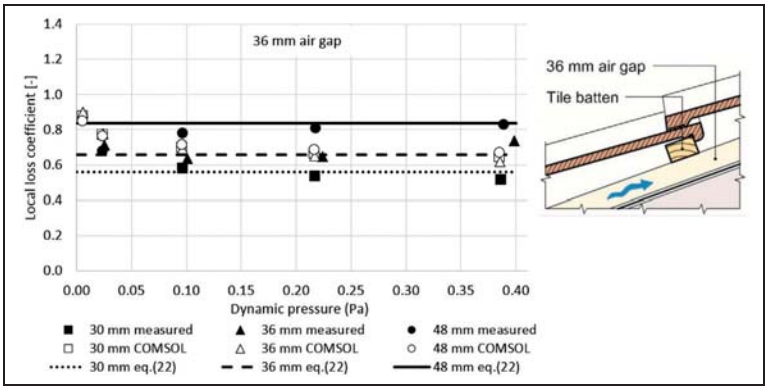

Figure 12. The filled symbols represent the results of the measurements, the open symbols represent results from the COMSOL calculations and the straight lines represent values according to equation (22).

Figure 12 shows the calculated results from equation (22) compared to the measured results for the 36 mm air gap

$$\xi = -\left(\frac{1}{\beta} - 1.375\right)^3 \tag{22}$$

$$\beta = \frac{A_1}{A_2} \tag{23}$$

Table 3 shows the average measured local loss coefficient by assuming a constant relation between the local loss coefficient and the dynamic pressure. In the table, the measured values are compared to the calculated values according to Hansen et al. (2013) and to results from equation (22) which is an improved solution based on the laboratory measurements.

Uncertainty of the tile batten measurements

Each calculated local loss coefficients of the tile batten consist of three measurements: two friction loss measurements (the friction loss between and below the tile batten) and a measurement of pressure loss including local losses by tile battens and friction. The uncertainty has only been calculated for part of the measurements as given by Table 4.

Table 3. Average measured and calculated local loss coefficients.

Air gap (mm)	Tile batten (mm)	Average measured local loss coefficient, ξ	Standard deviation, measured values	Calculated local loss coefficient, ξ, equations (9) to (12)	% Difference compared to measurements	Calculated local loss coefficient, ξ, equation (22)	% Difference compared to measurements
	30		0.006	0.58	−34	0.82	5
23	36	1	0.023	0.65	−53	0.94	−6
	48	1.19	0.04	0.77	−55	1.14	−4
	30	0.54	0.032	0.42	−28	0.56	4
36	36	0.67	0.055	0.48	−38	0.66	−2
	48	0.8	0.025	0.59	−35	0.83	4
	30	0.42	0.003	0.33	−28	0.43	2
48	36	0.5	0.013	0.39	−30	0.51	2
	48	0.67	0.028	0.48	−38	0.66	−2

Table 4. The uncertainty of the measurements is calculated for part of the measurements.

Dynamic pressure	23 mm cavity		48 mm cavity	
	0.1 Pa	0.4 Pa	0.1 Pa	0.4 Pa
Tile batten height (mm)	$\Delta\xi$ (%)	$\Delta\xi$ (%)	$\Delta\xi$ (%)	$\Delta\xi$ (%)
30	10.3	10.7	5.0	4.4
36	9.9	10.1	4.4	4.4
48	9.1	9.1	4.3	4.3

Air intake at eaves

Classic design. Figure 13 shows the local loss coefficient of the air intake design as a function of the dynamic pressure in the air cavity beneath the tile battens. The pressure is measured at the black dots in Figure 13. The figure shows results from one air gap of 50 mm with and without a fly net. The different series in the diagram are related to measurements performed with 23, 36 and 48 mm air gaps beneath the tile battens. The height of the tile batten is kept constant at 36 mm.

Modern design. Figure 14 gives the minor loss coefficient of the detail as a function of the dynamic pressure in the airflow beneath the tile batten. The pressure is measured at the black dots in Figure 14. The local loss coefficients in Figure 14 are corrected by subtracting the pressure loss caused by the passing of one tile batten. The figure shows results from one air gap of 25 mm with and without a fly net. The different series in the diagram are related to measurements performed with 23, 36 and 48 mm air gaps beneath the tile battens. The height of the tile batten is kept constant at 36 mm.

Discussion

The results show a good correspondence between the measured friction coefficient and the calculated friction coefficient. The calculated Reynolds numbers of Figure 8 indicate laminar flow. Therefore, the friction coefficient is inversely proportional to the Reynolds number.

Laboratory measuring model compared to tile roofing

The design of the laboratory measurements can be directly compared to using membranes on wooden boards for roofing. The use of metal sheeting or tiles implies an air gap between the roofing and the tile batten. An air gap above the tile batten roofing will affect the flow pattern of the airflow. It is likely that the increased cross-sectional area available for airflow will reduce the local loss coefficient. Consequently, the measured local loss coefficients of this study are conservative.

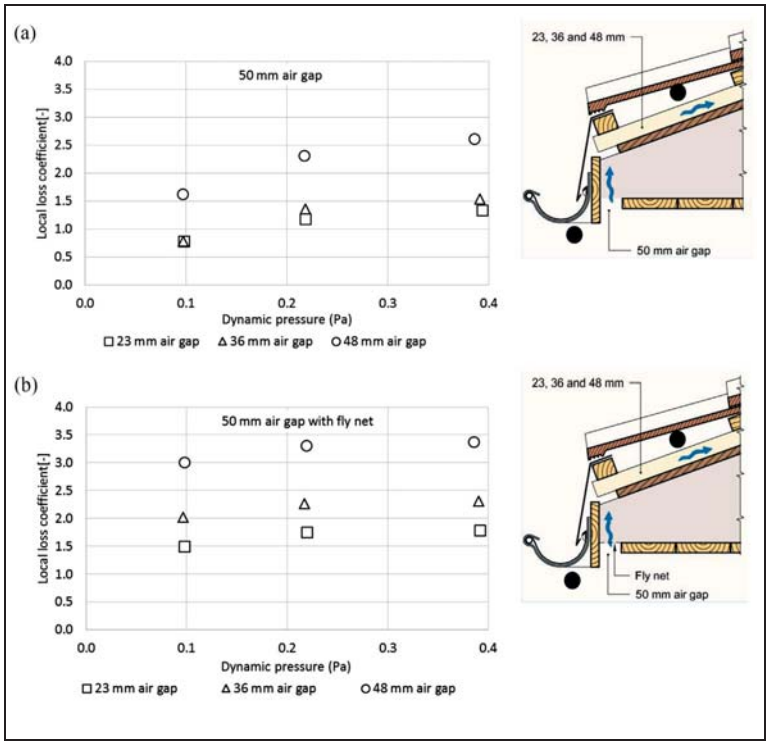

Figure 13. Measuring results of local loss coefficient for the classic eaves design as a function of dynamic pressure calculated for the air cavity beneath the tile batten. Diagram (a) without fly net and diagram (b) with fly net. The pressure is measured at the black dots.

The effect of roof slope is not covered by this study. However, the slope will affect the local loss at the eaves because the deflecting of the airflow entering the air cavity is dependent on the roof slope.

The height of the tile batten

In general, both the measurements and COMSOL simulations showed higher local loss coefficients compared to the calculations using the 'Danvak' handbook (equations (9) to (12)). Equations (9) to (12) are general values given a narrowing and expansion of the airflow. In this case, there is a small distance between the narrowing and expansion of the airflow possibly not causing completely laminar and undisturbed airflow when the air passes the expansion. Equation (22) is an

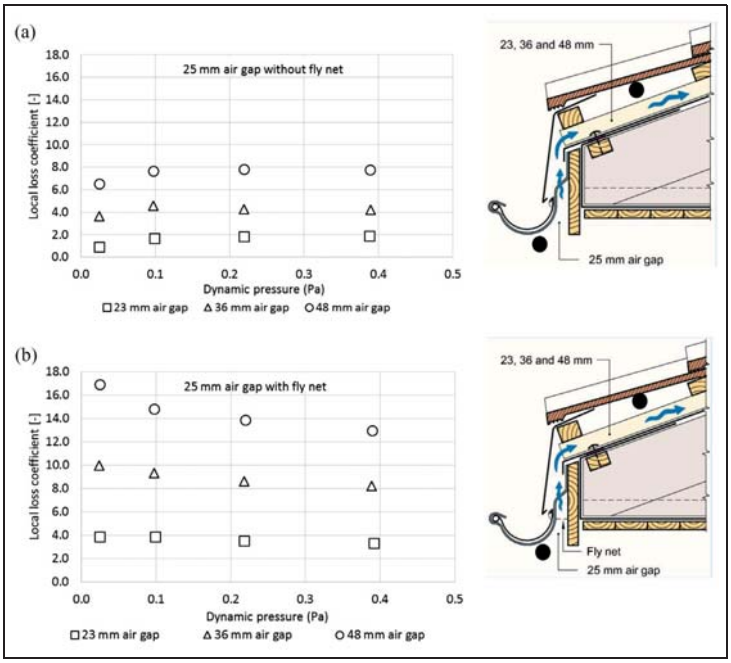

Figure 14. Measuring results of local loss coefficient for the modern eaves design as a function of dynamic pressure calculated for the air cavity beneath the tile batten. Diagram (a) without fly net and diagram (b) with fly net. The pressure is measured at the black dots.

improvement of equations (9) to (12) and is specific for the passing of sharp-edged tile battens. According to Kronvall (1980), a short distance between two obstacles in an airflow will cause a reduction of the total local loss coefficient given by the two obstacles. In this case, the small distance between the obstacles has caused an increased measured local loss coefficient compared to the calculated values. The calculations, simulations and the measurements all showed increasing local loss coefficients in line with increasing height of the tile batten. The maximum deviation between the average measured local loss coefficient and average calculated coefficient was 55%. The equivalent number for equation (22) was 6%. Hence, a sufficient correspondence between the calculated local loss coefficients for a batten passing given by equation (22) and the measurements was found.

The measurements and simulations of different dimensions of the tile batten indicated a constant correlation between the local loss coefficient and the dynamic pressure given a larger dynamic pressure than 0.10 Pa. However, both Hofseth

(2004) and Falk and Sandin (2013) found that the local loss coefficient was dependent on the air velocity and hence the dynamic pressure. The air velocity of Hofseth's results was 5–10 times larger than the air velocity of this study. This will of course influence the flow characteristics inside the air cavity. The air velocity of Falk and Sandin (2013) was of the same magnitude as this study. Measurements at low dynamic pressures mean that the measured pressure drop over the nine tile battens is very small, typically down to 0.1 Pa, which could imply increased measuring error, both because of the resolution of the pressure transmitter and fluctuations in the surrounding air.

However, the calculations of uncertainty do not interpret a correlation between the dynamic pressure and the magnitude of the uncertainty. On the other hand, the magnitude of uncertainty seems to increase by decreasing height of the air cavity below the tile batten. One possible explanation is that the relative measuring error of the cross-sectional areas increases by decreasing height of the air cavity. Based on this explanation and the constant relation between the uncertainty and the tile batten height, it is likely that the calculation of uncertainty from the 36 mm air gap will be somewhere between the two calculated uncertainties, that is, somewhere between 5% and 10%.

Sharp-edged and round-edged tile batten

The measurements showed a large difference in the local loss coefficients depending on the edge design of the tile batten. The local loss coefficient of the rounded tile battens was approximately 40% lower than the local loss coefficients of the sharp-edged tile battens. Idelchik (1994) also reported lowered local loss coefficients by the use of rounded orifices. There was a larger difference between the sharp-edged and round-edged tile batten for the 48 mm air gap compared to the 23 mm air gap. Compared to the calculated values according to equations (9) to (12), the smallest deviation was found for the rounded tile battens. The smallest deviation was found for the 23 mm air gap and the rounded tile batten.

Numerical analysis

It was found that the simplified COMSOL model shown in Figure 8 could reliably reproduce the results from the measurements. The smallest deviation between the simulations and the measurements was found for the smallest dynamic pressures. Many of the measurements include low Reynolds numbers, and the flow is laminar, but at the highest dynamic pressures, the flow is turbulent or in the transition zone. A challenge is that the Reynolds numbers are different in the different cross sections along the flow possibly changing between laminar and turbulent flow. The low Re k–ω model was used in the COMSOL simulations because of the geometry of the simulation model and the surface position of the static air pressure used in the calculation of the local losses. It was assumed that a more accurate calculation

of the flow characteristics close to the surface was important to obtain a more correct static pressure at the surface.

A simplification of the model is the assumption of uniform flow at the inlet of the model, below the tile batten. A close study into the second tile batten of Figure 8 shows that the air velocity is somewhat higher in the middle of the cross section and close to the lower surface compared to the air velocity close to the tile batten, also given in Figure 2. The smallest difference between the measurements and the simulations was found for the 36 mm tile batten and the air gaps of 23, 36 and 48 mm. The simulation results indicate that the tile batten height inflates less on the local loss coefficient compared to the measurements and the calculations.

The results indicate that the COMSOL software can be used to produce local loss coefficients where measurements of local loss coefficients of sharp-edged tile battens are not available. Given a larger dynamic pressure than 0.10 Pa, the COMSOL simulation indicates a constant local loss coefficient. Some of the measuring results also indicate an increasing local loss coefficient at lower dynamic pressures. This phenomenon is not easy to explain. The error by simplifying and calculating with a constant local loss coefficient at these small dynamic pressures will, however, be small because of low air velocities inside the cavity which, according to equation (7), gives small pressure losses.

Eaves design

The local loss coefficient increases by increasing height of the air gap beneath the tile batten. The explanation is the increasing airflow through the eaves construction by increasing air gap beneath the tile batten because the dynamic pressure is calculated at the passing of the tile battens. The measurements of the classic design show a large increase in the local loss coefficient by introduction of a fly net inside the 50 mm air gap at the eaves. The option without a fly net shows an increasing local loss coefficient by increasing dynamic pressures. The measurements for the option with a fly net indicate a constant relation between the dynamic pressure and the local loss coefficient for a dynamic pressure larger than 0.2 Pa. The measurements and the literature review conducted by Kronvall (1980) also indicated a constant local loss coefficient independent of the Reynolds number. The measurements include narrowing and expansion when the air enters the air space inside the eaves construction. Furthermore, the measurements include narrowing and expansion when the air enters the air cavity below the roofing. The geometry of the eaves design makes it difficult to compare the results to calculated results from equations in the literature.

The modern eaves design of Figure 13 shows increasing local loss coefficients compared to the classic solution. This can partly be explained by the decreased gap in the air cavity compared to the classic design. The measurements include pressure loss by narrowing and friction loss in the 25 mm air cavity. Furthermore, the measurements include a bend, narrowing and expansion by passing of the lowest tile batten of the roof. As with the classic solution, the local loss coefficient increases in line with the height of the air gap, thereby increasing mass flow through the air

cavity. Installation of a fly net inside the air cavity leads to approximately doubling of the local loss coefficients. The increase is large for the smallest dynamic pressures. The dynamic pressure is still calculated in the cross section below the tile batten. Installation of fly net of course reduces the effective airflow area, thereby increasing the local loss coefficient.

The local loss coefficients with the classic design correspond to the local loss coefficient given by four tile batten passings without a fly net and six tile batten passings with a fly net. The local loss coefficient given by the modern design without a fly net corresponds to approximately 16 tile batten passings. By installing a fly net, the local loss coefficient corresponds approximately to 30 tile batten passings. Thiis et al. (2007) showed that an increased local loss coefficient and thereby a reduction in the air velocity inside the air cavity was effective to reduce snow penetration into the air cavity.

Measures to increase ventilation of pitched roofs

To increase the ventilation of a typical roof construction, a decrease in the height of the tile batten is positive as well as an increase in the counter batten height. The use of round-edged tile battens was also found to lower the local loss coefficient, by approximately 40%, thereby increasing the ventilation of the roof compared to a sharp-edged tile batten. To increase the ventilation of pitched wooden roofs, the results show that a classic eaves design without a fly net is the preferred eaves solution.

Conclusion

This study has found a large difference in the local loss coefficients depending on the edge design of the tile batten. The local loss coefficients of the round-edged tile battens were approximately 40% lower than the local loss coefficients of the sharp-edged tile battens. The measurements and simulations of different dimensions of the tile batten indicated a constant correlation between the local loss coefficient and the dynamic pressure given a larger dynamic pressure than 0.10 Pa. The COMSOL model used in the study could reliably reproduce the results from the measurements. Increased height of the counter batten as well as the use of rounded tile battens was found to be effective at increasing the ventilation of pitched wooden roofs. Furthermore, the measurements showed considerably lower local loss coefficients for the classic eaves design compared to the modern design. Installation of fly net in the ventilation gap was found to approximately double the local loss coefficient.

Declaration of conflicting interests

The author(s) declared no potential conflicts of interest with respect to the research, authorship and/or publication of this article.

Funding

The author(s) disclosed receipt of the following financial support for the research, authorship, and/or publication of this article: The authors gratefully acknowledge the financial support by the Research Council of Norway and several partners through the Centre of Research-based Innovation 'Klima 2050' (www.klima2050.no).

References

Blom P (1990) *Venting of insulated, pitched roofs*. PhD thesis, Institute of Building Technology, Norwegian Technical University, Trondheim (in Norwegian).

Blom P (2001) Venting of attics and pitched, insulated roofs. *Journal of Building Physics* 25: 32–50.

Edvardsen K and Ramstad T (2014) *Trehus Håndbok 5* (Wood Frame Houses Handbook No 5). Oslo: SINTEF Building and Infrastructure (in Norwegian).

Falk J and Sandin K (2013) Ventilated rainscreen cladding: measurements of cavity air velocities, estimation of air change rates and evaluation of driving forces. *Building and Environment* 59: 164–176.

Geving S (2011) *Fuktskader Årsaker, Utbedringer og Tiltak* (Moisture Damages, Causes and Repair Measures). Oslo: SINTEF Building and Infrastructure (in Norwegian).

Gullbrekken (2017) Ventilated wooden roofs: influence of local weather conditions – measurements. In: *NSB 2017 – 11th Nordic symposium on building physics*, Trondheim, 11–14 June.

Hansen HE, Kjerulf-Jensen P and Stampe OB (2013) *Varme og Klimateknik Danvak Grundbog* (Heat and Climate Technique Danvak), 4th edn. Glostrup: Danvak (in Danish).

Hofseth V (2004) *Studie av luftede takkonstruksjoner* (Study of ventilated roof constructions). Trondheim: NTNU (in Norwegian).

Idelchik IE (1994) *Handbook of Hydraulic Resistance*. Boca Raton, FL: CRC Press.

Kronvall J (1980) *Air flows in building components*. PhD thesis, Lund University, Lund.

Roels S and Langmans J (2016) Highly insulated pitched roofs resilient to air flow patterns: guidelines based on a literature review. *Energy and Buildings* 120: 10–18.

Samuelson I (1998) Hygrothermal performance of attics. *Journal of Thermal Envelope and Building Science* 22: 132–146.

Thiis TK, Barfoed P, Delpech P, et al. (2007) Penetration of snow into roof constructions – wind tunnel testing of different eave cover designs. *Journal of Wind Engineering and Industrial Aerodynamics* 95: 1476–1485.

Tobiasson W, Buska J and Greatorex A (1994) Ventilating attics to minimize icings at eaves. *Energy and Buildings* 21: 229–234.

Uvsløkk S (1996) The importance of wind barriers for insulated timber frame constructions. *Journal of Building Physics* 20: 40–62.

Walker TS and Forest TW (1995) Field measurements of ventilation rates in attics. *Building and Environment* 30: 333–347.

Paper 7

L. Gullbrekken, S. Uvsløkk, H.O Hygen, T. Kvande, B. Time.

Air cavity design guidelines for pitched wooden roofs in cold climate

Submitted.

Paper VII

This paper is awaiting publication and is therefore not included.